COMMUNICATION

ChemComm
www.rsc.org/chemcomm

A novel route to multimetallic nuclearity-controlled d^8 metal-chalcogen compounds

Rubén Mas-Ballesté,[a] William Clegg,[b] Agustí Lledós*[a] and Pilar González-Duarte*[a]

[a] *Departament de Química, Universitat Autònoma de Barcelona, E-08193 Bellaterra, Barcelona, Spain; E-mail: Pilar.Gonzalez.Duarte@uab.es*

[b] *Department of Chemistry, University of Newcastle, Newcastle upon Tyne NE1 7RU, UK*

This submission was created using the RSC ChemComm Template (DO NOT DELETE THIS TEXT)
(LINE INCLUDED FOR SPACING ONLY - DO NOT DELETE THIS TEXT)

The synthetic strategy here reported, that involves the self-assembly of the $\{Pt_2S_2\}$ core in [(dppp)Pt(μ-S)$_2$Pt(dppp)] metalloligand, constitutes the first example of the use of $[L_2Pt(\mu\text{-}S)_2PtL_2]$ compounds as building blocks to obtain multimetallic aggregates containing a $\{Pt_2S_2\}_n$ core.

Control of the size of metal chalcogenide compounds is of great interest because of its potential effect on their electrical[1] and optical properties.[2] Despite novel approaches to the synthesis of high nuclearity platinum complexes have been reported recently,[3] the chemistry of noble-metal-sulfido clusters has been disregarded if compared with that of aggregates containing the first transition series metals and molybdenum.[4] Here, we report on a novel synthetic route based on the self-assembly of $[L_2Pt(\mu\text{-}S)_2PtL_2]$ compounds, which leads to multimetallic aggregates containing a $\{Pt_2S_2\}_n$ core. The synthetic strategy allows control of the nuclearity of the cluster and can be extended to other metals with square–planar coordination.

The outstanding nucleophilicity of the sulfur atoms in the $\{Pt_2S_2\}$ core accounts for the significant number of known homo- and heterometallic derivatives of $[L_2Pt(\mu\text{-}S)_2PtL_2]$, L = phosphine, identified to date,[5] as well as for its reaction with organic electrophiles[6] and protons.[7] Further development of this chemistry is now addressed to the use of compounds $[L_2Pt(\mu\text{-}S)_2PtL_2]$ as building blocks of multimetallic aggregates containing a $\{Pt_2S_2\}_n$ core. The synthetic strategy involves first expansion of the $\{Pt_2S_2\}$ rings to $[\{Pt_2S_2\}PtL'_2]$ fragments containing labile terminal L' ligands, which are then replaced by bridging sulfide ligands. As a result, the PtL'_2 fragment evolves to a $\{Pt_2S_2\}$ linking unit between two $\{Pt_2S_2\}$ rings, thus affording a new $[\{Pt_2S_2\}_2\{Pt_2S_2\}]$ core. Its subsequent evolution to $[\{Pt_2S_2\}_3PtL'_2]$ lays the foundation for a new cycle. In this work we present the synthesis and characterization of three complexes derived from $[Pt_2(\mu\text{-}S)_2(dppp)_2]$ (**1**) (Scheme 1) and provide evidence for the lability of chloride ligands in the $[\{Pt_2S_2\}PtCl_2]$ fragment.

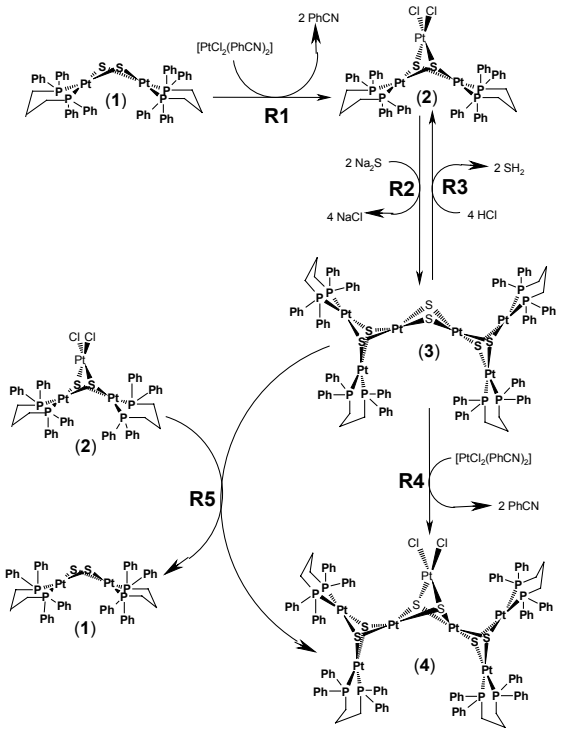

Scheme 1

By reacting during 6 hours at room temperature equimolar quantities of $[Pt_2(\mu\text{-}S)_2(dppp)_2]$ (**1**) with $[PtCl_2(PhCN)_2]$ in benzene, the compound $[\{Pt_2(\mu_3\text{-}S)_2(dppp)_2\}PtCl_2]$ (**2**) is obtained (yield 82%) as an orange solid. Slow evaporation of a solution of **2** in CH_2Cl_2 afforded yellow crystals. The X-ray structure consists of discrete trinuclear molecules and solvent molecules.† Although the latter show disorder, the structure of the complex (Figure 1) has been unequivocally determined. Thus, the central Pt_3S_2 unit consists of a non-equilateral triangle of platinum atoms capped above and below by two sulfur atoms, thus describing a trigonal bipyramid. Each platinum atom has approximate square-planar coordination. Significantly, among the wide family of derivatives obtained from $[L_2Pt(\mu\text{-}S)_2PtL_2]$ metalloligands, L = phosphine, no previous example of the $P_4Cl_2Pt_3S_2$ core observed in **2** had been determined by X-ray diffraction. In fact, as a result of reactions comparable to R1, three different alternatives have been proposed: formation of a mixture of an hexametallic $[\{Pt_2(\mu_3\text{-}S)_2(Ptolyl)_4\}M_2(\mu\text{-}Cl)_2\{Pt_2(\mu_3\text{-}S)_2(Ptolyl_3)_4\}]^{2+}$ and a trimetallic $[\{Pt_2(\mu_3\text{-}S)_2(Ptolyl_3)_4\}MCl_2]$ (M = Pd, Pt)[8] species, or formation of only an hexametallic $[\{Pt_2(\mu_3\text{-}S)_2(PPh_3)_4\}Pd_2(\mu\text{-}Cl)_2\{Pt_2(\mu_3\text{-}S)_2(PPh_3)_4\}]^{2+}$,[9] or a trimetallic $[\{Pt_2(\mu_3\text{-}S)_2(PPh_3)_4\}PtCl_2]$[10] complex. The $^{31}P\{^1H\}$-NMR spectrum of **2** in $CDCl_3$, shows only one signal centered at –8.08 ppm with ^1J(Pt-P) = 2978 Hz, thus indicating that ^{31}P nuclei are equivalent in solution.

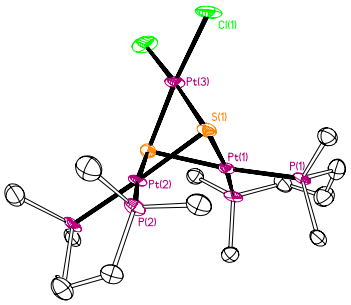

Figure 1. Molecular structure of **2** with the key atoms labeled and 50% probability ellipsoids. H atoms, phenyl rings and CH_2Cl_2 solvent molecules have been omitted.

† Electronic Supplementary Information (ESI) available: [details of any supplementary information available should be included here]. See http://www.rsc.org/suppdata/cc/b0/b000000a/

The lability of the chloro ligands in **2** becomes apparent in the characterization of this compound by ESI MS. Thus, depending on the recording conditions and on the solvent used to obtain mass data, the following cationic species have been identified: $[\{Pt_2(\mu_3\text{-}S)_2(dppp)_2\}PtCl]^+$ (m/z = 1509.5), $[\{Pt_2(\mu_3\text{-}S)_2(dppp)_2\}PtCl(CH_3CN)]^+$ (m/z = 1550.8), $[\{Pt_2(\mu_3\text{-}S)_2(dppp)_2\}Pt(CH_3CN)_2]^{2+}$ (m/z = 778.2), or $[\{Pt_2(\mu_3\text{-}S)_2(dppp)_2\}PtCl(CH_3OH)]^+$ (m/z =1541.6). Additional evidence for this lability is provided by the fact that a solution of **2** in dmso yields the unprecedented complex $[\{Pt_2(\mu_3\text{-}S)_2(dppp)_2\}PtCl(dmso)]Cl$, whose synthesis and characterization is here reported.[11] Moreover, the addition of an stoichiometric amount of dppp to **2** affords complex $[Pt_3(\mu_3\text{-}S)_2(dppp)_3]Cl_2$, recently reported.[12]

On the basis of its ability to exchange the chloride ions, a suspension of complex **2** in methanol was made to react during one hour at room temperature with a stoichiometric amount of $Na_2S{\cdot}9H_2O$. Concentration of the filtered orange solution thus obtained, followed by addition of ether, allowed isolation and characterization of $[\{Pt_2(\mu_3\text{-}S)_2(dppp)_2\}_2\{Pt_2(\mu\text{-}S)_2\}]$ (**3**) (yield 61%). The $^{31}P\{^1H\}$-NMR spectrum of **3** in dmso-d_6 shows a broad signal centered at -7.9 ppm with a ^1J(Pt-P) value of *ca.* 3000 Hz, and the ^{195}Pt-NMR spectrum in the same solvent consists of two signals, one singlet at δ = -3524 ppm (PtS_4) and one triplet centered at δ = -4425 ppm (S_2PtP_2) with ^1J(Pt-P) = 3002 Hz. Definite evidence for the hexametallic nature of **3** was provided by the MALDI-TOF mass spectrum, showing a major peak at m/z = 3013.5, which is fully consistent with the molecular mass of the cation $[\{Pt_2(\mu_3\text{-}S)_2(dppp)_2\}Pt(\mu\text{-}S)(\mu\text{-}SH)Pt\{Pt_2(\mu_3\text{-}S)_2(dppp)_2\}]^+$.

Comparison of the nucleophilicity of the $\{Pt_2S_2\}$ core in complexes **3** and **1** was established through determination of their basic character. Thus, the titration of **1** and **3** with HCl was monitored by $^{31}P\{^1H\}$-NMR. The addition of a stoichiometric amount of HCl to **3** leads to **2** quantitatively, while formation of $[PtCl_2(dppp)]$ from **1** requires a significant excess of HCl.[12] Additional evidence for the greater basicity of the $\{Pt_2S_2\}$ core in **3** than in **1** comes from the ability of the former to displace the $\{PtCl_2\}$ fragment from **2** to afford **1** and $[\{Pt_2(\mu_3\text{-}S)_2(dppp)_2\}Pt_2(\mu_3\text{-}S)_2PtCl_2\{Pt_2(\mu_3\text{-}S)_2(dppp)_2\}]$ (**4**), as indicated in Scheme 1. An alternative way to obtain **4** is by reacting **3** with a stoichiometric amount of $[PtCl_2(PhCN)_2]$ in acetonitrile during three hours at room temperature (yield 54%). Complex **4** was characterized by mass and NMR techniques. The MALDI-TOF spectrum has a major signal at m/z = 1640.2, which can be assigned to the $[\mathbf{4}+2H]^{2+}$ cation (theoretical m/z = 1640). $^{31}P\{^1H\}$-NMR measurements of **4** in dmso-d_6 show a broad signal centered at -9.3 ppm with ^1J(Pt-P) of *ca.* 3000 Hz. The ^{195}Pt- NMR spectrum consists of two singlets (δ = -3519, -3418 ppm) corresponding to the platinum nuclei in PtS_4 and $PtCl_2S_2$ fragments, and two triplets (δ = -4403 ppm, ^1J(Pt-P)= 2997 Hz, and δ = -4420 ppm, ^1J(Pt-P)= 2970 Hz), which can be assigned to the two different platinum nuclei present as S_2PtP_2 in **4**.

The thermodynamical feasibility of the reactions given in Scheme 1 has been corroborated by means of DFT calculations performed in complexes **1**-**4**, where dppp has been modeled by two PH_3 ligands.[13] The calculated reaction energies are given in Table 1. Geometry optimization of **1**t-**4**t afford their structural data, that of **2**t being in good agreement with the X-ray determined data for **2**. As regards the HOMO orbitals of **1**t and **3**t, they essentially consist of an antibonding combination of p_π orbitals of the sulfur atoms pointing outwards the hinged $\{Pt_2S_2\}$ ring, thus accounting for the observed coordinating ability of the sulfur atoms. Interestingly, the energy level of the HOMO for **3**t (-2.46 eV) is 1.95 eV higher than for **1**t (-4.41 eV), which is in accord with the greater basicity found experimentally for the $\{Pt_2S_2\}$ core in **3** as compared to **1**.

In summary, we have provided a new insight into the chemistry of $[L_2Pt(\mu\text{-}S)_2PtL_2]$ compounds and presented a potential synthetic strategy for obtaining multimetallic aggregates containing a $\{Pt_2S_2\}_n$ core.

Table 1. B3LYP reaction energies in gas phase.

Reaction	R1	R3	R4	R5
Energy (kcal/mol)	-8.5	-41.2	-49.7	-40.4

Thanks are due to Prof. O. Rossell and I. Angurell for their assistance in the recording of the ^{195}Pt-NMR spectra. Financial support from the *Ministerio de Ciencia y Tecnología* of Spain (projects BQU2001-1976 and BQU2002-04110-CO2-02) is gratefully acknowledged. RMB is indebted to the *Universitat Autònoma de Barcelona* for a pre-doctoral scholarship.

Notes and references

† Crystal data for **2**: $C_{54}H_{52}Cl_2P_4Pt_3S_2.6CH_2Cl_2$, M = 2054.7, orthorhombic, *Pnma*, a = 19.982(3), b = 18.607(2), c = 19.372(2) Å, V = 7202.5(16) Å^3, Z = 4, T = 160 K, R = 0.091.

1 M. Lazell, P. O'Brien, D. J. Otaway, P.-H. Park, *J. Chem. Soc., Dalton Trans*., 2000, 4479; M. Lazell, P. O'Brien, *Chem. Commun.,* 1999, 2041.

2 V. W.-W. Yam, *Acc. Chem. Res.*, 2002, **35**, 555; V. W.-W.Yam, K-L. Yu, E. C-C.Cheng, P. K-Y. Yeung, K.-K. Cheung, N. Zhu, *Chem Eur. J.* 2002, **8**, 4122; M. Feliz, J. M. Garriga, R. Llusar, S. Uriel, M. G. Humprey, N.T. Lucas, M. Samoc, B. Luther-Davis, *Inorg. Chem.,* 2001, **40**, 6132.

3 C. H. Tao, K. M. C. Wong, N. Y. Zhu, V. W.-W. Yam, *New J. Chem.*, 2003, **27**, 150; C. K. Hui, B. W-K. Chu, N. Y. Zhu, V. W.-W. Yam, *Inorg. Chem.,* 2002, **41**, 6178; B. T. Sterenberg, R. Ramachandran, R. J. Puddephatt, *Journal of Cluster Science.* 2001, **12**, 49; W. Schuh, G. Wachtler, G. Laschboer, H. Kopacka, K. Wurst, P. Peringer, *Chem. Commun.,* 2000, 1181.

4 M. Hidai, S. Kuwata, Y. Mizobe, *Acc. Chem. Res.*, 2000, **33**, 46.

5 X. Xu, S.-W. A. Fong, Z. Li, Z.-H. Loh, F. Zhao, J. J. Vittal, W. Henderson, S.-B. Khoo, T. S. A. Hor, *Inorg. Chem.,* 2002, **41**, 6838; M. Capdevila, Y. Carrasco, W. Clegg, R. A. Coxall, P. González-Duarte, A. Lledós, J. A. Ramírez, *J. Chem. Soc., Dalton Trans*., 1999, 3103; S.-W. A. Fong, T. S. A. Hor, *J. Chem. Soc., Dalton Trans*. 1999, 639 and references therein; V. W.-W. Yam, P. K-Y.Yeung, K.-K. Cheung, *Angew. Chem., Int. Ed. Eng.,* 1996, **35**, 739.

6 R. Mas-Ballesté, M. Capdevila, P. A. Champkin, W. Clegg, R. A. Coxall,. A. Lledós, C. Mégret, P. González-Duarte, *Inorg. Chem.,* 2002, **41**, 3218.

7 G. Aullón, M. Capdevila, W. Clegg, P. González-Duarte, A. Lledós, R. Mas-Ballesté, *Angew. Chem., Int. Ed. Eng.,* 2002, **41**, 2776; S.-W. A. Fong, W. T. Yap, J. J. Vittal, T. S. A. Hor, W. Henderson, A. G. Oliver, C. E. F. Rickard, *J. Chem. Soc., Dalton Trans.,* 2001, 1986; S.-W. A. Fong, J. J. Vittal, W. Henderson, T. S. A. Hor, A. G. Oliver, C. E. F. Rickard, *Chem. Commun.,* 2001, 421.

8 S. Narayan, V. K. Jain, *Transition Met. Chem.*, 2000, **25**, 400.

9 C. E. Briant, T. S. A. Hor, N. D. Howells, D. M. P. Mingos, *Chem. Commun.,* 1983, 1118.

10 B. H. Aw, K. K. Looh, H. S. O. Chan, K. L. Tan, T. S. A. Hor, *J. Chem. Soc., Dalton Trans.,* 1994, 3177.

11 In order to obtain $[\{Pt_2(\mu_3\text{-}S)_2(dppp)_2\}PtCl(dmso)]Cl$, complex **2** was dissolved in the minimum amount of dmso. Addition of diethyl ether caused precipitation of a yellowish solid, which was filtered off and washed with diethyl ether. Yield: 67%. NMR in CDCl3: $^{31}P\{^1H\}$-NMR: δ_A = -7.1 ppm, ^1J(Pt-P_A)= 3022 Hz; δ_B = -7.8 ppm, ^1J(Pt-P_B)= 3051 Hz; ^{1}H-NMR δ(coordinated dmso) = 2.85 ppm; ^{13}C-NMR δ(coordinated dmso) = 44.4 ppm; ESI-MS: m/z= 1587.7.

12 R. Mas-Ballesté, G.Aullón, P. A. Champkin, W. Clegg, C. Mégret, P. González-Duarte, A. Lledós, *Chem. Eur. J.,* 2003, **9**, 5023.

13 Gas phase DFT calculations with the B3LYP functional were carried out using GAUSSIAN 98 set of programs. Effective core potentials and their related double-ζ basis set known as LANL2DZ were used for Pt, P,Cl and S atoms, supplemented with polarization functions in P, Cl and S atoms. The 6-31G basis set was used for H, C and N atoms adding polarization functions in N atom. A thermodynamic consideration for the **R2** reaction requires take account the solvent effects but, unfortunately, PCM calculation for compound **3** was unsuccessful due to the size of the system, and thus the R2 energy reaction is not given.

Unusual C-H allylic activation in the {Pt^{II}(cod)} fragment bonded to a {Pt_2S_2} core

Rubén Mas-Ballesté,[a] Paul A. Champkin,[b] William Clegg,[b] Pilar González-Duarte[*,a], Agustí Lledós,[*,a] and Gregori Ujaque[a]

[a] Departament de Química, Universitat Autònoma de Barcelona, E-08193 Bellaterra, Barcelona, Spain. Fax: (+34)935811363; Tel: (+34)935813101; E-mail: Pilar.Gonzalez.Duarte@uab.es agusti@klingon.uab.es [b] School of Natural Sciences (Chemistry), University of Newcastle, Newcastle upon Tyne NE1 7RU, UK

Abstract

Complexes [{$Pt_2(\mu_3\text{-}S)_2(dppp)_2$}Pt(cod)]$Cl_2$ (**1**) and [{$Pt_2(\mu_3\text{-}S)_2(cod)_2$}Pt(dppp)]$Cl_2$ (**3**), where dppp = 1,3-bis(diphenylphosphino)propane and cod = 1,5-cyclooctadiene, have been synthesized by reacting [$Pt_2(\mu\text{-}S)_2(dppp)_2$] and [$PtCl_2$(cod)] (1:1), and [$Pt(SH)_2$(dppp)] and [$PtCl_2$(cod)] (1:2), respectively. Complex **1** has not allowed substitution of cod by the chelating dppp ligand. Remarkably, the reaction of **1** with methoxide anion yields [{$Pt_2(\mu_3\text{-}S)_2(dppp)_2$}Pt($C_8H_{11}$)]Cl (**2**), which entails deprotonation of cod instead of the insertion of CH_3O^- into the olefinic bond. Nor has replacement of the deprotonated cod ligand in **2** by dppp been achieved. Combination of experimental data and DFT calculations in **2** are consistent with the binding of $C_8H_{11}^-$ to platinum(II) by means of one η^2-alkene and one η^1-allyl bond. The structures of **1** and **2** have been confirmed by single-crystal X-ray diffraction. Analogous to **1**, the reaction of **3** with sodium methoxide causes the subsequent deprotonation of the two cod ligands, yielding [{$Pt_2(\mu_3\text{-}S)_2$(cod)(C_8H_{11})}Pt(dppp)]Cl (**4**) and [{$Pt_2(\mu_3\text{-}S)_2(C_8H_{11})_2$}Pt(dppp)] (**5**). In contrast to **1**, replacement of cod by dppp in **3** and **4** leads to **1** and **2**, respectively. Also, the substitution of one $C_8H_{11}^-$ ligand by dppp in **5** leads to **2**. On the basis of DFT calculations, with inclusion of solvent effects, the factors governing the chemical behavior of the $\{Pt(cod)\}^{2+}$ fragment bonded to a [$Pt_2(\mu\text{-}S)_2L_4$] (L_2 = dppp, cod or $C_8H_{11}^-$) metalloligand are discussed.

Introduction

Activation of the C–H bond in olefins bound to metal centers is relevant in organometallic chemistry because of its significance in many catalytic processes.[1] Frequently, this activation is achieved by reacting the metal-olefin complex with a base. However, this reaction may not only cause deprotonation of the olefin, but, alternatively, the insertion of the base in the double bond.[2] Both reactions are depicted in Scheme 1 for a {Pt(η^2-propene)} fragment, where for the deprotonation reaction only the more usual C–H allylic activation has been taken into account. While the nucleophilic attack at olefinic bonds coordinated to palladium(II) and platinum(II) has been well studied, unlike palladium, examples of base-promoted olefin deprotonation reactions in neutral platinum-olefin complexes are very scarce.[3] In addition, the study of the reactivity of cationic platinum-olefin complexes, which show an enhanced electrophilicity at the olefinic moiety,[4,3] has often been hampered by the lability of the unsaturated ligand in these complexes.[5] With respect to the {M^{II}(cod)} fragment in palladium or platinum complexes, the reaction with a wide range of bases has led in most cases to the insertion of these species in the olefinic bonds,[5] base-promoted deprotonation being observed only if the attacking species is a tertiary amine.[7]

In the quest to explore the remarkable chemistry of the {$Pt_2(\mu\text{-}S)_2$} core, its influence on the reactivity of a {Pt^{II}(cod)} fragment attracted our interest. The striking nucleophilicity of the bridging sulfur atoms together with the flexible hinge angle between the two $Pt^{II}S_2$ planes in [L_2{$Pt(\mu\text{-}S)_2Pt$}L_2] (L = phosphine) metalloligands account for: (a) their outstanding behavior as precursors to a large family of homo- and hetero-metallic complexes;[8] (b) their spontaneous evolution in the presence of organic electrophilic agents, such as CH_2Cl_2;[9] (c) the cascade of reactions following protonation of the bridging sulfur atoms in {Pt_2S_2};[10] and (d) the first evidence of fast intramolecular S–H···S proton transfer in a transition metal complex.[11] Thus, on the basis of the high electron density on the sulfur atoms in [L_2{$Pt(\mu\text{-}S)_2Pt$}L_2] compounds, it was reasonable to expect that their coordination to a

$\{Pt^{II}(cod)\}$ fragment should have an effect on the electrophilicity of the cod ligand, and possibly modify the reactivity of the $\{Pt^{II}(cod)\}$ fragment towards attack by nucleophiles.

In this paper we report the synthesis and characterization of $[\{Pt_2(\mu_3\text{-}S)_2(dppp)_2\}Pt(cod)]Cl_2$ (**1**) and $[\{Pt_2(\mu_3\text{-}S)_2(cod)_2\}Pt(dppp)]Cl_2$ (**3**), whose cationic species contain one or two $\{Pt^{II}(cod)\}$ fragments, respectively. Both cations, in contrast with the general behavior of cationic olefin complexes of platinum, do not undergo spontaneous loss of the unsaturated ligand, and thus have allowed exploration of their reactivity towards a strong nucleophile such as $NaCH_3O$. Unlike previous reports on the attack of $NaCH_3O$ on the $\{Pt^{II}(cod)\}$ fragment,[12] the above reactions have not promoted insertion of the methoxide anion, but only deprotonation of cod, thus leading to $[\{Pt_2(\mu_3\text{-}S)_2(dppp)_2\}Pt(C_8H_{11})]Cl$ (**2**), $[\{Pt_2(\mu_3\text{-}S)_2(cod)(C_8H_{11})\}Pt(dppp)]Cl$ (**4**) and $[\{Pt_2(\mu_3\text{-}S)_2(C_8H_{11})_2\}Pt(dppp)]$ (**5**). Moreover, only C–H allylic and not vinylic activation of the cod ligand in (**1**), (**3**) and (**4**) has been observed. Interestingly, one of the two cod ligands, preferably in neutral (as in **3** and **4**) but also in anionic form (as in **5**), can be replaced by dppp in complexes **3**–**5**. This, together with the fact that this replacement does not occur in **1** and **2**, shows the non-innocent role of the $[(dppp)\{Pt(\mu\text{-}S)_2Pt\}(dppp)]$ metalloligand on the stability of the platinum-bonded olefin. Complexes **1** and **2,** as solvated chloride and perchlorate salts respectively, have been characterized by X-ray crystallography, and their structures are discussed. Theoretical calculations have been performed in order to obtain an insight into the factors contributing to the unconventional reactivity observed in this work for the $\{Pt^{II}(cod)\}$ fragment.

Results and Discussion

Experimental results

The sequence of reactions carried out in this study is shown in Scheme 2. NMR parameters and mass determinations for the complexes **1**–**5** thus obtained are given in Table 1. Details of the synthetic pathways followed are given in the Experimental Section.

Complex **1** was formed as the only product of the following reaction in benzene solution:

$$[(dppp)\{Pt(\mu\text{-}S)_2Pt\}(dppp)] + [PtCl_2(cod)] \rightarrow [\{Pt_2(\mu_3\text{-}S)_2(dppp)_2\}Pt(cod)]Cl_2\ (\mathbf{1}) \quad \mathbf{(A)}$$

Remarkably, all attempts to replace the cod ligand in **1** by dppp or chloride anions were unsuccessful. Thus, different reaction conditions, such as the solvent and temperature of the reaction as well as the molar ratio of the reagents, never led to the already known $[Pt_3(\mu_3\text{-}S)_2(dppp)_3]Cl_2$ complex.[10] These observations are consistent with previously reported results for related compounds containing the $\{Rh^I(cod)\}$ fragment bonded to a $\{Pt_2(\mu\text{-}S)_2\}$ core, $[\{Pt_2(\mu_3\text{-}S)_2(PPh_3)_4\}Rh(cod)]^+$ and $[\{Pt_2(\mu_3\text{-}S)_2(\text{-}diop)_2\}Rh(cod)]^+$).[13] However, in contrast to the striking stability towards substitution of the cod ligand in **1**, this complex reacts with $NaCH_3O$ or Na_2S under mild conditions, affording $[\{Pt_2(\mu_3\text{-}S)_2(dppp)_2\}Pt(C_8H_{11})]Cl$ (**2**). While this formula agreed well with the ESI MS and MALDI TOF parameters of **2** in solution, the coordinative behavior of the deprotonated cod ligand, $(C_8H_{11})^-$, was deduced from the DEPT-135 NMR spectrum, displaying five different CH and three different CH_2 groups. These features are consistent with $(C_8H_{11})^-$ being bound to platinum(II) by means of one η^2-alkene and one η^1-allyl bond. Full structural characterization of **2** has required a combination of crystallography together with theoretical calculations, both discussed below. On the basis of the three sets of data (NMR, X-ray and theoretical calculations) it has been deduced that the isomer labeled as *allyl A* in Figure 1 corresponds to **2** either in the solid phase or in solution.

Interestingly, the reaction leading from **1** to **2** can easily be reversed. Thus, addition of a stoichiometric amount of dilute HCl to a solution of **2** converts it to **1**. The ^{2}H-NMR spectrum of a

solution of **2** after addition of DCl instead of HCl reveals an allylic position for the added hydrogen atom, and thus confirms that the base-promoted deprotonation of cod in **1** corresponds to a C–H allylic activation. Additionally, we have observed that the behavior of the anionic deprotonated $(C_8H_{11})^-$ ligand in **2** towards replacement by dppp or chloride anions is comparable to that of neutral cod in **1**, both being substitutionally inert ligands.

Complex **3**, an analog of **1**, but with one dppp ligand replaced by cod, has been obtained in accordance with the reaction:

$$[Pt(SH)_2(dppp)] + 2[PtCl_2(cod)] \rightarrow [\{Pt_2(\mu_3\text{-}S)_2(cod)_2\}Pt(dppp)]Cl_2\ (\mathbf{3}) + 2HCl \quad \mathbf{(B)}$$

which requires the slow addition of a solution of $[Pt(SH)_2(dppp)]$ to a solution of $[PtCl_2(cod)]$, so that an excess of the latter reagent is always present in the reaction medium. Otherwise, a mixture of complexes **1** and **3** is obtained, formation of **1** probably being due to the reaction:

$$2[Pt(SH)_2(dppp)] + [PtCl_2(cod)] \rightarrow [\{Pt_2(\mu_3\text{-}S)_2(dppp)_2\}Pt(cod)]Cl_2\ (\mathbf{1}) + 2SH_2 \quad \mathbf{(C)}$$

Overall, reactions A and B lead to pure complexes **1** and **3**, respectively, under the experimental conditions here described. A mixture of both **1** and **3** has been obtained only if reactions B and C are allowed to proceed simultaneously, which requires the presence of $[Pt(SH)_2(dppp)]$ as well as a $[Pt(SH)_2(dppp)]$ / $[PtCl_2(cod)]$ ratio greater than 1/2. Notably, the reaction of $[Pt_2(\mu\text{-}Se)_2(PPh_3)_4]$ with $[PtCl_2(cod)]$, which is comparable to reaction A, affords a mixture of $[\{Pt_2(\mu_3\text{-}Se)_2(PPh_3)_4\}Pt(cod)]^{2+}$ and $[\{Pt_2(\mu_3\text{-}Se)_2(cod)_2\}Pt(PPh_3)_2]^{2+}$, closely related to **1** and **3**, respectively.[14]

The acid-base reactions involving **3** compare well with those of **1**. Thus, the addition of one equivalent of $NaCH_3O$ to a solution of **3** yields $[\{Pt_2(\mu_3\text{-}S)_2(cod)(C_8H_{11})\}Pt(dppp)]Cl$ (**4**), which, after subsequent additions of base, evolves to $[\{Pt_2(\mu_3\text{-}S)_2(C_8H_{11})_2\}Pt(dppp)]$ (**5**). Within the same context of the acid-base chemistry, the reactions from **3** to **4,** and eventually to **5,** are easily reversed by addition of the corresponding amount of dilute hydrochloric acid. With respect to the binding modes of the $(C_8H_{11})^-$ ligands in **4** and **5**, ^{13}C DEPT 135 NMR data clearly indicate that they all bind to platinum(II) by means of one η^2-alkene and one η^1-allyl bond, as already found in **2**. As theoretical calculations for the latter

complex and other model compounds show that the *allyl A* isomeric form (Figure 1) has the greatest stability (described below), the same disposition has been assumed for all $(C_8H_{11})^-$ ligands in **4** and **5**.

The replacement reaction of cod by dppp ligands in **3**, **4** and **5** shows marked differences from the results observed for the same reaction with **1** and **2**. Thus, the reaction of **3** with dppp promotes replacement of one of the two cod ligands and leads to **1**. That of **4** with dppp entails substitution of the uncharged cod ligand only and yields **2**. Reacting **5** with dppp also affords **2** as the only product, even though this reaction involves replacement of one of the two deprotonated $(C_8H_{11})^-$ ligands present in **5**. These results indicate that **1** and **2** are particularly stable complexes, not only substitutionally inert, but also the only products obtained in the reaction of **3**, **4** and **5** with dppp. Comparison of both families of complexes (**1**, **2** *vs*. **3-5**) clearly indicates that the presence of the [(dppp){Pt(μ-S)$_2$Pt}(dppp)] moiety is responsible for the outstanding stability of **1** and **2**.

NMR characterization of complexes **4** and **5** requires consideration of their corresponding isomeric forms, which are depicted in Figure 2. In addition, the NMR parameters of the related complexes **1–3** provide a reference for a comparative analysis. All NMR data are given in Table 1. Thus, the $^{13}C\{^1H\}$ and ^1H NMR spectra provide evidence that the carbon and hydrogen atoms of cod in **3**, in contrast to **1**, are not symmetrically equivalent, as shown by the two groups of signals assigned to the CH groups. Consequently, deprotonation of cod in **3** to afford **4** gives rise to two isomers as long as the character of $(C_8H_{11})^-$ corresponds to the *allyl A* form exclusively. This assumption is fully validated by the ^{13}C DEPT 135 NMR spectrum of **4**, which displays two sets of signals, each set including five CH and three CH_2 groups. These data not only denote two different dispositions of the $(C_8H_{11})^-$ ligand in **4**, but also show that their binding to platinum occurs by means of η^2-alkene and η^1-allyl coordination modes. The choice of the *allyl A* with respect to the *allyl B* form is discussed below. The coexistence of isomers **4.1** and **4.2** (Figure 2) in solution is corroborated by the $^{31}P\{^1H\}$ NMR of **4** showing two superimposed double doublets.

Following the same lines of reasoning as above, deprotonation of the two cod ligands in **3** should give rise to **5** in six isomeric forms, as shown in Figure 2. The coexistence in solution of all or several of these isomers accounts for the multiplet signal displayed for each carbon nucleus of $(C_8H_{11})^-$ in the $^{13}C\{^1H\}$ NMR spectra. In parallel, the $^{31}P\{^1H\}$ NMR spectrum of **5** consists of a broad signal.

Theoretical Study

Binding Mode of the $(C_8H_{11})^-$ Ligand. Deprotonation of the cod ligand can occur *via* a vinylic or an allylic proton, thus giving rise to different coordination modes of the $(C_8H_{11})^-$ ligand. Whereas in the former case only one isomer can be obtained (*vinyl* in Figure 1), the abstraction of an allylic proton can generate two isomers, depending on which of the two terminal allyl carbon atoms is bonded to the metal (*allyl A and ally B* in Figure 1). Thus, three different isomers must be considered. The relative stabilities of these isomers in the gas phase and in methanol solution were evaluated for a series of $[L_2Pt(COD)]^z$ ($z = 0$, $L_2 = 2SH^-$, $2Cl^-$; $z = +2$, $L_2 = [Pt_2(\mu\text{-}S)_2(PH_3)_2]$, $2PH_3$, and $2SH_2$) complexes (Table 2). The relative stabilities of the three isomers are practically the same for all the complexes studied, both in the gas phase and in solution. The total charge of the complex does not affect the relative stabilities: very similar relative energies among the isomers are obtained for the neutral and dicationic species. The vinyl isomer is highly unstable compared to both allylic isomers. Regarding the two allylic isomers, for all the complexes studied allyl A is more stable than allyl B by a range of 4.5–8 kcal/mol in the gas phase and 3–7 kcal/mol in solution. The coordination geometry of the platinum center in isomer B shows a high distortion from planarity. In contrast, isomer A presents a less strained structure. These structural features could explain the higher stability of isomer A.

The relative energies calculated for a model of complex **2** ($L_2 = [Pt_2(\mu\text{-}S)_2(PH_3)_2]$) fully agree with the complete series of the studied complexes. From these theoretical values, the vinyl isomer can be discarded, in agreement with the spectroscopic data indicating that the product of the deprotonation reaction contains a Pt-allyl group. Moroever, the allyl A isomer can be proposed as the observed isomer

for complex **2**, and the preference for this binding mode of the $(C_8H_{11})^-$ ligand can be extended to complexes **4** and **5**.

Stability of $[L_2Pt(cod)]^z$ (z = 0, +2) Complexes Towards cod Displacement. The cod ligand is usually a somewhat labile ligand, which can be displaced easily by ligands with higher coordinating ability such as bidentate phosphines. However, this is not the case in compound **1**. In order to elucidate the reasons for the surprising stability of the cod ligand in **1** towards substitution by dppp, the reaction energy (ΔE_{LE}) for the ligand exchange reaction **(D)** has been calculated for a series of eight related $[L_2Pt(cod)]^z$ complexes, taking $H_2P\text{-}(CH_2)_3\text{-}PH_2$ (dhpp) as a model of the dppp ligand.

$$[L_2Pt(cod)]^z + dppp \rightarrow [L_2Pt(dppp)]^z + cod \quad \textbf{(D)}$$

The complexes of the series are neutral (z = 0) when L ligands are SH^-, I^-, Br^- or Cl^-, and cationic (z = +2) when L ligands are PH_3, SH_2, $[Pt_2(\mu\text{-}S)_2(dhpp)_2]$ (complex **1**) or $[Pt_2(\mu\text{-}S)_2(dhpp)(cod)]$ (complex **3**). Consideration of a series of $[L_2Pt(cod)]$ complexes with ligands L of different natures should enable us to put the energetic values for the ligand exchange obtained for complexes **1** and **3** into a general context. The computed ΔE_{LE} values are shown in Table 3.

The results indicate that substitution of cod by dppp is, in all studied cases, highly favored on thermodynamic grounds. The process is highly exothermic, with ΔE_{LE} ranging from –18.7 to –37.5 kcal/mol. The substitution of a cod ligand by dppp is more exothermic for cationic complexes than for neutral ones; this statement agrees well with the higher lability of olefinic ligands generally observed for cationic Pt-alkene complexes.[5] Our results justify the replacement of cod by dppp ligands observed in **3** and **4**, but they can not explain the stability towards cod displacement exhibited by complex **1**. Indeed they suggest that the factors hampering the exchange of the cod ligand by dppp in **1** should be of a kinetic nature.

The bond dissociation energies (BDE) for cod and dppp ligands in this series of complexes were also evaluated (see Table 3). Determination of these thermodynamic parameters can provide a mechanistic insight, because BDE give an approximate estimation of the energy barrier for a

dissociative ligand-exchange process. The results presented here show that the Pt-cod bond energies are higher for cationic $[L_2Pt(cod)]$ complexes than for neutral ones. High and similar values of $BDE_{Pt\text{-}cod}$ have been calculated for cationic complexes with $L_2 = [Pt_2(\mu\text{-}S)_2(dhpp)_2]$ and $[Pt_2(\mu\text{-}S)_2(dhpp)(cod)]$, despite the very different behavior towards the cod/dppp exchange observed in **1** and **3**. The high $BDE_{Pt\text{-}cod}$ obtained indicates that the dissociative mechanism is highly unfavorable in **1** and **3**, and suggests an associative mechanism for the replacement of cod by dppp. This mechanistic proposal agrees with others found in the literature; for instance, the ligand-exchange of olefins in d^8 square-planar complexes is supposed to go through an associative mechanism.[15] Nevertheless, associative mechanisms are subject to the achievability of a transition state with five ligands coexisting in the coordination sphere of the metal center. In the $[L_2Pt(cod)]^z$ complexes under study, when L is bulky, as for the $[Pt_2(\mu\text{-}S)_2(dppp)_2]$ metalloligand, the transition state for the associative mechanism would be highly unstable or may not even exist. Thus, the high steric hindrance due to $[Pt_2(\mu\text{-}S)_2(dppp)_2]$ in **1** hampers the associative mechanism for the replacement of cod ligand by dppp to yield $[Pt_3(\mu_3\text{-}S)_2(dppp)_3]$ and confers a remarkable kinetic stability towards cod dissociation on **1**. Molecular models of the reactant ($[\{Pt_2(\mu_3\text{-}S)_2(dppp)_2\}Pt(cod)]^{+2}$) and product ($[Pt_3(\mu_3\text{-}S)_2(dppp)_3]^{+2}$) for the cod/dppp exchange reaction illustrate the difficulties encountered by dppp when approaching the platinum atom bound to cod and $[Pt_2(\mu\text{-}S)_2(dppp)_2]$ metalloligand simultaneously (Figure 3).

The cod/dppp ligand-exchange is experimentally observed in **3**, bearing the metalloligand $[Pt_2(\mu\text{-}S)_2(dppp)(cod)]$. It is likely that, when cod has substituted one dppp ligand, the lower bulkiness of the metalloligand allows the associative mechanism to take place. The different hindrance imposed by the presence of cod or dppp in the $[Pt_2(\mu\text{-}S)_2(dppp)(L)]$ fragment can be inferred from Figure 3. In conclusion, the theoretical study indicates that, despite the replacement of cod by dppp in **1** to yield $[\{Pt_2(\mu_3\text{-}S)_2(dppp)_2\}Pt(dppp)]^{2+}$ being an exothermic process, the reaction is kinetically unfavorable because neither associative nor dissociative mechanisms are possible with a reasonable energetic barrier. This insight could be extended to the behavior of the reported complexes containing the

$\{Pt_2(\mu_3\text{-}S)_2Rh(cod)\}^{2+}$ core, where cod has shown an enhanced stability towards ligand exchange reactions.[13]

Deprotonation vs. Nucleophilic Attack on the cod Ligand. As far as the reactivity of complexes **1** and **3** towards MeO^- is concerned, the reaction proceeds with the abstraction of an allylic proton instead of the common insertion of the methoxide anion in the double bond. DFT calculations using a continuum solvation model were carried out to try to understand this unexpected reactivity. The inclusion of solvent effects is mandatory to obtain a reliable estimation of reaction energies, given the changes in the charges experienced by the species throughout the reaction. The reaction energy for both processes, deprotonation (reaction **E)** and nucleophilic attack (reaction **F**) in methanol ($\varepsilon = 32.63$), for a set of complexes of formula $[L_2Pt(cod)]^z$ ($z = 0$, $L_2 = 2SH^-$, $2Cl^-$; $z = +2$, $L_2 = [Pt_2(\mu\text{-}S)_2(PH_3)_2]$, $2PH_3$, and $2SH_2$) were evaluated (Table 4).

$$[L_2Pt(cod)]^z + CH_3O^- \rightarrow [L_2Pt(C_8H_{11})]^{z-1} + CH_3OH \quad \textbf{(E)}$$

$$[L_2Pt(cod)]^z + CH_3O^- \rightarrow [L_2Pt(C_8H_{12}OCH_3)]^{z-1} \quad \textbf{(F)}$$

These results show that, for all the different complexes studied, both reactions are highly exothermic, the cationic presenting a higher exothermicity than the neutral species. Comparing the reaction energies for both processes, the insertion of methoxide anion in a cod double bond is thermodynamically more favorable than deprotonation for all the studied species. Nevertheless, these differences in the reaction energy are lower for cationic species than for neutral ones. Given these tendencies, although the nucleophilic attack is always thermodynamically favored, the deprotonation of the cod ligand becomes more feasible for cationic complexes. These features suggest that the experimentally observed reactivity for **1** and **3** towards MeO^-, giving rise to deprotonation, is a kinetically controlled process.

To evaluate the aforementioned hypothesis, the reaction profiles for the insertion of methoxide and the deprotonation of the cod ligand were calculated for two different $[L_2Pt(cod)]$ complexes, one neutral ($L_2 = 2Cl^-$) and one of a cationic nature ($L_2 = [Pt_2(\mu\text{-}S)_2(PH_3)_4]$). To study methoxide insertion the

C_{sp2}-$O_{methoxide}$ distance was selected as the reaction coordinate. The reaction profiles for the nucleophilic attack found for both complexes in the gas phase and in methanol do not present any barrier. This is not a surprising result, which had already been found by Norrby *et al*. in a thorough theoretical study of nucleophilic attack on cationic (η^3-allyl)palladium complexes.[16] In this study, no transition state could be located for the reaction between an anionic nucleophile and a cationic (allyl)palladium complex. The authors concluded that this reaction does not have an energy barrier in the gas phase, and that the barrier observed in real reactions can largely be attributed to the desolvation energy of the reacting ions. For the addition of anionic nucleophiles to cationic Pd-allyl complexes a transition state was found in solution only when constructing a two-dimensional potential energy surface.[16] The exploration of the bidimensional potential surface for the reactions under study greatly increases the computational requirements, and it is beyond the scope of this work.

The deprotonation reaction profiles in the gas phase and in solution for both complexes are shown in Figure 4. The selected reaction coordinate for this process is the H_{allyl}-$O_{methoxide}$ distance, which varies from 1.6 Å to 1.0 Å . In the case of the neutral $[Cl_2Pt(cod)]$ complex, the reaction has no barrier in the gas phase, whereas it shows an energy barrier of ca. 6 kcal/mol in solution. For the cationic $[Pt_2(\mu_3\text{-}S)_2(PH_3)_4\}Pt(cod)]^{2+}$ complex, the reaction does not present any barrier, either in the gas phase or in solution. To obtain more accurate reaction profiles it would also be necessary to construct a two-dimensional potential energy surface in solution. Nevertheless, the exploration of these potential surfaces also demands too much computer time, and was not performed.

Although the obtained results are not definitely conclusive, they can provide qualitative ideas about the unexpected reactivity exhibited by the cod ligand in **1**. The fact that in solution the cationic species do not present a barrier for proton abstraction, but neutral species do, suggests that deprotonation of **1** may be easier than that of $[Cl_2Pt(cod)]$. Moreover, although the insertion process is always thermodynamically more favorable than deprotonation, the energy differences between the two processes are reduced for cationic species, also suggesting that the deprotonation reaction is more

feasible for cationic compounds. These results are consistent with the hypothesis that the observed reactivity of complex **1** with methoxide anion is a consequence of kinetic factors. It is likely that the bulkiness of the $[Pt_2(\mu\text{-}S)_2(dppp)_2]$ metalloligand causes steric interactions with the incoming nucleophile and also plays a role in favoring deprotonation.

Molecular Structures

*X-ray Crystal Structure of $[\{Pt_2(\mu_3\text{-}S)_2(dppp)_2\}Pt(cod)]Cl_2$ (**1**)*

The crystal structure of this complex consists of $[\{Pt_2(\mu_3\text{-}S)_2(dppp)_2\}Pt(cod)]^{2+}$ cations (Figure 5, Table 5) and Cl^- counterions held together by electrostatic interactions, and chloroform solvent molecules. The cation has no crystallographic symmetry, but has an approximately D_{3h} Pt_3S_2 core. The molecular structure of the trinuclear cation can be considered as formed by one [(dppp){Pt(μ-S)$_2$Pt}(dppp)] metalloligand linked to a {Pt(cod)} moiety through two sulfur atoms. The central Pt_3S_2 unit consists of a triangle of platinum atoms capped above and below by two sulfur atoms, thus describing a distorted trigonal bipyramid. These two triply bridging sulfido ligands lie essentially equidistant, 1.524 Å above and 1.516 Å below, the Pt_3 plane. However, deviation from the ideal geometry is evidenced by the dihedral angles between pairs of the three PtS_2 planes, which range from 114.4º to 124.8º. The geometric features of the Pt_3S_2 unit compare well with those observed in the $[\{Pt_2(\mu_3\text{-}S)_2(dppp)_2\}Pt(C_8H_{11})]^+$ derivative, described below, and with related complexes containing the $P_6Pt_3S_2$ core with monodentate and chelating phosphine ligands.[8b,10,17] Moreover, the overall structure of $[\{Pt_2(\mu_3\text{-}S)_2(dppp)_2\}Pt(cod)]^{2+}$ bears a close resemblance to that of its selenium analog containing a Pt_3Se_2 core.[14]

Each platinum atom in $[\{Pt_2(\mu_3\text{-}S)_2(dppp)_2\}Pt(cod)]^{2+}$ has square-planar coordination, distortion from the ideal geometry being mainly due to the reduction of the S–Pt–S angles from 90º. The two {PtS_2(dppp)} subunits show an antisymmetric arrangement of the PtP_2C_3 rings, both in a chair conformation, which become symmetry-equivalent in solution according to NMR data.

*X-ray Crystal Structure of [{$Pt_2(\mu_3\text{-}S)_2(dppp)_2$}$Pt(C_8H_{11})$]($ClO_4$) (**2**)*

The crystal structure of this complex consists of $[\{Pt_2(\mu_3\text{-}S)_2(dppp)_2\}Pt(C_8H_{11})]^+$ cations (Figure 6, Table 6) and ClO_4^- counterions held together by electrostatic interactions, and solvent molecules. Main structural features of the trinuclear cation can be described analogously to the parent $[\{Pt_2(\mu_3\text{-}S)_2(dppp)_2\}Pt(cod)]^{2+}$ complex, both consisting of a central Pt_3S_2 unit with a trigonal bipyramidal geometry. Distortion from the ideal geometry is slightly greater for $[\{Pt_2(\mu_3\text{-}S)_2(dppp)_2\}Pt(C_8H_{11})]^+$, where the dihedral angles between PtS_2 planes range from 112.7º to 125.7º. However, the binding of the deprotonated cod ligand to platinum deserves special consideration, as disorder of this ligand and the solvent molecules across a mirror plane (which contains all three Pt atoms, bisects each diphosphine ligand, and relates the two bridging sulfide ligands to each other) resulted in serious overlap of the atomic arrangements (Figure 7) and hampered reliable determination of the C–C distances and positions of H atoms (see the Experimental section for details of the disorder treatment). As shown in Figure 8, the C(29)–C(30) distance of 1.38 Å in the deprotonated cod ligand is consistent with a double bond and thus with one η^2-alkene binding mode of $(C_8H_{11})^-$ to platinum. Moreover, the Pt(3)–C(34) distance of 2.23 Å is compatible with a second coordination mode of either allylic (*allyl A* type) or vinylic nature. Concomitantly, the position of C(33), and thus the C(32)–C(33) and C(33)–C(34) distances, could be interpreted as indicative of an η^1-vinyl binding mode for the cod ligand, though the difference in these bond lengths is small (and insignificant statistically, in view of the relatively large standard uncertainties for these disordered atoms). In contrast, NMR data for $[\{Pt_2(\mu_3\text{-}S)_2(dppp)_2\}Pt(C_8H_{11})]^+$ are consistent with η^1-allyl rather than η^1-vinyl bonding, and DFT calculations show not only that the Pt(η^1-vinyl) coordination is strongly disfavored with respect to η^1-allyl, but also that the allyl A isomer (Figure 1) is the energetically preferred form. Comparison of the structural data obtained by crystallography and DFT (Figure 8) shows that this apparent inconsistency is mainly due to the observed position of C(33), which is particularly affected by overlap with a solvent molecule in the disorder model and hence is especially

unreliable. We thus deduce that the binding of $(C_8H_{11})^-$ to platinum probably occurs by means of η^2-alkene and η^1-allyl coordination modes in the solid state and in solution.

Concluding Remarks

The chemistry of $[\{Pt_2(\mu_3\text{-}S)_2(dppp)_2\}Pt(cod)]^{2+}$ has shown to be remarkable on the basis of (a) the high stability of the cod ligand towards substitutiton by dppp, and (b) the ease of proton abstraction from the cod ligand as a result of the nucleophilic attack by the methoxide anion. The preference of cod for deprotonation rather than the usual insertion of the nucleophile into the olefinic bond is also shown in the reaction of $[\{Pt_2(\mu_3\text{-}S)_2(cod)_2\}Pt(dppp)]^{2+}$ and $[\{Pt_2(\mu_3\text{-}S)_2(cod)(C_8H_{11})\}Pt(dppp)]^{+}$ with sodium methoxide. Overall, the unprecedented behavior of cod in three cationic complexes containing a $[\{Pt_2(\mu_3\text{-}S)_2\}Pt(cod)]^{2+}$ moiety (as **1**, **3** and **4**) reveals the strong influence of the $\{Pt_2(\mu\text{-}S)_2\}$ core on the reactivity of the $\{Pt(cod)\}^{2+}$ fragment. According to DFT calculations on a series of $[L_2Pt(cod)]^z$ species, the competition between proton abstraction and base insertion is highly dependent on the charge of the complex, the former reaction appearing as more feasible in cationic (as **1** and **3**) than in neutral platinum complexes.

Concerning the substitution of cod (in neutral or anionic form) by dppp, the five complexes obtained behave differently. Those containing the $\{Pt_2(\mu_2\text{-}S)_2(dppp)_2\}$ moiety (as **1** and **2**) are substitutionally inert. By contrast, those based on the $\{Pt_2(\mu_2\text{-}S)_2(dppp)L\}$ moiety with L = cod or $C_8H_{11}^-$ (as **3**, **4** and **5**) undergo the substitution reaction readily. However, DFT calculations show that replacement of cod by dppp in **1** or **3** is an exothermic process. Consequently, kinetic effects should account for the reluctance of cod to be replaced by dppp in **1** and **2**. These effects can be attributed to the steric hindrance imposed by the $\{Pt_2(\mu_2\text{-}S)_2(dppp)_2\}$ unit, which disfavors an associative pathway for the ligand exchange in **1**. This factor, combined with the high binding energy we have found for the cod ligand in a series of cationic platinum complexes, precludes the substitution of cod by dppp in **1**.

Finally, the unusual reactivity exhibited by the cod ligand in complexes containing the [{Pt(μ_3-S)$_2$Pt}Pt(cod)]$^{2+}$ moiety, and the dependence of such reactivity on electronic and steric factors involving the {Pt_2S_2} core, allow envisaging new perspectives. On the basis of the results here reported it can be proposed that the coordination of [$Pt_2(\mu$-S)$_2L_4$] metalloligands to a transition metal ML'_n fragment can be an effective tool for modifying its chemical properties. In addition, these modifications could be modulated by a fine tuning of the nature of the terminal ligands bound to the central {Pt_2S_2} core.

Experimental Section

Materials and Methods. All reactions were carried out under an atmosphere of pure dinitrogen, and conventionally dried and degassed solvents were used throughout. These were Purex Analytical Grade from SDS. Solutions of NaOMe in MeOH (4.74 M) and DCl in D_2O (35% wt, 99.9% D) were purchased from Aldrich. Metal complexes of formula [$PtCl_2$(dppp)] and [$PtCl_2$(cod)] were prepared according to published methods.[18] The synthesis of [Pt(SH)$_2$(dppp)][10] and [(dppp)Pt(μ-S)$_2$Pt(dppp)][8b,9] has already been reported.

Complexes **1–5** have been characterized by NMR and mass spectroscopy. ^{1}H, ^{13}C{^{1}H} and ^{31}P{^{1}H} NMR spectra were recorded from samples in $(CD_3)_2SO$ solution at room temperature, using a Bruker AC250 spectrometer. ^{13}C and ^{1}H chemical shifts are relative to $SiMe_4$, and ^{31}P chemical shifts to external 85% H_3PO_4. The ^{2}H NMR spectra of the product reaction of **2** with DCl was recorded from $(CH_3)_2SO$ solution using a Bruker Avance500 spectrometer. The ESI MS measurements were performed on a VG Quattro Micromass Instrument. Experimental conditions are given elsewhere.[9] MALDI mass spectra were obtained on a Voyager DE-RP (PerSeptive Biosystems, Framighan) time-of-flight (TOF) mass spectrometer equipped with a nitrogen laser (337 nm 3ns pulse). The accelerating voltage in the ion source was 20 kV. Data were acquired in the reflector mode operation with a delay time value of 60 ns. Experiments were performed using the matrix 2,5-dihydroxy-benzoic acid [DHB, Aldrich]. Matrix solutions were prepared by dissolving 10 mg of DHB in 10 mL of CH_3CN/H_2O 50%

(v/v). Equal volumes (1μL + 1μL) of matrix solution and diluted samples (10^{-2} M in CH_3CN) were mixed and spotted onto the stainless steel sample plate. The mixture dried in air before being introduced into the mass spectrometer. Microanalytical data have been omitted because those referring to the carbon content were unsatisfactory, as already reported in some related phosphine platinum complexes.[9,10,11,19]

Synthesis of [{Pt$_2$(μ_3-S)$_2$(dppp)$_2$}Pt(cod)]Cl$_2$ (1). To a stirring solution of [Pt$_2$(μ_3-S)$_2$(dppp)$_2$] (0.5 g, 0.39 mmol) in benzene (100 mL) was added solid [PtCl$_2$(cod)] (0.15 g, 0.39 mmol). The resulting clear solution was stirred for 5 h at room temperature, during which time complex **1** formed as a white solid. It was then filtered off and washed with diethyl ether. Yield 78%. X-ray quality crystals were grown by slow evaporation of a solution of **1** in $CHCl_3$. $^{31}P\{^1H\}$-NMR (162.1 MHz, d_6-dmso): δ_P = –4.1 ppm, $^1J_{Pt-P}$ = 3069 Hz. ^{1}H-NMR (250 MHz, d_6-dmso): δ_{CH} = 4.54; δ_{CH2} = 2.53. $^{13}C\{^1H\}$-NMR (101.26 MHz, d_6-dmso): δ_{CH} = 96.91; δ_{CH2} = 28.93. ^{1}H- and $^{13}C\{^1H\}$-NMR data refer to cod ligand exclusively. ESI-MS: m/z: 790.9 (M^{2+}/2).

Synthesis of [{Pt$_2$(μ_3-S)$_2$(dppp)$_2$}Pt(C$_8$H$_{11}$)]Cl (2). To a suspension of **1** (0.5 g, 0.30 mmol) in benzene (75 mL) was added an equimolar amount of NaMeO in methanol (63 μL of a 4.74 M solution). After 8 hours of stirring at room temperature the suspension was concentrated to ca. 20 mL under reduced pressure. Addition of diethyl ether to the filtrated solution yielded a pale yellow solid. Yield 62%. $^{31}P\{^1H\}$-NMR (162.1 MHz, d_6-dmso): δ_P = –6.26 ppm, $^1J_{Pt-P}$ = 3006 Hz. ^{1}H-NMR (250 MHz, d_6-dmso): δ_{CH} = 4.27,4.04, 3.09, 2.81, 2.27; δ_{CH2} = 2.82, 2.01 (m). $^{13}C\{^1H\}$-NMR (101.26 MHz, d_6-dmso): δ_{CH} = 83.29, 81.35, 75.18, 54.25, 26.29; δ_{CH2} = 33.94, 29.02, 28.26. ^{1}H- and $^{13}C\{^1H\}$-NMR data refer to $(C_8H_{11})^-$ ligand exclusively. ESI-MS: m/z: 790.5 [(M^++H^+)/2]; MALDI-TOF-MS: m/z: 1581.1 (M^+).

Synthesis of [{Pt$_2$(μ_3-S)$_2$(cod)$_2$}Pt(dppp)]Cl$_2$ (3). A solution of [Pt(SH)$_2$(dppp)] (0.22 g, 0.33 mmol) in benzene (50 mL) was added dropwise to a stirred solution of [PtCl$_2$(cod)] (0.25 g, 0.67 mmol) in the same solvent (50 mL) and the reaction mixture left to stir for 6 h at room temperature. After this

time the solution was concentrated to ca. 25 mL and the yellow solid thus formed was filtered off and dried. Yield 45%. $^{31}P\{^{1}H\}$-NMR (162.1 MHz, d_6-dmso): δ_P = –2.61 ppm; $^{1}J_{Pt-P}$ = 3193 Hz. ^{1}H-NMR (250 MHz, d_6-dmso): δ_{CH} = 5.49, 4.99; δ_{CH2} = 2.5 (m). $^{13}C\{^{1}H\}$-NMR (101.26 MHz, d_6-dmso): δ_{CH} = 100.96, 98.84; δ_{CH2} = 30.15. ^{1}H- and $^{13}C\{^{1}H\}$-NMR data refer to cod ligand exclusively. ESI-MS: m/z: 638.9 [$(M^{2+})/2$].

Synthesis of [{$Pt_2(\mu_3\text{-}S)_2(cod)(C_8H_{11})$}Pt(dppp)]Cl (4). To a solution of **3** (0.10 g, 0.07 mmol) in benzene (25 mL) was added a methanol solution of NaMeO (17 μL of a 4.74 M solution). The resulting solution was left to stir for 4 h after which time it was concentrated to ca. 5 mL and filtered. Addition of diethyl ether to the filtrate caused precipitation of complex **4** as a pale yellow solid. Yield 28%. $^{31}P\{^{1}H\}$-NMR (162.1 MHz, d_6-dmso): δ_P = –3.75 ppm. ^{1}H-NMR (250 MHz, d_6-dmso): δ_{CH} = 5.3–5.1, 4.8–4.6. $^{13}C\{^{1}H\}$-NMR (101.26 MHz, d_6-dmso): δ_{CH} = 96.42–95.04 (m), 85.16, 84.47, 83.42, 83.19, 79.05, 78.31, 54.60, 54.50, 28.01, 27.27; δ_{CH2} = 34.55, 34.25, 30.47–29.70 (m), 28.95, 28.80, 28.55, 28.14. ^{1}H- and $^{13}C\{^{1}H\}$-NMR data refer to olefinic ligands exclusively. ESI-MS: m/z: 638.7 [$(M^{+}+H^{+})/2$]; MALDI-TOF-MS: m/z: 1277.1 (M^{+}).

Synthesis of [{$Pt_2(\mu_3\text{-}S)_2(C_8H_{11})_2$}Pt(dppp)] (5) The same procedure as that followed for complex **4** yielded complex **5** from **3** (0.10 g, 0.074 mmol) and a methanol solution of NaMeO (43 μL of a 4.74 M solution). Yield 31%. $^{31}P\{^{1}H\}$-NMR (162.1 MHz, d_6-dmso): δ_P = –6.09 ppm. ^{1}H-NMR (250 MHz, d_6-dmso): δ_{CH} = 5.2–3.8. $^{13}C\{^{1}H\}$-NMR (101.26 MHz, d_6-dmso): δ_{CH} = 85.06–83.22 (m), 79.20–78.02 (m), 73.10–72.34 (m), 54.43–54.08 (m), 26.80–25.30 (m); δ_{CH2} = 35.63–34.28 (m), 29.40–27.80 (m). ^{1}H- and $^{13}C\{^{1}H\}$-NMR data refer to $(C_8H_{11})^{-}$ ligand exclusively.; ESI-MS: m/z: 638.9 [$(M+2H^{+})/2$]; MALDI-TOF-MS: m/z: 1276.9 ($M+H^{+}$).

Evolution with time of a solution of [{$Pt_2(\mu_3\text{-}S)_2(dppp)_2$}Pt(cod)]$Cl_2$ (1) or [{$Pt_2(\mu_3\text{-}S)_2(dppp)_2$}Pt($C_8H_{11}$)]Cl (2) in the presence of dppp. To a solution of complex **1** or **2** in

either CH_2Cl_2, CH_3CN or MeOH was added a 5:1 molar excess of dppp at room temperature. This solution was monitored for 48 h by taking one aliquot every 12 h, evaporating it to dryness and recording the $^{31}P\{^1H\}$-NMR spectrum in d_6-dmso. The above experiments were also performed in the same solvents but under reflux conditions. NMR data revealed that the possible ligand exchange reactions never occurred.

Reaction between [{Pt$_2$(μ_3-S)$_2$(cod)$_2$}Pt(dppp)]Cl$_2$ (3) and dppp. To a solution of **3** (25 mg, 0.02 mmol) in CH_2Cl_2 (15 mL) was added dppp (8 mg, 0.02 mmol). After 2 hours of stirring at room temperature the solvent was removed *in vacuo*, leaving the product as a white solid. The $^{31}P\{^1H\}$-NMR spectrum of this solid in d_6-dmso solvent showed that complex **1** was the only compound present in solution.

Reaction between [{Pt$_2$(μ_3-S)$_2$(cod)(C$_8$H$_{11}$)}Pt(dppp)]Cl (4) or [{Pt$_2$(μ_3-S)$_2$(C$_8$H$_{11}$)$_2$}Pt(dppp)] (5) with dppp. To a solution of 0.02 g of **4** (0.015 mmol) or **5** (0.016 mmol) in CH_2Cl_2 (15 mL) was added 8 mg (0.02 mmol) of dppp . After 2 hours of stirring at room temperature the resulting solution was analyzed by $^{31}P\{^1H\}$-NMR as indicated above. The NMR data showed that in both reactions complex **2** was the only compound present in solution.

Reaction between [{Pt$_2$(μ_3-S)$_2$(dppp)$_2$}Pt(C$_8$H$_{11}$)]Cl (2) and HCl or DCl. To a solution of **2** (0.20 g, 0.12 mmol) in benzene (25 mL) was added an equimolar amount of HCl in water (30 μL of a 4 M HCl solution). After 15 minutes of stirring at room temperature the solid formed was filtered off and analyzed by $^{31}P\{^1H\}$-NMR. These data confirmed that the only product obtained was complex **1**. The same experiment was carried out but with addition of an equimolar amount of DCl in D_2O (13 μL of a 9.3 M DCl solution) instead of HCl. The solid thus obtained was analyzed by $^{31}P\{^1H\}$-NMR, confirming complex **1** as the only product in both cases. In addition, the ^2H-NMR spectrum of the compound obtained after addition of DCl shows a resonance at 2.47 ppm.

Reaction of [{$Pt_2(\mu_3\text{-}S)_2(cod)(C_8H_{11})$}Pt(dppp)]Cl (4) or [{$Pt_2(\mu_3\text{-}S)_2(C_8H_{11})_2$}Pt(dppp)] (5) with HCl. A solution containing 20 mg of **4** (0.015 mmol) or **5** (0.016 mmol) in CH_3CN (15 mL) was acidified by addition of 20 μL or 40 μL, respectively, of 1.0 M HCl in water. After 15 min of stirring at room temperature the solvent was evaporated to dryness. Characterization of the solid residue by $^{31}P\{^1H\}$-NMR indicated that complex **3** was the only end-product in both acid-base reactions.

X-ray crystallography. Data for complexes **1** and **2** were measured on Bruker SMART 1K CCD diffractometers.[20] For **1**, Mo Kα radiation (λ = 0.71073 Å) was used, while the small size and poorly diffracting nature of the crystals of **2** necessitated the use of synchrotron radiation (λ = 0.6900 Å) at CCLRC Daresbury Laboratory SRS station 9.8.[21] Crystallographic data are given in Table 7. Both structures were found to contain solvent, some of which could be modeled with ordered atomic sites and some of which is disordered; for **1**, three ordered chloroform molecules were located, and other highly disordered solvent was handled by the SQUEEZE procedure in the program PLATON,[22] while for **2**, one ordered dichloromethane molecule was located (on a mirror plane), and other disordered solvent was fitted with a number of partially occupied atom sites giving no recognizable molecular geometry. For each structure, only the ordered solvent is included in the formulae given in Table 7. The cation of **2** lies on a crystallographic mirror plane, across which the deprotonated COD ligand lies. The atoms of the two disorder components and those of some of the disordered solvents overlap each other, rendering the geometry of these moieties unreliable. Restraints were applied to the anisotropic displacement parameters of the ligand, but no geometrical constraints or restraints were used for these atoms. The perchlorate anion is also disordered across a mirror plane. H atoms were included in ideal positions for ordered parts of both structures. Refinement was on all unique F^2 values in each case.[23] The largest features in final difference syntheses lie close to heavy atoms and disordered parts of the structures.

Computational Details. Calculations were performed using the GAUSSIAN98 series of programs.[24] Geometry optimizations were done using the density functional theory (DFT) with the hybrid B3LYP functional.[25] Effective core potentials (ECP) and their associated double-ζ LANL2DZ

basis set were used for platinum, phosphorus, sulfur, iodine, bromine and chlorine atoms,[26] adding an extra series of *d*-polarization functions in the case of P, S, I, Br and Cl.[27] The 6-31G basis set was used for the C and H atoms.[28] Solvent effects were taken into account by means of the COSMO solvation model.[29] Energies were calculated with methanol (ε = 32.63) as solvent, keeping the optimized geometry for the isolated species (single-point calculations).

Supporting information available: For **1** and **2**, details of crystal structure determination, atomic coordinates, bond lengths and angles, and displacement parameters. This material is available free of charge via the Internet at http://pubs.acs.org. Observed and calculated structure factor lists are available from the authors upon request.

Acknowledgment. Financial support from the *Ministerio de Ciencia y Tecnología* of Spain (projects BQU2001-1976 and BQU2002-04110-CO2-02), the EPSRC (UK) and Ineos Acrylics is gratefully acknowledged. RMB is indebted to the *Universitat Autònoma de Barcelona* for a pre-doctoral scholarship.

References

(1) (a) R. H. Crabtree, *The Organometallic Chemistry of the Transition Metals,* John Wiley and Sons: New York, 2001.

(2) (a) Hahn, C.; Morvillo, P.; Herdtweck, E., Vitagliano, A. *Organometallics* **2002**, *21*, 1807. (b) Vicente, J.; Chicote, M-T.; MacBeath, C.; Fernández-Baeza, J.; Bautista, D. *Organometallics* **1999**, *18*, 2677. (c) Hamed, O.; Henry, P. M. *Organometallics* **1997**, *16*, 4903.

(3) Bandoli, G.; Dolmella, A.; Fanizzi, F. P.; Di Masi, N. G.; Maresca, L.; Natile, G. *Organometallics* **2002**, *21*, 4595.

(4) Bandoli, G.; Dolmella, A.; Di Masi, N. G.; Fanizzi, F. P.; Maresca, L.; Natile, G. *Organometallics* **2001**, *20*, 805.

(5) (a) Albietz, P. J.; Yang, K.; Lachicotte, R. J.; Eisenberg, R. *Organometallics* **2000**, *19*, 3543. (b) Fusto, M.; Giordano, F.; Orabona, I.; Ruffo, F.; Panunzi, A. *Organometallics* **1997**, *16*, 5981.

(6) (a) Macchioni, A.; Bellachioma, G.; Cardaci, G.; Travaglia, M.; Zuccacia, C.; Milani, B.; Corso, G.; Zangrado, E.; Mestroni, G.; Carfagna, C.; Formica, M. *Organometallics* **1999**, *18*, 2677. (b) Hoel, G. R.; Stockland, R. A.; Anderson, G. K.; Ladipo, F. T.; Braddock-Wilking, J.; Rath, N. P.; Mareque-Rivas, J. C. *Organometallics* **1998**, *17*, 1155.

(7) (a) Peters, J. C.; Harkins, S. B.; Brown, S. D.; Day, M. W. *Inorg. Chem.* **2001**, *40*, 5083. (b) Dahan, F.; Agami, C.; Levisalles, J.; Rose-Munch, F. *Chem. Commun.* **1974**, 505.

(8) (a) Fong, S.-W. A.; Hor, T. S. A. *J. Chem. Soc., Dalton Trans*. **1999**, 639, and references therein. (b) Capdevila, M.; Carrasco, Y.; Clegg, W.; Coxall, R. A.; González-Duarte, P.; Lledós, A.; Ramírez, J. A. *J. Chem. Soc., Dalton Trans*. **1999**, 3103. (c) Yam V. W.-W.; Yeung P. K.-Y.; Cheung K.-K. *Angew. Chem Int. Ed. Engl.* **1996**, *35*, 739.

(9) Mas-Ballesté, R.; Capdevila, M.; Champkin, P. A.; Clegg, W.; Coxall, R. A.; Lledós, A.; Mégret, C.; González-Duarte, P. *Inorg. Chem.* **2002**, *41*, 3218.

(10) Mas-Ballesté, R.; Aullón, G.; Champkin, P. A.; Clegg, W.; Mégret, C.; González-Duarte, P.; Lledós, A. *Chem. Eur. J.* **2003**, *9*, 5023.

(11) Aullón, G.; Capdevila, M.; Clegg, W.; González-Duarte, P.; Lledós, A.; Mas-Ballesté, R. *Angew. Chem. Int. Ed. Engl.* **2002**, *41*, 2776.

(12) (a) Aucott, S. M.; Slawin, A. M. Z.; Wollins, J. D. *J. Chem. Soc., Dalton Trans*. **2000**, 2559. (b) Bhattacharyya, P.; Slawin, A. M. Z.; Smith, M. B., *J. Chem. Soc., Dalton Trans*. **1998**, 2467. (c) Slawin, A. M. Z.; Smith M. B.; Wollins, J. D. *J. Chem. Soc., Dalton Trans*. **1996**, 3659. (d) Giordano, F.; Vitagliano, A. *Inorg. Chem.* **1981**, *20*, 633. (e) Bamberi, G.; Forsellini, E.; Gonziani, R. *J. Chem. Soc., Dalton Trans*. **1972**, 525.

(13) (a) Brunner, H.; Weber, M.; Zabel, M. *J. Organomet. Chem*. **2003**, *684*, 6. (b) Briant, C. E.; Gilmour, D. I.; Luke, M. A.; Mingos, D. M. P. *J. Chem. Soc., Dalton Trans*. **1985**, 851.

(14) Yeo, J. S. L.; Vittal, J. J.; Henderson, W.; Hor, T. S. A. *Inorg. Chem.* **2002**, *41*, 1194.

(15) (a) Canovese, L.; Visentin, F.; Uguagliati, P.; Crociani, B. *J. Chem. Soc., Dalton Trans*. **1996**, 1921. (b) Johnson, L. K.; Killian, C. M.; Brookhart, M. *J. Am. Chem. Soc.* **1995**, *117*, 6414. (c) van Asselt, R.; Elsevier, C. J.; Smeets, W. J. J.; Spek A. L. *Inorg. Chem.* **1994**, *33*, 1521.

(16) Hagelin, H.; Akermark, B.; Norrby, P.-O. *Chem. Eur. J.* **1999**, *5*, 902.

(17) (a) Li, Z.; Mok, H. F.; Batsanov, A. S.; Howard, J. A. K.; Hor, T. S. A. *J. Organomet. Chem*. **1999**, *575*, 223. (b) Pilkington, M. J.; Slawin, A. M. Z.; Williams, D. J.; Woollins, J. D. *J. Chem. Soc., Dalton Trans*. **1992**, 2425. (c) Bushnell, G. W.; Dixon, K. R.; Ono, R.; Pidcock, A. *Can. J. Chem*. **1984**, *62*, 696.

(18) Brown, M. P.; Puddephatt, R. J.; Rashidi, M.; Seddon, K. R., *J. Chem. Soc., Dalton Trans.* **1977**, 951.

(19) Capdevila, M.; González-Duarte, P.; Foces-Foces, C.; Hernández Cano F.; Martínez-Ripoll, M. *J. Chem. Soc., Dalton Trans*. **1990**, 143.

(20) *SMART* and *SAINT* software, Bruker AXS Inc., Madison, WI, USA, 2001.

(21) Cernik, R. J.; Clegg, W.; Catlow, C. R. A.; Bushnell-Wye, G.; Flaherty, J. V.; Greaves, G. N.; Burrows, I.; Taylor, D. J.; Teat, S. J.; Hamichi, M. *J. Synchrotron Rad*. **1997**, *4*, 279.

(22) Spek, A. L. *PLATON*. University of Utrecht, The Netherlands, 2001.

(23) Sheldrick, G. M. *SHELXTL*, version 6. Bruker AXS Inc., Madison, WI, USA, 2001.

(24) M. J. Frisch, G. W. Trucks, H. B. Schlegel, G. E. Scuseria, M. A. Robb, J. R. Cheeseman, V. G. Zakrzewski, J. A. Montgomery, R. E. Stratmann, J. C. Burant, S. Dapprich, J. M. Millam, A. D. Daniels, K. N. Kudin, M. C. Strain, O. Farkas, J. Tomasi, V. Barone, M. Cossi, R. Cammi, B. Mennucci, C. Pomelli, C. Adamo, S. Clifford, J. Ochterski, G. A. Petersson, P. Y. Ayala, Q. Cui, K. Morokuma, D. K. Malick, A. D. Rabuck, K. Raghavachari, J. B. Foresman, J. Cioslowski, J. V. Ortiz, B. B. Stefanov, G. Liu, A. Liashenko, P. Piskorz, I. Komaromi, R. Gomperts, R. L. Martin, D. J. Fox, T. Keith, M. A. Al-Laham, C. Y. Peng, A. Nanayakkara, C. Gonzalez, M. Challacombe, P. M. W. Gill, B. Johnson, W. Chen, M. W. Wong, J. L. Andres, C. Gonzalez, M. Head-Gordon, E. S. Replogle, J. A. Pople, *Gaussian98 (Revision A.7)*; Gaussian Inc.: Pittsburgh, PA, 1998.

(25) (*a*) Becke, A. D. *J. Chem. Phys.* **1993**, *98*, 5648. (*b*) Lee, C.; Yang, W.; Parr, R. G. *Phys. Rev. B* **1988**, *37*, 785.

(26) (*a*) Hay, P. J.; Wadt, W. R. *J. Chem. Phys.* **1985**, *82*, 299. (*b*) Hay, P. J.; Wadt, W. R. *J. Chem. Phys.* **1985**, *82*, 270.

(27)Höllwarth, A.; Böhme, M.; Dapprich, S.; Ehlers, A. W.; Gobbi, A.; Jonas, V.; Köhler, K. F.; Stegman, R.; Veldkamp, A.; Frenking, G. *Chem. Phys. Lett.* **1993**, *208*, 237.

(28)Hehre, W. J.; Ditchfield, R.; Pople, J. A. *J. Chem. Phys.* **1972**, *56*, 2257.

(29) Barone, V.; Cossi, M. *J. Phys. Chem,* **1998**, *102*, 1995.

Table 1. NMR Parameters and Mass Determinations for the Complexes **1**–**5**

Complex	MS	Calculated MW	$\delta(^{31}P)$ ppm[a]	$^{1}J_{Pt-P}$ Hz	$\delta(^{1}H)$ of cod ligand ppm[a]	$\delta(^{13}C)$ of cod ligand ppm[a]
$[Pt_2(\mu\text{-}S)_2(dppp)_2]$	ESI: 1279	1279.1	–0.08	2615		
1	ESI: 790.9[b]	1582.4	–4.12	3069	CH: 4.54; CH_2: 2.53	CH: 96.91; CH_2: 29.82
2	ESI: 790.5[c] MALDI:1581.1	1581.4	–6.26	3006	CH: 4.27, 4.04, 3.09, 2.81, 2.27; CH_2: 2.82 (m), 2.01 (m)	CH: 83.29, 81.35, 75.18, 54.25, 26.29; CH_2: 33.94, 29.02, 28.26
$[Pt(SH)_2(dppp)]$	ESI: 640.1[d]	673.6	–1.30	2760		
3	ESI: 638.9[b]	1278.1	–2.61	3193	CH: 5.49, 4.99; CH_2: 2.5 (m)	CH: 100.96, 98.84; CH_2: 30.15
4	ESI: 638.7[c] MALDI: 1277.1	1277.1	–3.75 (m)		CH: 5.1-5.3 (br), 4.6-4.8 (br);	CH: 96.42–95.04 (m), 85.16, 84.47, 83.42, 83.19, 79.05, 78.31, 54.60, 54.50, 28.01, 27.27; CH_2: 34.55, 34.25, 30.47–29.70 (m) 28.95, 28.80, 28.55, 28.14
5	ESI: 638.9[c] MALDI: 1276.9	1276.1	–6.09 (m)		CH: 3.8-5.2 (br, m)	CH: 85.06–83.22 (m), 79.20–78.02 (m), 73.10–72.34 (m), 54.43–54.08 (m), 26.80–25.30 (m); CH_2: 35.63–34.28 (m), 29.40–27.80 (m)

[a] In d_6-dmso. [b] $M^{2+}/2$. [c] The formic acid added for ESI-MS measurements on **2** causes formation of **1**; on **4** and **5** causes formation of **3**. [d] $[(dppp)Pt(SH)]^+$ fragment. Abbreviations: m, multiplet; br, broad.

Table 2. Relative Energies (kcal/mol) for the Different Isomers of Complexes $[L_2Pt(C_8H_{11})]$

	Gas Phase			Solution[a]		
	Allyl (A)	Allyl (B)	Vinyl	Allyl (A)	Allyl (B)	Vinyl
2 Cl^-	0.0	5.4	31.7	0.0	3.1	28.9
2 SH^-	0.0	4.6	29.8	0.0	4.2	27.3
$[Pt_2(\mu\text{-}S)_2(PH_3)_4]$	**0.0**	**7.8**	**34.7**	**0.0**	**7.1**	**32.9**
2 PH_3	0.0	5.5	27.4	0.0	4.4	27.3
2 SH_2	0.0	7.3	32.3	0.0	6.4	32.5

[a] Calculated in methanol (ε= 32.63) using COSMO continuum solvation model

Table 3. Reaction Energies for the cod/dppp Ligand Exchange Reaction and Pt-cod and Pt-dppp Bond Dissociation Energies in $[L_2Pt(cod)]$ Complexes (in kcal/mol)

L_2	$2SH^-$	$2I^-$	$2Br^-$	$2Cl^-$	$[Pt_2(\mu\text{-}S)_2(dhpp)_2]$[a]	$[Pt_2(\mu\text{-}S)_2(dhpp)(cod)]$	2 PH_3	2 SH_2
ΔE_{LE}	−18.7	−23.7	−23.2	−22.5	**−28.2**	**−28.7**	−33.6	−37.5
$BDE_{(Pt\text{-}cod)}$	42.2	57.4	65.5	73.6	**78.9**	**81.7**	116.5	140.1
$BDE_{(Pt\text{-}dppp)}$	60.7	81.1	88.7	96.1	**107.1**	**110.4**	150.1	177.6

[a] dhpp = $H_2P(CH_2)_3PH_2$

Table 4. Reaction Energies (in kcal/mol) for MeO^- Insertion or deprotonation reactions in $[L_2Pt(cod)]$ Complexes.[a]

L_2	$2SH^-$	$2Cl^-$	$[Pt_2(\mu\text{-}S)_2(PH_3)_4]$	$2PH_3$	$2SH_2$
Insertion	−28.4	−41.3	**−50.8**	−62.9	−69.2
Deprotonation	−12.7	−23.9	**−40.0**	−52.5	−58.5

[a] Calculated in methanol (ε= 32.63) using COSMO continuum solvation model

Table 5. Selected Bond Lengths (Å) and Angles (deg) for **1**

Pt(1)–S(1)	2.375(4)	Pt(1)–S(2)	2.365(3)
Pt(2)–S(1)	2.372(3)	Pt(2)–S(2)	2.381(3)
Pt(3)–S(1)	2.342(3)	Pt(3)–S(2)	2.326(3)
Pt(1)–P(1)	2.261(3)	Pt(1)–P(2)	2.260(4)
Pt(2)–P(3)	2.263(3)	Pt(2)–P(4)	2.264(3)
Pt(3)–C(55)	2.195(13)	Pt(3)–C(58)	2.198(10)
Pt(3)–C(59)	2.218(10)	Pt(3)–C(62)	2.216(12)
C(55)–C(62)	1.346(16)	C(58)–C(59)	1.399(16)
S(1)–Pt(1)–S(2)	79.82(10)	S(1)–Pt(2)–S(2)	79.55(10)
S(1)–Pt(3)–S(2)	81.29(11)	P(1)–Pt(1)–P(2)	92.59(13)
P(3)–Pt(2)–P(4)	93.72(11)		

Table 6. Selected Bond Lengths (Å) and Angles (deg) for **2**

Pt(1)–S(1)	2.3592(11)	Pt(2)–S(1)	2.3705(11)
Pt(3)–S(1)	2.3789(11)	Pt(1)–P(1)	2.2558(11)
Pt(2)–P(2)	2.2519(12)	Pt(3)–C(29)	2.064(13)
Pt(3)–C(30)	2.103(10)	Pt(3)–C(34)	2.230(10)
S(1)–Pt(1)–S(1′)	81.42(5)	S(1)–Pt(2)–S(1′)	80.95(5)
S(1)–Pt(3)–S(1′)	80.60(5)	P(1)–Pt(1)–P(1′)	94.93(6)
P(2)–Pt(2)–P(2′)	95.72(6)		

Table 7. Crystallographic Data for **1** and **2**

Complex	**1**	**2**
Formula	$C_{62}H_{64}P_4Pt_3S_2^{2+}\cdot 2Cl^-\cdot 3CHCl_3$	$C_{62}H_{63}P_4Pt_3S_2^{+}\cdot ClO_4^-\cdot CH_2Cl_2$
Form wt	2011.4	1765.8
Cryst syst	Monoclinic	Monoclinic
Space group	$P2_1/n$	$P2_1/m$
a (Å)	13.5107(7)	12.8372(12)
b (Å)	20.5840(10)	14.8717(14)
c (Å)	28.7743(14)	19.6316(19)
β (deg)	99.474(2)	106.160(2)
V (Å^3)	7893.1(7)	3599.8(6)
Z	4	2
T (K)	160	120
Reflns measd	42657	24256
Unique reflns	10305	10158
R_{int}	0.078	0.041
R (F, $F^2 > 2\sigma$)	0.046	0.035
R_w (F^2, all data)	0.119	0.099
S (F^2, all data)	0.966	1.013
max, min el dens (e Å^{-3})	1.61, −1.57	1.58, −1.71

Figure Captions

Figure 1. Possible binding modes of the $(C_8H_{11})^-$ ligand in a $[L_2Pt(C_8H_{11})]$ complex.

Figure 2. Labeling of the carbon atoms of cod ligand in **3** and possible isomers of **4** and **5**.

Figure 3. Molecular models of complexes $[\{Pt_2(\mu\text{-}S)_2(cod)_2\}Pt(dppp)]^{2+}$ (A), $[\{Pt_2(\mu\text{-}S)_2(dppp)_2\}Pt(cod)]^{2+}$ (B) and $[Pt_3(\mu_3\text{-}S)_2(dppp)_3]^{2+}$ (C). Arrows indicate the space available for the attack of an additional ligand.

Figure 4. Deprotonation reaction profiles in gas phase and solution for complexes $[PtCl_2(cod)]$ and **1**.

Figure 5. Molecular structure of **1** with the key atoms labeled and 50% probability ellipsoids. H atoms, Cl^- anions and CH_3Cl solvent molecules have been omitted.

Figure 6. Molecular structure of **2** with the key atoms labeled and 50% probability ellipsoids. H atoms, ClO_4^- anions and CH_2Cl_2 solvent molecules have been omitted.

Figure 7. Representation of the overlap of atomic arrangements corresponding to $\{Pt(C_8H_{11})\}$ fragment in **2**.

Figure 8. (A) Structural parameters obtained by X-ray diffraction for complex **2**. Numbers in bold characters are inconsistent with the proposal of an allyl A structure for the deprotonated cod ligand. (B) Structural parameters calculated by means of DFT calculations for the allyl A isomer.

Figure 1.

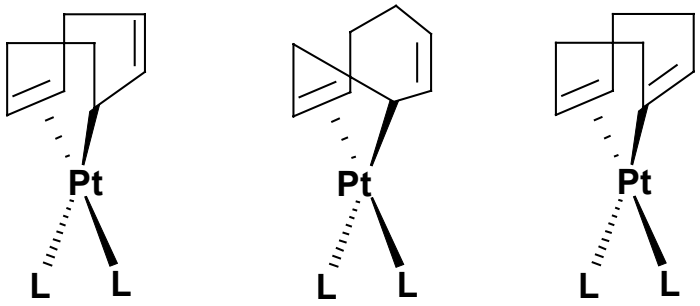

Figure 2

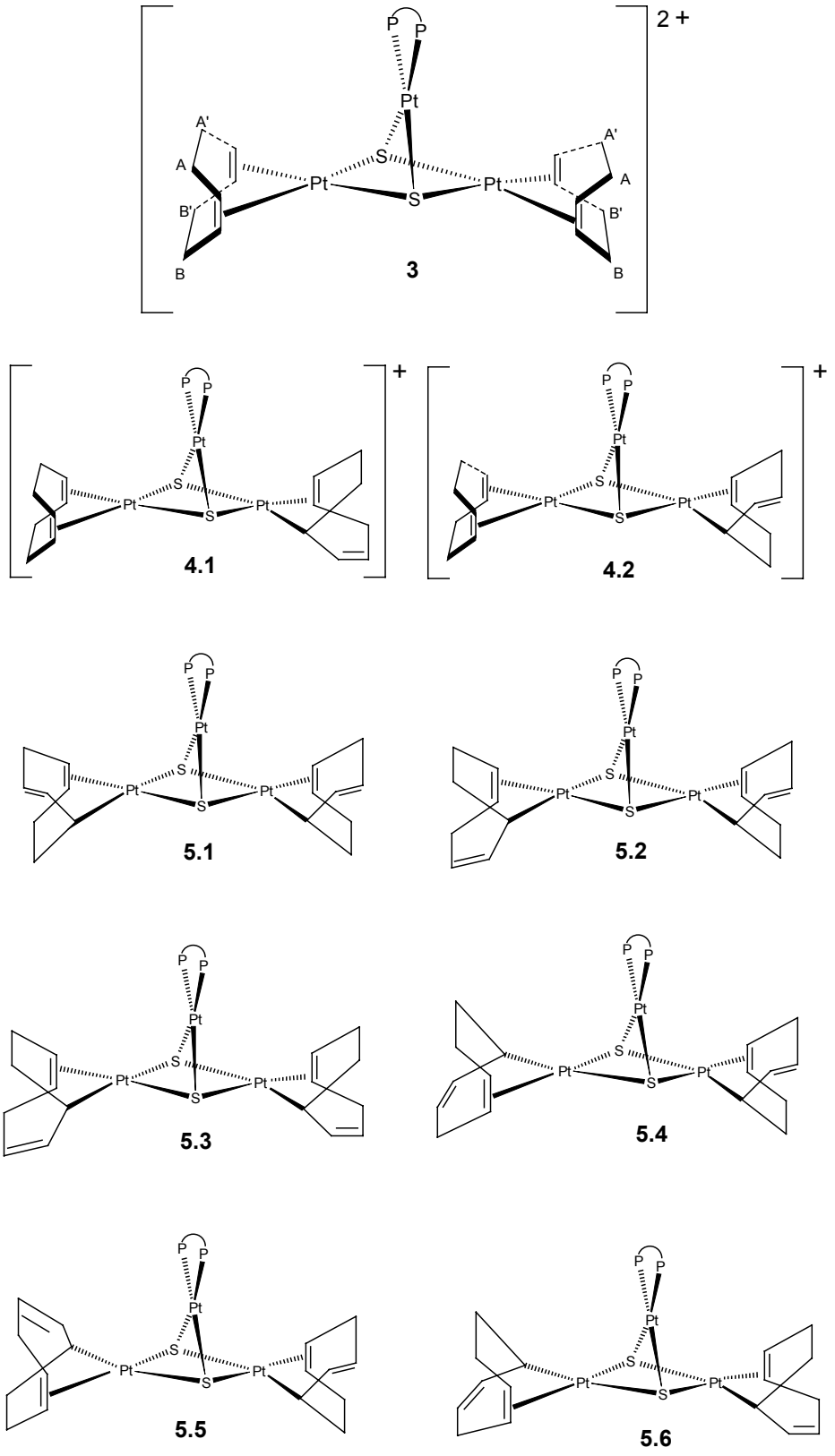

Figure 3

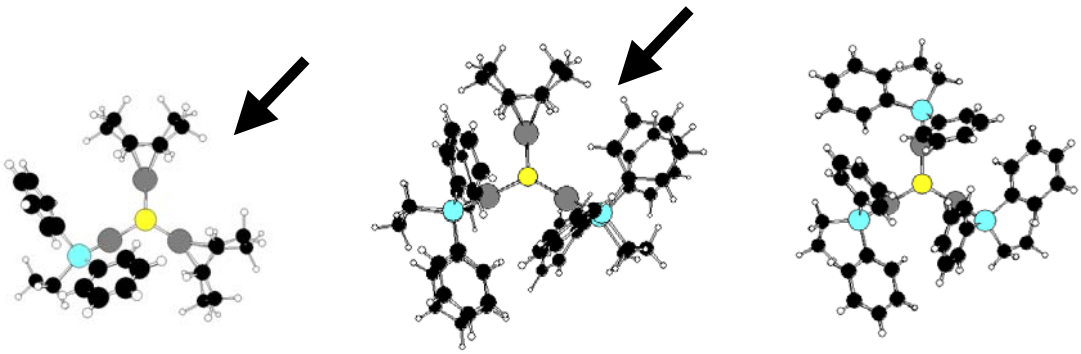

(A) (B) (C)

Figure 4

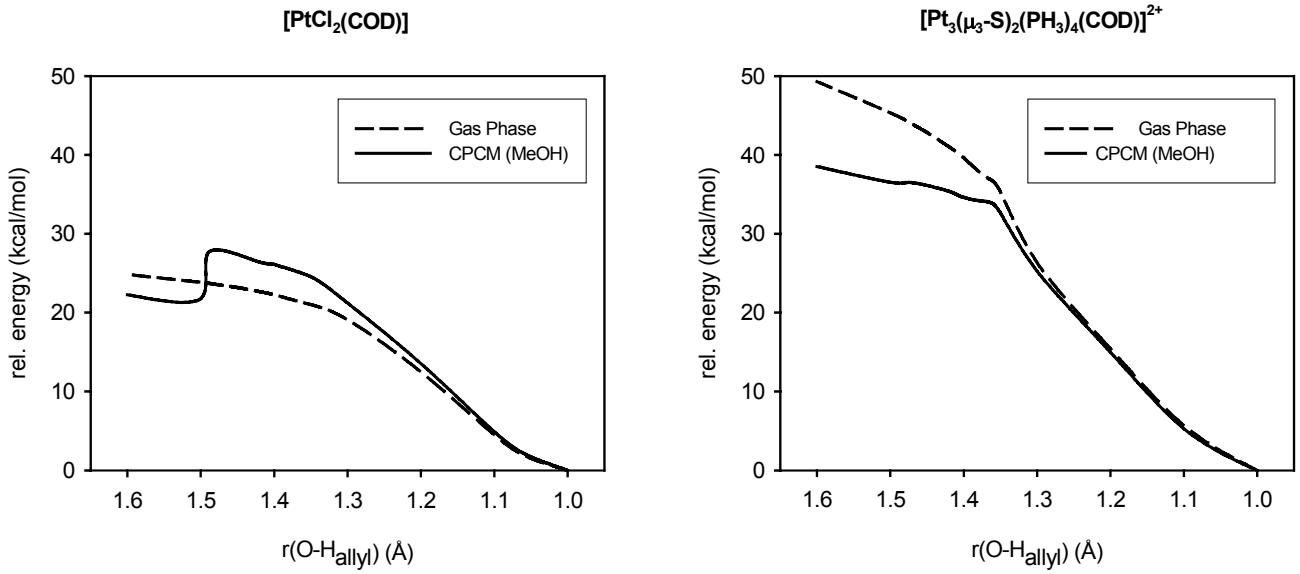
[PtCl2(COD)]
[Pt3(μ3-S)2(PH3)4(COD)]2+
Gas Phase
CPCM (MeOH)
rel. energy (kcal/mol)
r(O-Hallyl) (Å)
0
10
20
30
40
50
1.6
1.5
1.4
1.3
1.2
1.1
1.0

Figure 5

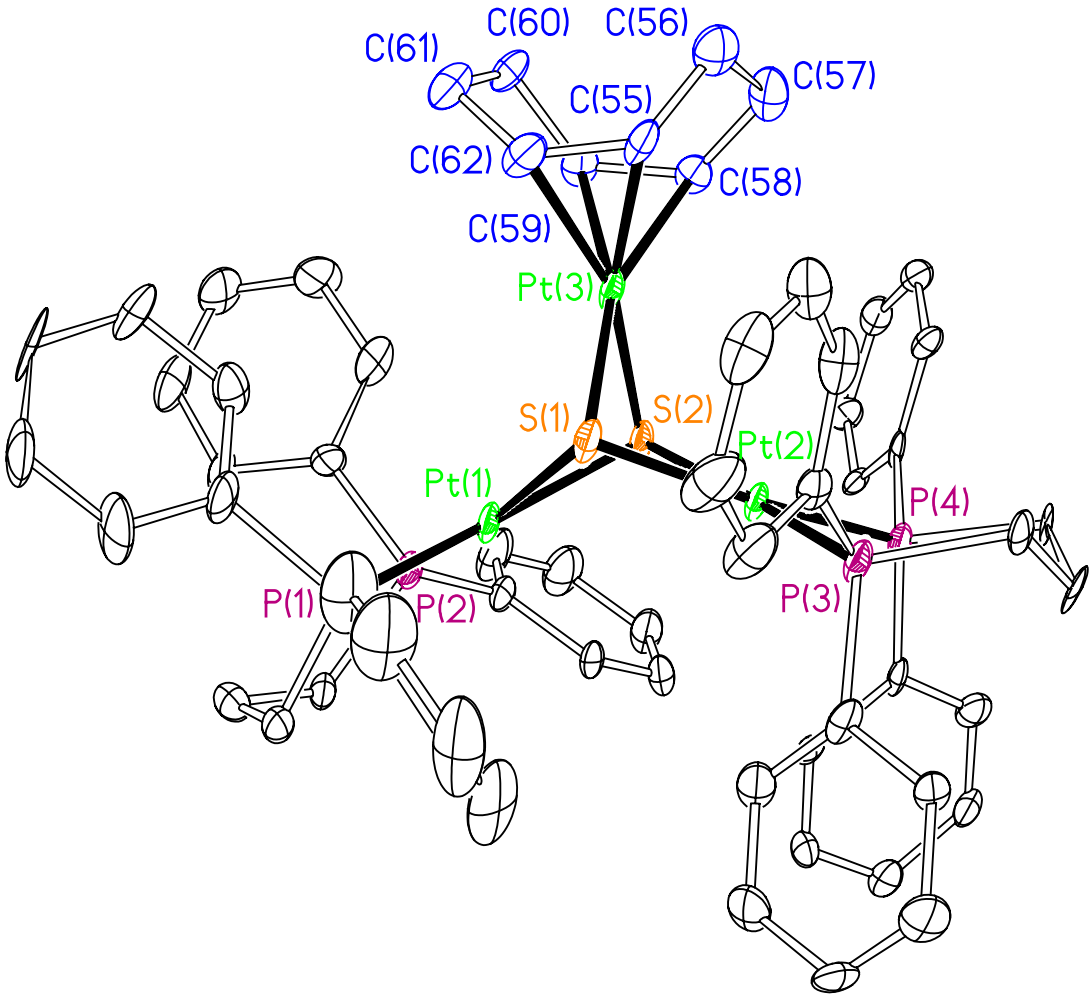

Figure 6

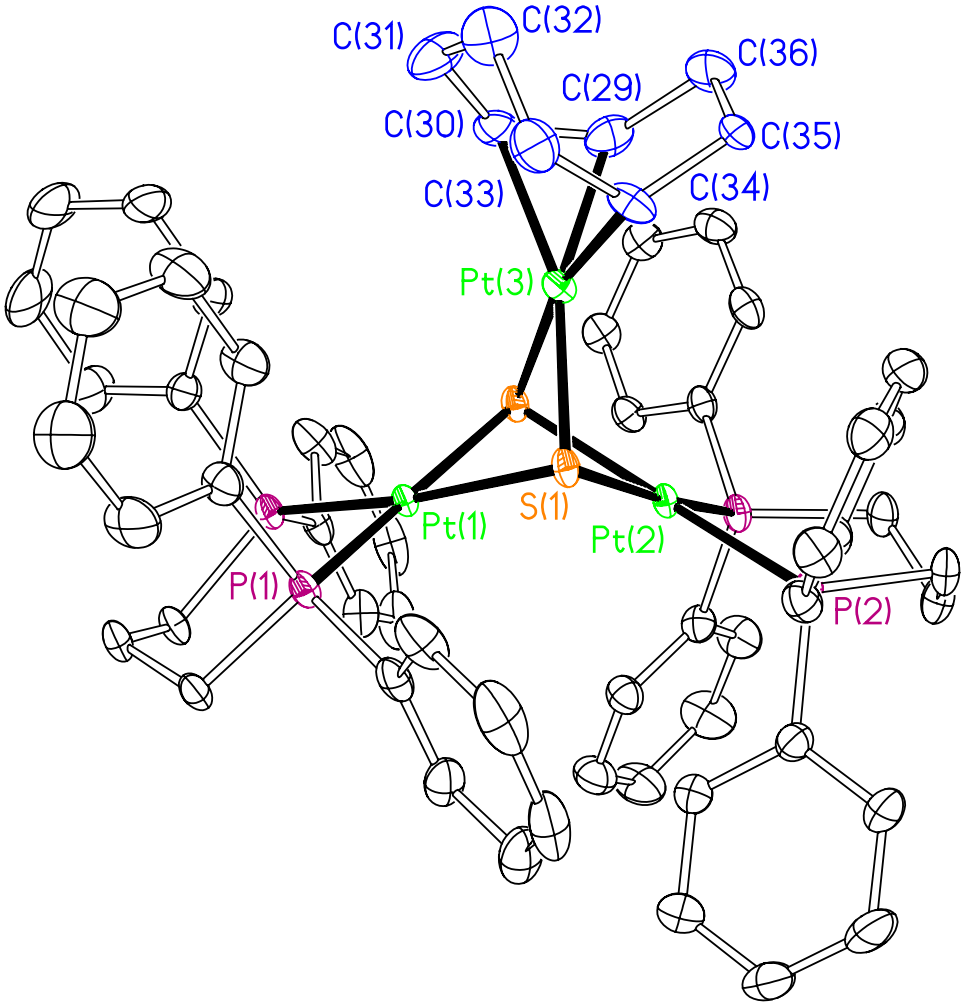

Figure 7

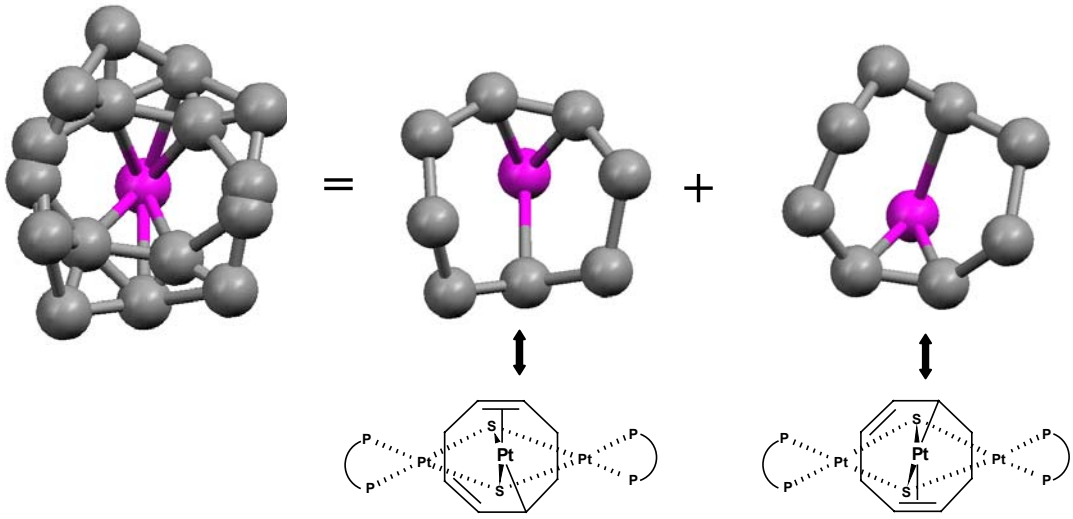

Figure 8

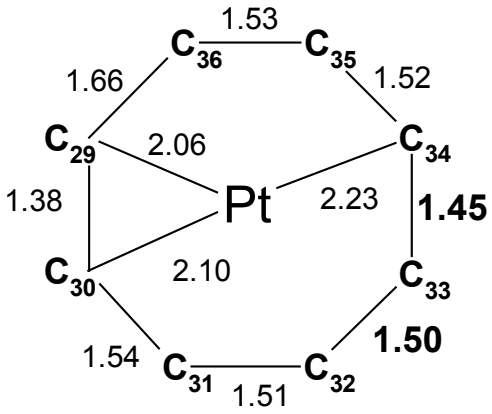
1.53
C36
C35
1.66
1.52
C29
2.06
C34
1.38
Pt
2.23
1.45
C30
2.10
C33
1.54
C31
1.51
C32
1.50

(A)

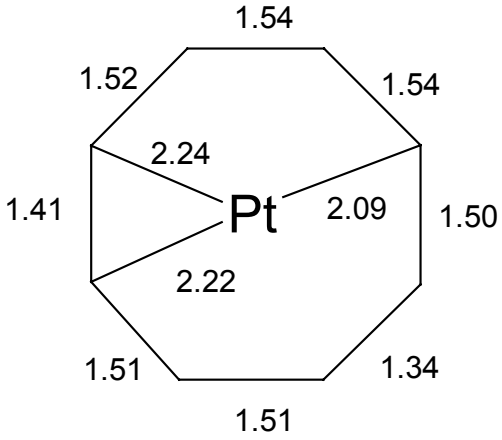
1.54
1.52
1.54
2.24
1.41
Pt
2.09
1.50
2.22
1.51
1.34
1.51

(B)

Scheme 1

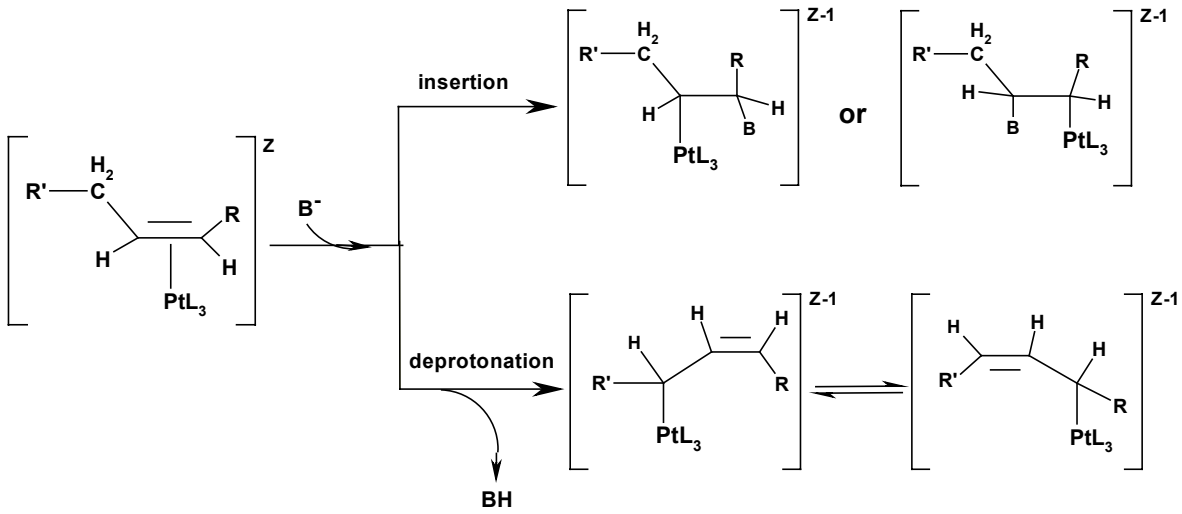

Scheme 2

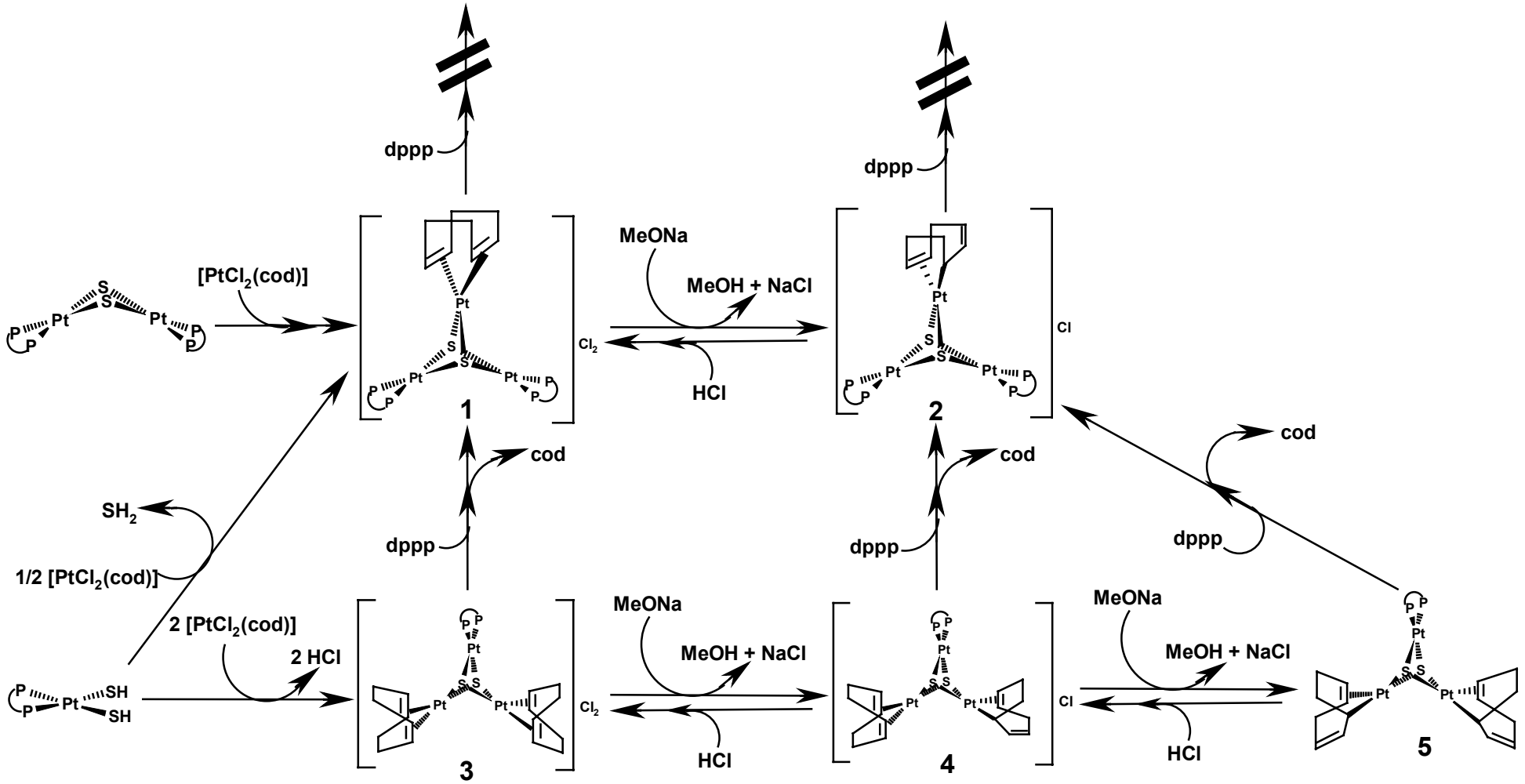
dppp
[PtCl2(cod)]
MeONa
MeOH + NaCl
HCl
Cl2
Cl
1
2
cod
SH2
1/2 [PtCl2(cod)]
2 [PtCl2(cod)]
2 HCl
3
4
5

Inorg. Chem. **2002**, *41*, 3218–3229

Diverse Evolution of [{$Ph_2P(CH_2)_nPPh_2$}Pt(μ-S)$_2$Pt{$Ph_2P(CH_2)_nPPh_2$}] (n = 2, 3) Metalloligands in CH_2Cl_2

Rubén Mas-Ballesté,[†] Mercè Capdevila,[†] Paul A. Champkin,[‡] William Clegg,[‡] Robert A. Coxall,[‡] Agustí Lledós,[†] Claire Mégret,[†] and Pilar González-Duarte*,[†]

Departament de Química, Universitat Autònoma de Barcelona, E-08193 Bellaterra, Barcelona, Spain, and Department of Chemistry, University of Newcastle, Newcastle upon Tyne NE1 7RU, U.K.

Received July 6, 2001

The nucleophilicity of the {Pt_2S_2} core in [{$Ph_2P(CH_2)_nPPh_2$}Pt(μ-S)$_2$Pt{$Ph_2P(CH_2)_nPPh_2$}] (n = 3, dppp (**1**); n = 2, dppe (**2**)) metalloligands toward the CH_2Cl_2 solvent has been thoroughly studied. Complex **1**, which has been obtained and characterized by X-ray diffraction, is structurally related to **2** and consists of dinuclear molecules with a hinged {Pt_2S_2} central ring. The reaction of **1** and **2** with CH_2Cl_2 has been followed by means of ^{31}P, ^{1}H, and ^{13}C NMR, electrospray ionization mass spectrometry, and X-ray data. Although both reactions proceed at different rates, the first steps are common and lead to a mixture of the corresponding mononuclear complexes [Pt{$Ph_2P(CH_2)_nPPh_2$}(S_2CH_2)], n = 3 (**7**), 2 (**8**), and [Pt{$Ph_2P(CH_2)_nPPh_2$}Cl_2], n = 3 (**9**), 2 (**10**). Theoretical calculations give support to the proposed pathway for the disintegration process of the {Pt_2S_2} ring. Only in the case of **1**, the reaction proceeds further yielding [Pt_2(dppp)$_2$\{μ-(SCH_2SCH_2S)-*S*,*S*′}]Cl_2 (**11**). To confirm the sequence of the reactions leading from **1** and **2** to the final products **9** and **11** or **8** and **10**, respectively, complexes **7**, **8**, and **11** have been synthesized and structurally characterized. Additional experiments have allowed elucidation of the reaction mechanism involved from **7** to **11**, and thus, the origin of the CH_2 groups that participate in the expansion of the $(SCH_2S)^{2-}$ ligand in **7** to afford the bridging $(SCH_2SCH_2S)^{2-}$ ligand in **11** has been established. The X-ray structure of **11** is totally unprecedented and consists of a hinged {(dppp)Pt(μ-S)$_2$Pt(dppp)} core capped by a CH_2SCH_2 fragment.

Introduction

Evolution of the chemistry of [L_2Pt(μ-S)$_2$PtL_2] as a metalloligand precursor to higher nuclearity aggregates has proceeded so rapidly since the first report of [Pt_2(PMe_2Ph)$_4$-(μ-S)$_2$] by Chatt and Mingos in 1970[1] that it appears difficult to further extend the present knowledge of the synthesis and structural aspects of the corresponding homo- and heterometallic derivatives. The recent developments in the synthesis, structures, and reactivities of sulfide-bridged aggregates with the {Pt_2S_2} core have been excellently reviewed by Fong and Hor,[2] who have made important contributions to this field.[3] The high nucleophilicity of the bridging sulfur atoms together with the flexible hinge angle between the two $Pt^{II}S_2$ planes explains the large family of derivatives based on the {Pt_2S_2} core and the varied coordination geometries about the heterometal in complexes containing the [L_2Pt-(μ-S)$_2$PtL_2] metalloligand.[4]

Despite the formidable body of structural and related data on this family of compounds, several points remained open to consideration. On one hand, the synthetic routes reported for complexes of formula [L_2Pt(μ-S)$_2$PtL_2] were not straightforward, reports on their crystal structures were scarce, and most of the sulfide-bridged aggregates containing the {Pt_2S_2} core had been achieved with PPh_3 as terminal ligand.[2,3] These observations led us to report a convenient synthesis (90% yield), monitored by means of ^{31}P NMR, for [(dppe)Pt(μ-

* Corresponding author. E-mail: Pilar.Gonzalez.Duarte@uab.es.
[†] Universitat Autònoma de Barcelona.
[‡] University of Newcastle.

(1) Chatt, J.; Mingos, D. M. P. *J. Chem. Soc. A* **1970**, 1243.
(2) Fong, S.-W. A.; Hor, T. S. A. *J. Chem. Soc., Dalton Trans*. **1999**, 639.
(3) Selected recent references: (a) Li, Z.; Loh, Z.-H.; Mok, K. F.; Hor, T. S. A. *Inorg. Chem.* **2000**, *39*, 5299. (b) Li, Z.; Xu, X.; Khoo, S. B.; Mok, K. F.; Hor, T. S. A. *J. Chem. Soc., Dalton Trans*. **2000**, 2901. (c) Liu, H.; Jiang, C.; Yeo, J. S. L.; Mok, K. F.; Liu, L. K.; Hor, T. S. A.; Yan, Y. K. *J. Organomet. Chem*. **2000**, *595*, 276. (d) Fong, S.-W. A.; Vittal, J. J.; Henderson, W.; Hor, T. S. A.; Oliver, A. G.; Rickard, C. E. F. *Chem. Commun*. **2001**, 421.
(4) (a) Capdevila, M.; Clegg, W.; González-Duarte, P.; Jarid, A.; Lledós, A. *Inorg. Chem*. **1996**, *35*, 490. (b) Aullón, G.; Ujaque, G.; Lledós, A.; Alvarez, S.; Alemany, P. *Inorg. Chem*. **1998**, *37*, 804.

10.1021/ic0107173 CCC: $22.00
Published on Web 05/17/2002

Scheme 1

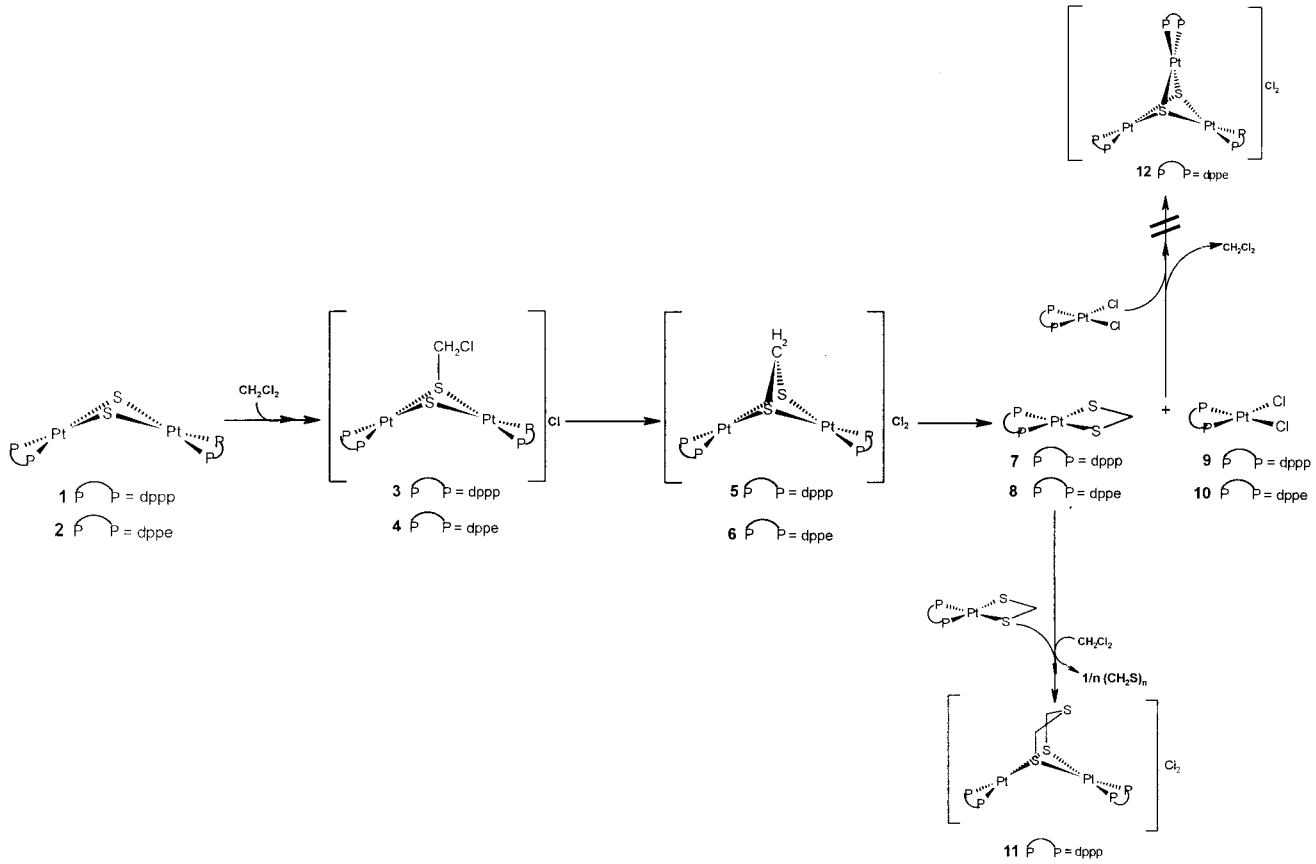

$S)_2Pt(dppe)]$, its X-ray crystal structure,[5] and the synthesis and full structural characterization in the solid phase as well as in solution by multinuclear NMR of a series of pentanuclear complexes of formula $[M\{Pt_2(dppe)_2(\mu_3\text{-}S)_2\}_2]$, ($M^{II}$ = Zn, Cd, Hg, Cu).[5,6] These constituted the first examples structurally characterized by X-ray diffraction where the heterometal is tetrahedrally coordinated to two $[L_2Pt(\mu\text{-}S)_2PtL_2]$ metalloligands.

Another question there has been insufficient information to address is the reaction pathway by which the $[L_2Pt(\mu\text{-}S)_2PtL_2]$ metalloligands react with organic electrophilic agents, such as $PhCH_2Br$[1] and CH_3I,[7] as a consequence of the nucleophilicity of the sulfide bridges. A particular case of this well-established reaction is the surprising progression of $[L_2Pt(\mu\text{-}S)_2PtL_2]$ compounds when they are dissolved in CH_2Cl_2.[2] Thus, in recent years, several different species have been characterized as a result of this reaction (Table 1). The apparent dispersion of the compounds obtained, the lack of a systematic study of the reactions involved and the possible relationship between the nucleophilic character of the $\{Pt_2S_2\}$ core and the nature of the terminal ligands suggested to us that this whole question deserves further analysis.

Table 1. Complexes Obtained upon Exposure of $[L_2Pt(\mu\text{-}S)_2PtL_2]$ Metalloligands in CH_2Cl_2

complex	terminal ligand	experimental evidences	ref.
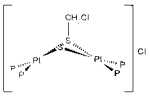	P= PPh_3 P_2= dppf [a]	NMR	8, 9
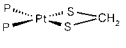	P= PMe_2Ph P= dppy [b]	NMR and X-ray diffraction	10, 11
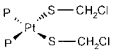	P_2= dppf [a] P= PPh_3	NMR	9, 12

[a] dppf = $[FeC_5H_4PPh_2)_2]$. [b] dppy = $PPh_2(C_5H_5N)$.

Here we report a detailed study of the multistage pathway followed in the reaction of the $[(P\cap P)Pt(\mu\text{-}S)_2Pt(P\cap P)]$ metalloligands, where P∩P = dppe or dppp, with CH_2Cl_2, Scheme 1. On the basis of multinuclear NMR, electrospray ionization mass spectrometry (ESI MS), and X-ray crystallographic data, we show that both reactions proceed at different rates and eventually afford different products. Overall, the complexity of the reaction of the $[(P\cap P)Pt(\mu\text{-}S)_2Pt(P\cap P)]$ metalloligands with CH_2Cl_2 explains the diversity of the compounds reported in closely related systems, Table 1, and evidences the influence of the terminal ligands on the reactivity of the $\{Pt(\mu\text{-}S)_2Pt\}$ core.

(5) Capdevila, M.; Carrasco, Y.; Clegg, W.; González-Duarte, P.; Lledós, A.; Sola, J.; Ujaque, G. *J. Chem. Soc., Chem. Commun.* **1998**, 597.
(6) Capdevila, M.; Carrasco, Y.; Clegg, W.; Coxall, R. A.; González-Duarte, P.; Lledós, A.; Ramírez, J. A. *J. Chem. Soc., Dalton Trans.* **1999**, 3103.
(7) (a) Ugo, R.; La Monica, G.; Cenini, S.; Segre, A.; Conti, F. *J. Chem. Soc. A* **1971**, 522. (b) Briant, C. E.; Gardner, C. J.; Hor, T. S. A.; Howells, N. D.; Mingos, D. M. P. *J. Chem. Soc., Dalton Trans.* **1984**, 2645.

Experimental Section

Materials and Methods. All the manipulations were carried out at room temperature under an atmosphere of pure dinitrogen, and conventionally dried and degassed solvents were used throughout. These were Purex Analytical Grade from SDS. Metal complexes of formula $[PtCl_2(P\cap P)]$, P∩P = dppe or dppp, were prepared according to published methods.[13] The synthesis of [(dppe)Pt-(μ-S)$_2$Pt(dppe)] (**2**) has already been reported.[5]

Elemental analyses were performed on a Carlo-Erba CHNS EA-1108 analyzer. The microanalytical data for crystals of **11** have been omitted because they are unsatisfactory, as already found in some related phosphine platinum complexes.[14] ^{1}H, ^{13}C{^{1}H}, and ^{31}P{^{1}H} NMR spectra of the complexes **1**, **2**, and **7**−**11** and the ^{31}P{^{1}H} NMR spectrum of **11′** (**E** + **E′** in Scheme 2) were recorded from samples in $(CD_3)_2SO$ solution at room temperature using a Bruker AC250 spectrometer. ^{13}C and ^{1}H chemical shifts are relative to $SiMe_4$, and ^{31}P chemical shifts, to external 85% H_3PO_4. The ^{2}H NMR spectrum of **11′** was recorded from $(CH_3)_2SO$ solution using a Bruker AM400 spectrometer, and the ^{1}H NMR spectrum was recorded from $(CD_3)_2SO$ solution using a Bruker Avance500. The ^{31}P{^{1}H} NMR spectra of **1**, **2**, and **3** were simulated on a Pentium-200 computer using the gNMR V4.0.1 program by P. H. M. Budzelaar from Cherwell Scientific Publishing.[15]

To analyze the course of the reaction of **1** or **2** in CH_2Cl_2, a solution of 50 mg of the corresponding pure compound in 25 mL of solvent was prepared at room temperature. At different times, aliquots were taken from the solution, they were evaporated to dryness, and the ^{1}H, ^{13}C, and ^{31}P NMR spectra of a fraction of the solid residue dissolved in d_6-DMSO were recorded. Another fraction was used in order to determine the mass of the species present by means of ESI MS measurements. These were performed on a VG Quattro Micromass Instrument. Experimental conditions were as follows: 10 μL of sample was injected at 15 μL/min; capillary-counter electrode voltage, 4.5 kV; lens-counter electrode voltage, 1.0 kV; cone potential, 55 V; source temperature, 90 °C; *m*/*z* range, 300−1600. The carrier was acetonitrile for the spectra recorded during the reaction of **1**, **2**, or **7** with CH_2Cl_2 or a 1:1 mixture of acetonitrile and water containing 1% formic acid in the case of the pure **1**, **2**, **7**, **8**, and **11** complexes. ESI MS data provided evidence for the formation of **3**, **4**, and **5**.

[Pt$_2$(dppp)$_2$(μ-S)$_2$] (1). $[PtCl_2(dppp)]$ (0.20 g, 0.3 mmol) was added to a benzene solution (75 mL) of $Na_2S\cdot 9H_2O$ (0.35 g, 1.6 mmol) and the mixture stirred at room temperature for 8 h. These reaction conditions were fixed after monitoring the reaction by ^{31}P NMR, as already reported for the dppe analogue.[6] The excess $Na_2S\cdot 9H_2O$, the formed NaCl, and the $[PtCl_2(dppp)]$ which did not react were filtered off. The solvent was removed under vacuum from the filtrate to yield the product as an orange solid. Yield 84%. Anal. Calcd for $C_{54}H_{52}P_4Pt_2S_2$: C, 50.70; H, 4.10; S, 5.01. Found: C, 50.83; H, 4.29; S, 5.12. X-ray quality crystals of this compound were obtained by slow evaporation of a solution of **1** in acetone.

[Pt(dppp)(S$_2$CH$_2$)] (7). To a suspension of $Na_2S\cdot 9H_2O$ (0.35 g, 1.6 mmol) in benzene (50 mL) were added solid $[PtCl_2(dppp)]$ (0.10 g, 0.15 mmol) and CH_2Cl_2 (0.5 mL, 7.8 mmol) with stirring. After 24 h, the excess $Na_2S\cdot 9H_2O$ and the white solid formed, NaCl, were filtered off. The filtrate was concentrated to dryness, giving a yellow solid. Recrystallization in acetonitrile afforded a yellow crystalline solid. Yield 43%. Anal. Calcd for $C_{28}H_{28}P_2PtS_2\cdot CH_3CN$: C, 49.58; H, 4.30; N, 1.93; S, 8.82. Found: C, 48.79; H, 4.20; N, 2.22; S, 8.90. A single crystal was chosen for X-ray diffraction.

[Pt(dppe)(S$_2$CH$_2$)] (8). Using the same procedure as that indicated for complex **7**, a yellow solid was obtained from the reaction of $[PtCl_2(dppe)]$ (0.085 g, 0.1 mmol) with $Na_2S\cdot 9H_2O$ (0.175 g, 0.8 mmol) and CH_2Cl_2 (0.5 mL, 7.8 mmol) in a benzene solution (25 mL). Yield 67%. Anal. Calcd for $C_{27}H_{26}P_2PtS_2$: C, 48.28; H, 3.90; S, 9.55. Found: C, 48.03; H, 4.10; S, 10.15. Recrystallization of **8** in acetone allowed isolation of yellow crystals. Unfortunately, the diffraction data were very weak and of inferior quality compared to those of **7**, allowing only a qualitative structure analysis.

[Pt$_2$(dppp)$_2${μ-(SCH$_2$SCH$_2$S)-*S*,*S*′}]Cl$_2$ (11). A pure solid sample of **7** (0.05 g, 0.07 mmol) was added to CH_2Cl_2 (5 mL) with stirring. After several days, the solution was concentrated to dryness affording a pale yellow solid. The residue was redissolved in toluene, and the filtered solution was concentrated to yield the expected product as a pale yellow solid, which was filtered and dried. Recrystallization of **11** from toluene gave colorless crystals suitable for X-ray diffraction.

To carry out the study of the mechanism involved in the reaction from **7** to **11**, 30 mg of **7** were dissolved in 1 mL of CD_2Cl_2. By a similar procedure as that followed for **11**, 15 mg (50% yield) of **11′** were obtained. Characterization of this solid was made by multinuclear NMR spectroscopy.

X-ray Crystallographic Characterization of Complexes 1, 7, and 11. A summary of crystal data, data collection, and refinement parameters for the three structural analyses is given in Table 2. Crystals were examined on a Bruker AXS SMART CCD area-detector diffractometer with graphite-monochromated Mo Kα radiation (λ = 0.71073 Å); measurements were made at 160 K. Cell parameters were obtained from a least-squares fit on the observed setting angles of all significant intensity reflections.

Table 2. Crystal Data, Data Collection, and Refinement for Complexes **1**, **7**, and **11**

	1·Me$_2$CO	**7**·MeCN	**11**·1.5PhMe
formula	$C_{57}H_{58}OP_4Pt_2S_2$	$C_{30}H_{35}NP_2PtS_2$	$C_{66.5}H_{68}Cl_2P_4Pt_2S_3$
fw	1337.2	730.7	1548.4
cryst size, mm^3	0.7 × 0.3 × 0.2	0.4 × 0.3 × 0.2	0.24 × 0.18 × 0.08
space group	$P2_1/c$	$P2_1/c$	$P2_1/c$
a, Å	22.025(8)	9.8365(5)	13.8539(5)
b, Å	14.753(5)	16.6498(9)	13.0377(5)
c, Å	16.502(5)	17.7108(9)	34.1386(13)
β, deg	101.470(14)	100.589(1)	91.7764(6)
V, Å^3	5255(3)	2851.2(3)	6163.3(4)
Z	4	4	4
ρ_{calcd}, g cm^{-3}	1.690	1.702	1.669
μ, cm^{-1}	55.6	52.0	48.7
$R(F)^a$ ($F^2 > 2\sigma(F^2)$)	0.0305	0.0226	0.0464
$R_w(F^2)^b$ (all data)	0.0543	0.0532	0.0982

^{a} $R(F) = \sum||F_o| - |F_c||/\sum|F_o|$. ^{b} $R_w(F^2) = [\sum[w(F_o^2 - F_c^2)^2]/\sum[w(F_o^2)^2]]^{1/2}$.

(8) Gukathasan, R. R.; Morris, R. H.; Walker, A. *Can. J. Chem.* **1983**, *61*, 2490.
(9) Zhou, M.; Lam, C. F.; Mok, K. F.; Leung, P.-H.; Hor, T. S. A. *J. Organomet. Chem.* **1994**, *476*, C32.
(10) Shaver, A.; Lai, R. D.; Bird, P. H.; Wickramasinghe, W. *Can. J. Chem.* **1985**, *63*, 2555.
(11) Yam, V. W.-W.; Kok-Yan, P.; Cheung, K.-K. *J. Chem. Soc., Chem. Commun.* **1995**, 267.
(12) Zhou, M.; Leung, P.-H.; Mok, K. F.; Hor, T. S. A. *Polyhedron* **1996**, *15*, 1737.
(13) Brown, M. P.; Puddephatt, R. J.; Rashidi, M.; Seddon, K. R. *J. Chem. Soc., Dalton Trans.* **1977**, 951.
(14) Capdevila, M.; González-Duarte, P.; Foces-Foces, C.; Hernandez-Cano, F.; Martínez-Ripoll, M. *J. Chem. Soc., Dalton Trans*. **1990**, 143.
(15) Budzelaar, P. H. M. *gNMR V4.01*; Cherwell Scientific Publishing Ltd.: Oxford, UK, 1997.

Table 3. ESI MS and NMR Data for Complexes **1**−**5** and **7**−**11**

cmpd	*m*/*z*	calcd MW[a]	δP (ppm)	$^1J_{Pt-P}$ (Hz)	δH(SCH_2) (ppm)	$^3J_{Pt-H}$(SCH_2) (Hz)	δC(SCH_2) (ppm)
1	1279.7	1279.13	−0.08[b]	2615[b]			
2	1251.7	1251.18	40.5[c]	2740[c]			
3	1328.2	1328.66	P_A: 2.1[d]	Pt−P_A: 2410[d]	4.19	28	54.6
			P_B: 1.6	Pt−P_B: 3165			
4	1300.0	1300.61	P_A: 46.2	Pt−P_A: 2678	4.10	?	?
			P_B: 45.3	Pt−P_B: 3421			
5	646.7[e]	1293.21					
7	686.4	685.68	−2.25	2705	5.45	37	38.6
8	671.9	671.65	39.4	2824	5.93	34	41.9
9			−3.7	3408			
10			43.4	3610			
11	669.5[e]	1341.31	−0.14	2909	4.19		37.1

[a] Only the neutral or cationic complex species is considered. [b] ^{31}P RMN parameters from the computer simulation for **1**: $\delta P = -0.07$ ppm; $^1J_{Pt-P} = 2612$ Hz; $^2J_{Pt-Pt} = 758$ Hz; $^3J_{Pt-P} = 28$ Hz; $^4J_{P-P} = 22$ Hz. [c] From ref 6. [d] ^{31}P RMN parameters from the computer simulation for **3**: $\delta P_A = 2.0$ ppm; $\delta P_B = 1.7$ ppm; $^1J_{Pt-P(A)} = 2412$ Hz; $^1J_{Pt-P(B)} = 3164$ Hz; $^2J_{Pt-Pt} = 750$ Hz; $^3J_{Pt-P(A)} = 42$ Hz; $^3J_{Pt-P(B)} = 33$ Hz; $^4J_{P(A)-P(A)} = 21$ Hz; $^4J_{P(B)-P(B)} = 23$ Hz; $^4J_{P(A)-P(B)} = 26$ Hz. [e] $M = m/z$ ($z = 2$).

Intensities were integrated from a series of 0.3° ω rotation frames covering at least a hemisphere of reciprocal space and were corrected for absorption and other effects by semiempirical methods based on redundant and symmetry-equivalent reflections.[16]

The structures were solved by direct methods and were refined by full-matrix least-squares on all unique F^2 values, with anisotropic displacement parameters for non-hydrogen atoms and with isotropic H atoms constrained with a riding model.[17] The largest residual electron density peaks were close to Pt atoms in each case. One toluene solvent molecule in the structure of **11** is disordered over an inversion center.

The main bond distances and angles for these complexes are given in Table 5.

Computational Details. Calculations were performed with the GAUSSIAN 98 series of programs.[18] The DFT (density functional theory) was applied with the B3LYP function.[19] Effective core potentials (ECPs) were used to represent the innermost electrons of the platinum atom[20a] as well as the electron core of P, S, and Cl atoms.[20b] The basis set for the metal was that associated with the pseudopotential,[20a] with a standard double-ζ LANL2DZ contraction.[18] The basis set for the P, S, and Cl atoms was that associated with the pseudopotential,[20b] with a standard double-ζ LANL1DZ contraction[18] supplemented with a set of d-polarization functions.[21] A 6-31G basis set was used for the C and H atoms.[22] Solvent effects were taken into account by means of PCM calculations[23] using standard options of PCM and cavity keywords.[18] Free energies of solvation were calculated with CH_2Cl_2 ($\epsilon = 8.93$) as solvent, keeping the geometry optimized for the isolated species (single-point calculations). Very recently, this approach has been successfully applied to the study of bimetallic polysulfides $Cp_2Fe_2S_4$.[24]

Results and Discussion

Experimental Study of the Reaction Pathway from 1 to 9 and 11, and from 2 to 8 and 10. The first information obtained on the reaction of [(dppp)Pt(μ-S)$_2$Pt(dppp)] (**1**) in CH_2Cl_2 (Scheme 1) was the series of ^{31}P NMR spectra recorded as a function of time (Figure 1). They indicated that **1** evolved to [(dppp)Pt(μ-S)(μ-SCH_2Cl)Pt(dppp)]Cl (**3**), which immediately transformed into a mixture of [Pt(dppp)(S_2CH_2)] (**7**) and [Pt(dppp)Cl_2] (**9**). Then, while the latter remained unchanged, **7** disappeared to give rise to [Pt_2(dppp)$_2$\{μ-(SCH_2SCH_2S)-*S*,*S*′\}]Cl_2 (**11**). However, the apparent complexity of this process together with the simultaneous presence of several species throughout the time since the exposure of **1** to CH_2Cl_2 made it necessary to obtain ^{1}H and ^{13}C NMR and ESI MS complementary data. NMR parameters and ESI-MS mass determinations for compounds **1**−**11** are shown in Table 3.

The ^{31}P NMR spectrum of **1** shows the same features as that of **2** already reported,[6] in good concordance with their similar structures in the solid phase.[5] In **1** and **2**, all the ^{31}P nuclei show the same chemical shift but are not magnetically equivalent. Interpretation of these spectra with the aid of computer simulations requires consideration of second-order effects due to $^2J_{Pt-Pt}$, $^3J_{Pt-P}$, and $^4J_{P-P}$ couplings. On the basis of ^{1}H and ^{13}C DEPT135 NMR data, it was reasonable to assume that the first species formed as a result of the

(16) Sheldrick, G. M. *SADABS*; Bruker AXS: Madison, WI, 1997.
(17) Sheldrick, G. M. *SHELXTL*, Version 5; Bruker AXS: Madison, WI, 1994.
(18) Frisch, M. J.; Trucks, G. W.; Schlegel, H. B.; Scuseria, G. E.; Robb, M. A.; Cheeseman, J. R.; Zakrzewski, V. G.; Montgomery, J. A., Jr.; Stratmann, R. E.; Burant, J. C.; Dapprich, S.; Millam, J. M.; Daniels, A. D.; Kudin, K. N.; Strain, M. C.; Farkas, O.; Tomasi, J.; Barone, V.; Cossi, M.; Cammi, R.; Mennucci, B.; Pomelli, C.; Adamo, C.; Clifford, S.; Ochterski, J.; Petersson, G. A.; Ayala, P. Y.; Cui, Q.; Morokuma, K.; Malick, D. K.; Rabuck, A. D.; Raghavachari, K.; Foresman, J. B.; Cioslowski, J.; Ortiz, J. V.; Stefanov, B. B.; Liu, G.; Liashenko, A.; Piskorz, P.; Komaromi, I.; Gomperts, R.; Martin, R. L.; Fox, D. J.; Keith, T.; Al-Laham, M. A.; Peng, C. Y.; Nanayakkara, A.; Gonzalez, C.; Challacombe, M.; Gill, P. M. W.; Johnson, B. G.; Chen, W.; Wong, M. W.; Andres, J. L.; Head-Gordon, M.; Replogle, E. S.; Pople, J. A. *Gaussian 98*, revision A.6; Gaussian, Inc.: Pittsburgh, PA, 1998.
(19) (a) Lee, C.; Yang, W.; Parr, R. G. *Phys. Rev.* **1988**, *B37*, 785. (b) Becke, A. D. *J. Chem. Phys.* **1993**, *98*, 5648. (c) Stephens, P. J.; Delvin, F. J.; Chabalowski, C. F.; Frisch, M. J. *J. Phys. Chem.* **1994**, *98*, 11623.
(20) (a) Hay, P. J.; Wadt, W. R. *J. Chem. Phys.* **1985**, *82*, 299. (b) Wadt, W. R.; Hay, P. J. *J. Chem. Phys.* **1985**, *82*, 284.
(21) Höllwarth, A.; Böhme, M.; Dapprich, S.; Ehlers, A. W.; Gobbi, A.; Jonas, V.; Köhler, K. F.; Stegman, R.; Veldkamp, A.; Frenking, G. *Chem. Phys. Lett.* **1993**, *208*, 237.
(22) Hehre, W. J.; Ditchfield, R.; Pople, J. A. *J. Chem. Phys.* **1972**, *56*, 2257.
(23) (a) Tomasi, J.; Persico, M. *Chem. Rev.* **1994**, *94*, 2027. (b) Amovilli, C.; Barone, V.; Cammi, R.; Cancès, E.; Cossi, M.; Mennucci, B.; Pomelli, C. S.; Tomasi, J. *Adv. Quantum Chem.* **1998**, *32*, 227.
(24) Blasco, S.; Demachy, I.; Jean, Y.; Lledós, A. *New J. Chem.* **2001**, *25*, 611.

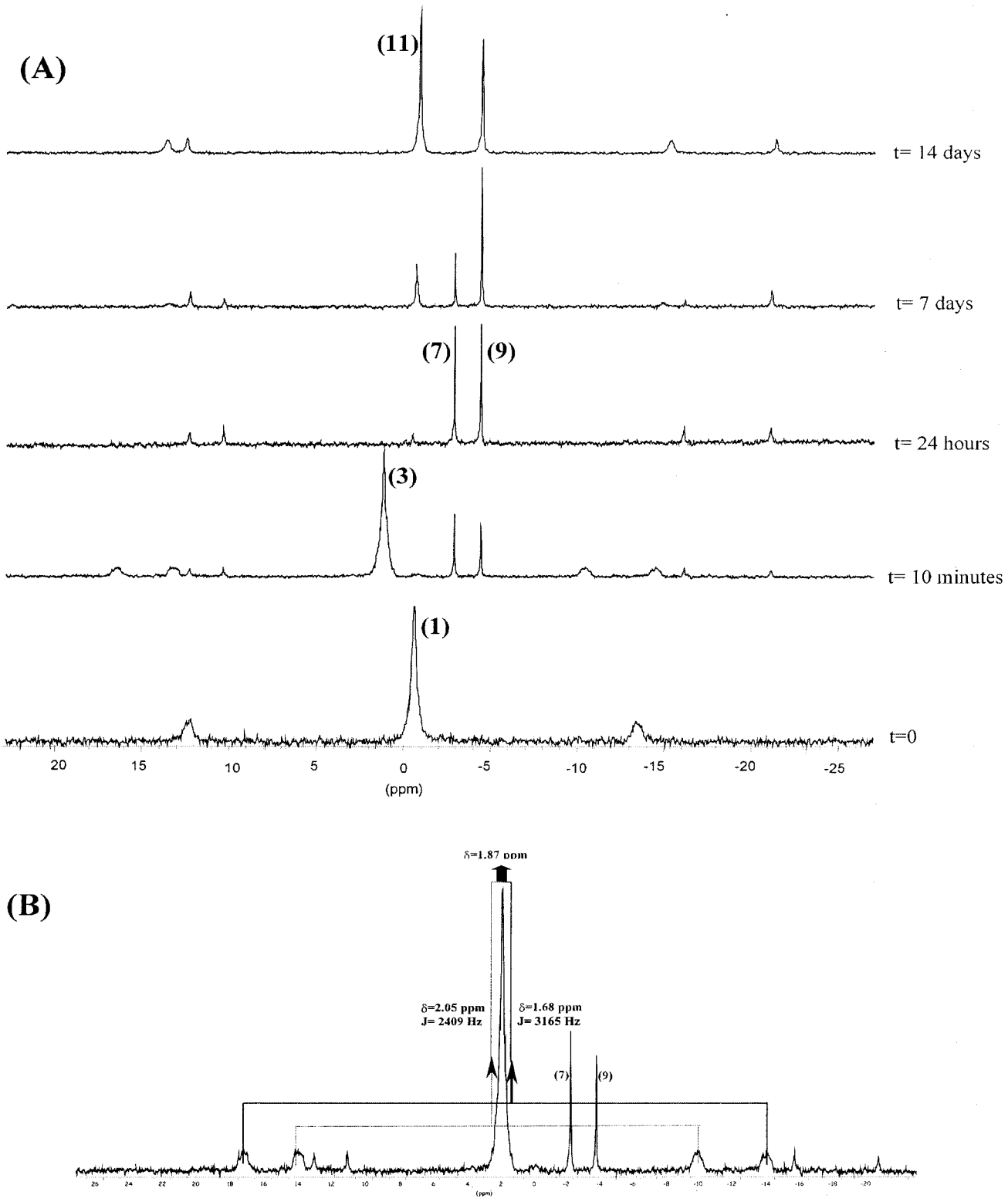

Figure 1. (A) Progression of **1** in CH_2Cl_2 as a function of time monitored by $^{31}P\{^1H\}$ NMR. Spectra of the different aliquots were recorded in d_6-DMSO. (B) Analysis of the $^{31}P\{^1H\}$ NMR spectra of **3**.

nucleophilic attack of **1** to CH_2Cl_2 solvent involved the binding of one CH_2Cl fragment to a sulfide bridge while the remaining chloride behaved as a counterion. ESI MS data clearly confirmed that the new species, **3**, could be formulated as [**1**.CH_2Cl]Cl (molecular weight of the cation of **3**, 1328.66). Its ^{31}P NMR spectrum consisting of only one signal with four satellites was indicative of the asymmetry of **3**, thus corroborating the attack of only one CH_2Cl_2 molecule. This spectrum, which is comparable to that reported for the analogue with PPh_3 as terminal ligand,[8] could be interpreted by considering that the two chemically nonequivalent ^{31}P nuclei in **3** show a very close chemical shift but different $^1J_{Pt-P}$ values. This difference could be attributed to the different nature and thus trans influence of the bridging S^{2-}

or SCH_2Cl^- ligands. The chemical shift values δP_A and δP_B were taken as the midpoint between the two satellites corresponding to the $^1J_{Pt-P(A)}$ and $^1J_{Pt-P(B)}$ couplings, respectively (Figure 1). These δP_A, δP_B, $^1J_{Pt-P(A)}$, and $^1J_{Pt-P(B)}$ values were used for a full computer simulation, which allowed a good match with the experimental spectrum.

ESI MS determinations not only led to the identification of [(dppp)Pt(μ-S_2CH_2)Pt(dppp)]Cl_2, **5** (molecular weight of its cation, 1293.21), which was undetected by NMR measurements run in parallel, but also evidenced the coexistence in solution of **1**, **3**, **5**, and **7**. The ^{31}P NMR spectra of the subsequent species formed, **7** and **9**, were consistent with a first-order analysis and showed only one chemical shift for each complex. This indicated that all the respective phosphorus nuclei were chemically and magnetically equivalent in solution. Further reaction of **7** affords **11**. On the basis of the whole set of the spectroscopic data obtained for **11** (ESI MS, ^{1}H, ^{13}C and ^{31}P NMR), it was possible to determine its structure, which would otherwise involve a second-order ^{31}P NMR spectrum. However, in this complex, the second-order effects appear to be small, and the ^{31}P NMR spectrum allows a first-order analysis. In addition, the only chemical shift that is observed in this spectrum at room temperature indicates a fast flipping of the thioether sulfur atom. ^{1}H and ^{13}C NMR data suggested that **7** and **11** included $(SCH_2S)^{2-}$ or $(SCH_2SCH_2S)^{2-}$ groups, respectively. The observation that the ^{31}P NMR parameters for **9** were coincident with those of the precursor of **1** led to its identification as the mononuclear [Pt(dppp)Cl_2] species.[13,25]

Analogous to **1**, the reaction of [(dppe)Pt(μ-S)$_2$Pt(dppe)] (**2**) with CH_2Cl_2 (Scheme 1) was followed by means of ^{31}P NMR spectra recorded as a function of time (Figure 2) and additional ^{1}H and ^{13}C NMR data and ESI MS measurements. The synthesis, X-ray structure, and NMR parameters of **2** have already been reported.[5,6] The subsequent ^{31}P NMR spectra evidenced that **2** afforded [(dppe)Pt(μ-S)(μ-SCH_2-Cl)Pt(dppe)]Cl (**4**), which transformed into a mixture of [Pt(dppe)(S_2CH_2)] (**8**) and [Pt(dppe)Cl_2] (**10**). Complexes **8** and **10** do not react further even if they are mixed at a 1:2 mole ratio, which is the appropriate stoichiometric molar ratio to obtain [$Pt_3(\mu_3$-S)$_2$(dppe)$_3$]Cl_2, **12**, already reported.[6] This complex is obtained from a solution of **2** in either CH_2Cl_2 or $CHCl_3$ containing traces of HCl.

Unlike **3**, the ^{31}P NMR spectrum of **4** showed two different chemical shifts corresponding to two chemically inequivalent phosphorus atoms, as already reported for a closely related species containing dppf, [Fe($C_5H_4PPh_2$)$_2$], instead of dppe as terminal ligand.[9] The ^{31}P NMR spectrum allowed determination of the coupling constants involving not only P−Pt ($^1J_{Pt-P(A)}$, $^1J_{Pt-P(B)}$) but also P−P ($^4J_{P(A)-P(B)}$) nuclei, as shown in Table 3. However, at room temperature, the conversion from **2** to **8** and **10** occurred in 2 h and thus hampered recording the ^{13}C NMR spectrum of **4** and determining neither the mass nor the NMR spectral features of the possible intermediate species [(dppe)Pt(μ-S_2CH_2)Pt(dppe)]-Cl_2 (**6**). While the ^{31}P NMR parameters for **10** coincided with those of [Pt(dppe)Cl_2], already known as a precursor of **2**, complex **8** could be fully characterized as indicated later. Analogously to complexes **7** and **9**, the ^{31}P NMR spectra of **8** and **10** were consistent with a first-order analysis.

Overall, the first stages of the reaction of **1** or **2** with CH_2-Cl_2 proceed at different rates but follow a common pathway, independent of the diphosphine nature, to give a mixture of two mononuclear complexes **7** and **9** or **8** and **10**. However, only in the case of dppp, the reaction does not stop at this point, but there is a second electrophilic attack of CH_2Cl_2 on the thiolate sulfur of **7** to afford the final unprecedented complex **11**. These results indicate that dppp confers a greater nucleophilicity to the sulfur atoms and are consistent with the information obtained by theoretical calculations. The proposed pathway is corroborated by the X-ray structures of **1**, **7**, and **11** (**8** only a qualitative analysis), which are in good concordance with NMR data in solution, and by the crystal structures of **2** and **12** previously reported.[5,6]

Theoretical Study of the Pathway from Bimetallic (1, 2) to Mononuclear Complexes (7, 9 and 8, 10). We have performed DFT calculations in order to determine the structural features of the intermediates and to obtain an energetic picture of the process. In the calculations we have modeled dppp and dppe real ligands by $H_2P(CH_2)_3PH_2$ (dhpp) and $H_2P(CH_2)_2PH_2$ (dhpe), respectively. Thus, the different species are labeled with the same number as the parent compound but with an additional t. Their main geometric parameters are collected in Table 4. The calculated structures agree with the analogous products structurally characterized in this work and with other related complexes reported in the literature.[7b,26−29]

The analysis of the NPA (natural population analysis) charges indicates that the sulfides in the dhpp containing compounds have a slightly more negative charge than those with dhpe. This is a consequence of the greater positive charge supported by the dhpp ligand. Thus, sulfides in **1t** appear to be more nucleophilic than in **2t**. The same feature has been found for all the species from **1t** to **7t** if compared with those from **2t** to **8t**.

The changes in the PPtP angle for both bidentate ligands along the reaction pathway deserve further analysis. Data in Table 4 show that the changes on the PPtP angle for the dhpe ligands are small (from 85.0° in **6t** to 88.4° in **10t**) but substantial in the case of dhpp (from 91.4° in **5t** to 98.5° in **9t**). Moreover, PPtP angles in dhpp are always closer to the values found for unidentate, unconstrained systems. As a consequence, dhpp appears to be more flexible, and the corresponding complexes less strained than those with dhpe. This fact may be the origin of the observed greater reactivity

(25) (a) Robertson, G. B.; Wickramasinghe, W. A. *Acta Crystallogr., Sect. C* **1987**, *43*, 1694. (b) Farrar, D. H.; Ferguson, G. *J. Crystallogr. Spectrosc. Res.* **1982**, *12*, 465.

(26) Bos, W.; Bour, J. J.; Schlebos, P. P. J.; Hageman, P.; Bosman, W. P.; Smits, J. M. M.; van Wietmarschen, J. A. C.; Beurskens, P. T. *Inorg. Chim. Acta* **1986**, *119*, 141.

(27) Forniés-Càmer, J.; Masdeu-Bultó, A. M.; Claver, C.; Cardir, C. J. *Inorg. Chem.* **1998**, *37*, 2626.

(28) Masdeu-Bultó, A. M.; Ruiz, A.; Castillón S.; Claver, C.; Hitchcook, P. B.; Chaloner, P. A.; Bo, C.; Poblet, J. M.; Sarasa, P. *J. Chem. Soc., Dalton Trans.* **1993**, 2689.

(29) Elduque, A.; Finestra, C.; López, J. A.; Lahoz, F. J.; Merchán, F.; Oro, L. A.; Pinillos, M. T. *Inorg. Chem.* **1998**, *37*, 824.

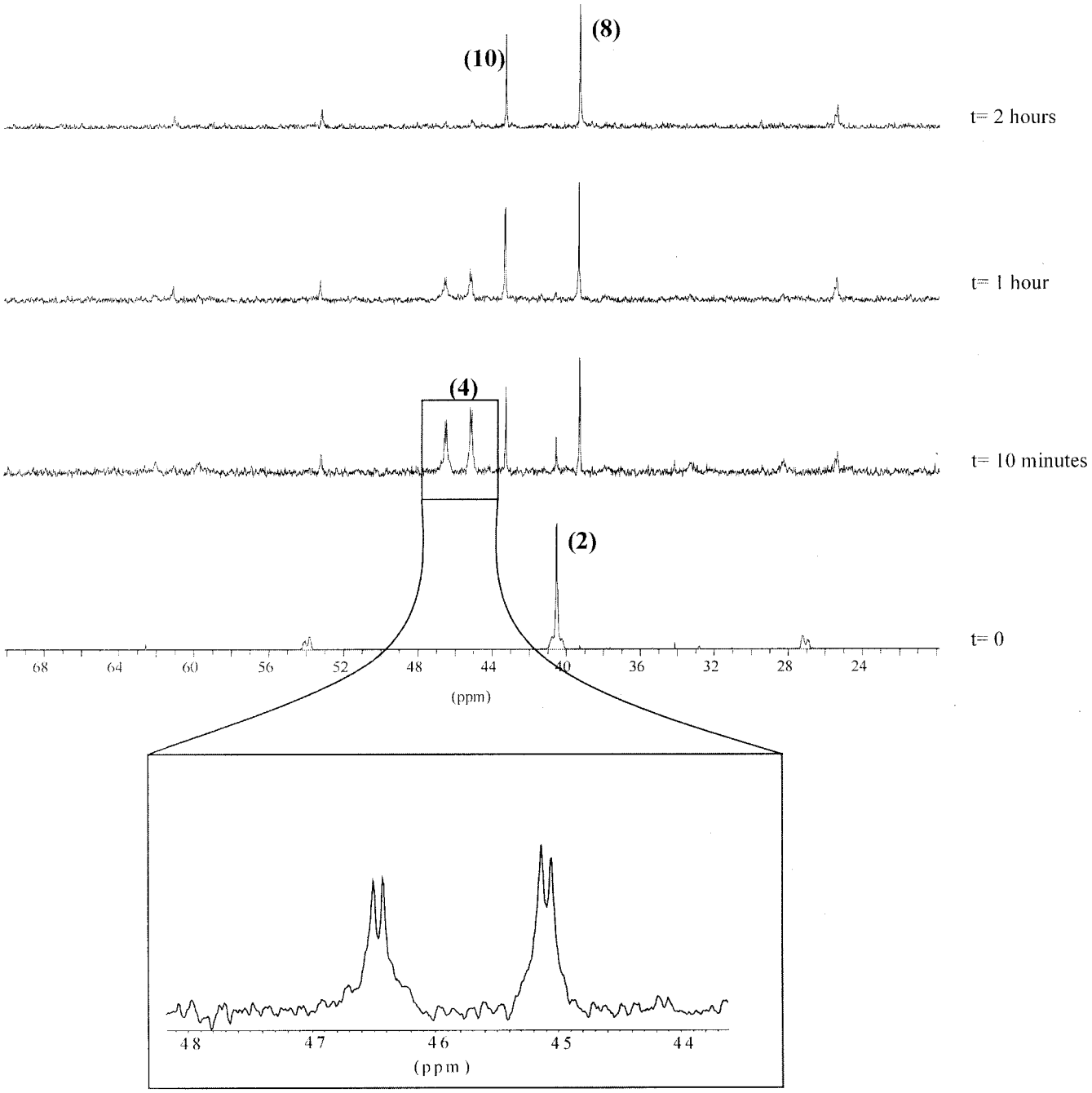

Figure 2. Progression of **2** in CH_2Cl_2 as a function of time monitored by $^{31}P\{^1H\}$ NMR. Spectra of the different aliquots were recorded in d_6-DMSO.

of the dppe containing species compared to those containing dppp. The influence of the bite angle of diphosphine ligands on the stability and catalytic behavior of metal complexes has been reviewed recently.[30]

Moreover, we have calculated the thermodynamics of the different steps of the reaction of **1t** or **2t** with dichloromethane by means of the polarizable continuum model (PCM).[23] If taking **1t** + CH_2Cl_2 and **2t** + CH_2Cl_2 as the zero of energy, the first intermediates, (**3t** + Cl^-) and (**4t** + Cl^-), are found 0.5 and 1.6 kcal/mol, respectively, above the corresponding reactants, whereas the second intermedi-

(30) Dierkes, P.; van Leeuwen, P. W. N. M. *J. Chem. Soc., Dalton Trans.* **1999**, 1519.

Table 4. Most Important Geometric Parameters[a] of the Optimized Structures **1t**−**10t**

structure	Pt−S	Pt−P	Pt···Pt	S···S	Pt−S−Pt	S−Pt−S	θ^b	P−Pt−P
1t	2.406	2.293	3.286	3.228	86.1	84.2	147.7	95.8
2t	2.399	2.299	3.301	3.216	87.0	84.2	148.9	86.6
3t	2.392	2.289	3.386	3.226	90.0	83.4	138.4	93.6
	2.458	2.336			87.1			
4t	2.400	2.282	3.331	3.087	87.9	79.3	126.9	86.0
	2.438	2.335			86.2			
5t	2.476	2.317	3.260	2.840	82.3	70.0	106.9	91.4
6t	2.470	2.318	3.251	2.842	82.3	70.2	107.1	85.0
7t	2.380	2.313		2.933		76.1		92.8
8t	2.376	2.317		2.928		76.1		85.6
9t		2.257						98.5
10t		2.253						88.4

[a] Distances in angstroms; angles in degrees. [b] Dihedral angle between the two PtS_2 planes.

ates, (**5t** + 2Cl$^-$) and (**6t** + 2Cl$^-$), lie 43.7 and 44.4 kcal/mol, respectively, above the reactants. Monometallic complexes are considerably stabilized: 27.2 kcal/mol (**7t** + **9t**) and 26.5 kcal/mol (**8t** + **10t**) below the reactants. ΔG values obtained for the second intermediates (more than 40 kcl/mol) are hardly compatible with their experimental detection at room temperature. However, the numerical values of the relative energies in solution of species differently charged (0 for the reactants, +1 and −1 for the first intermediate, and +2 and −2 for the second one) can only be given a semiquantitative significance. Calculations with inclusion of solvent effects cannot be given the same accuracy as those in the gas phase. When using the continuum model for the solvent, as in the PCM method, energies are dependent on the atomic radii used to define the cavity. This is especially important for charged species of small size as the Cl$^-$ anion. Even though this model hinders a quantitative determination of the energies of the charged species, the reaction profile obtained allows the following conclusions: (i) The driving force for the reaction is the greater stability of the two mononuclear compounds, **7t** and **9t** or **8t** and **10t**, with respect to the corresponding reactants, **1t** or **2t**, by more than 25 kcal/mol. (ii) The stabilities of the two intermediates in each of both reaction pathways are manifestly different. Whereas the first intermediate has almost the same free energy as the initial species, the second one appears as significantly more unstable. Thus, the formation of the second intermediate must be the rate-limiting step for the process.

Study of the Reaction Mechanism from 7 to 11. The synthesis of **11** from **7** allowed characterization of the former by X-ray, mass measurements, and corresponding NMR parameters in solution (Table 3). The stoichiometric molar ratio of **7** to CH_2Cl_2 in the reaction leading to **11** is 2:1. This fully confirmed that the molar ratio of **9** to **11** in the final solution obtained upon exposure of **1** in CH_2Cl_2 is 2:1, as observed by NMR data. Complex **7** is stable in acetonitrile, acetone, and methanol solvents even under open atmosphere. However, upon exposure of **7** to CH_2Cl_2, it converts to the final complex, **11**. On one hand, the complete characterization of **7** allowed confirmation of its existence as an intermediate species in the reaction of **1** with CH_2Cl_2 to give **9** and **11** (Scheme 1). On the other, the direct synthesis of **11** by reacting **7** with CH_2Cl_2 evidenced its involvement in this reaction. This finding, and comparison of the structures of **7** and **11**, raises the question of the source of the CH_2 groups that participate in the expansion of the $(SCH_2S)^{2-}$ ligand in **7** to afford the bridging $(SCH_2SCH_2S)^{2-}$ ligand in **11**. On the basis of all these data, we thought that replacement of CH_2Cl_2 by CD_2Cl_2 in the synthesis of **11** from **7** could cast light on the origin of these CH_2 groups as well as the mechanism involved in this reaction.

The reaction of **7** with CD_2Cl_2 was carried out by an analogous procedure to that followed for the synthesis of **11**, and the solid obtained, **11′**, was analyzed by means of the corresponding ^{1}H, ^{2}H, and ^{31}P NMR spectra. The ^{31}P NMR parameters for **11′** were coincident with those of **11** (Table 3), thus confirming that the same reaction had taken place. However, the comparison of the ^{1}H NMR spectra of **11′** and **11** indicated that the signal at 4.2 ppm, which is due to the protons of the $(SCH_2SCH_2S)^{2-}$ ligand, decreased by about 25% if the synthesis was run in CD_2Cl_2 instead of CH_2Cl_2. Also, in the ^{2}H NMR spectrum, there was only one signal at 4.3 ppm, thus indicating the insertion of the CD_2 group in the bridging ligand. These data showed that one-fourth of the protons in the $(SCH_2SCH_2S)^{2-}$ ligand had been replaced by deuterium. This allows the conclusion that for each pair of **11** formed, one species contains $(SCH_2SCH_2S)^{2-}$ and the other $(SCH_2SCD_2S)^{2-}$ as bridging ligands. Or, when the reaction is run in CH_2Cl_2 to give $[Pt_2(dppp)_2\{\mu$-(SCH_2SCH_2S)-$S,S'\}]Cl_2$ (**11**), one-fourth of the CH_2 groups of the bridging ligand comes from the CH_2Cl_2 solvent and three-fourths from the starting material, [Pt(dppp)(S_2CH_2)] (**7**). All these observations are consistent with the reaction mechanism proposed in Scheme 2.

Accordingly, the first step in the reaction of **7** with CD_2Cl_2 to give **11′**, which comprises species **E** and **E′**, involves the electrophilic attack of a CD_2Cl_2 molecule on one sulfur atom of the dithiolate $(SCH_2S)^{2-}$ ligand in **7**. Then, cleavage of the {PtS_2C} ring in the intermediate species **A** yields a mononuclear species **B**. This includes two $(SCX_2Cl)^-$ terminal ligands, one with X = H and the other with X = D. Although **B** has not been detected in this work, analogues with PPh_3[9] and dppf[12] have been reported previously. Both $(SCX_2Cl)^-$ (X = H or D) groups in **B** are capable of carrying out an electrophilic attack on a second molecule of **7**, but only if this is done by $(SCD_2Cl)^-$ will the CD_2 fragment from the initial CD_2Cl_2 molecule be inserted into the final complex. Thus, the attack of **B** on **7** gives rise to the intermediate species **C** and **C′** where the formation of the $(SCH_2SCX_2S)^{2-}$ (X = H, D) ligand is already apparent. The loss of the SCX_2 fragment, which can afford possible oligomeric forms,[31] triggers formation of the intermediate **D** and **D′** species. The former was detected by ESI MS in the reaction of **7** with the CH_2Cl_2 solvent. An internal rearrangement of the Pt−S bonds in **D** and **D′** yields the final species **E** and **E′**, where the $(SCH_2SCX_2S)^{2-}$ ligand bridges two {Pt(dppp)} units. Overall, the proposed mechanism (Scheme 2) accounts for the inherent ability of **7** to react with the CH_2Cl_2 solvent and gives an insight into the source of the CH_2 groups, which give rise to the $(SCH_2SCH_2S)^{2-}$ ligand in the unprecedented complex **11**.

The fact that none of the intermediate species involved in the reaction mechanism is observed by ^{31}P NMR suggests that the evolution from **7** to **A** is the rate determining step. To confirm this assumption, the reaction of **7** at different concentrations in CH_2Cl_2 was monitored by ^{31}P NMR. These data were in good agreement with a pseudo-first-order rate law, and the calculated rate constant (9.8×10^{-3} h^{-1}) was independent of the initial concentration of **7**.

Molecular Structures. The crystal structure of complex **1** consists of neutral dinuclear [(dppp)Pt(μ-$S)_2$Pt(dppp)] species devoid of crystallographic symmetry elements, and acetone solvent molecules. Both types of molecules have only

(31) Schmidt, M.; Weissflog, E. *Angew. Chem., Int. Ed. Engl.* **1977**, *17*, 51.

Scheme 2

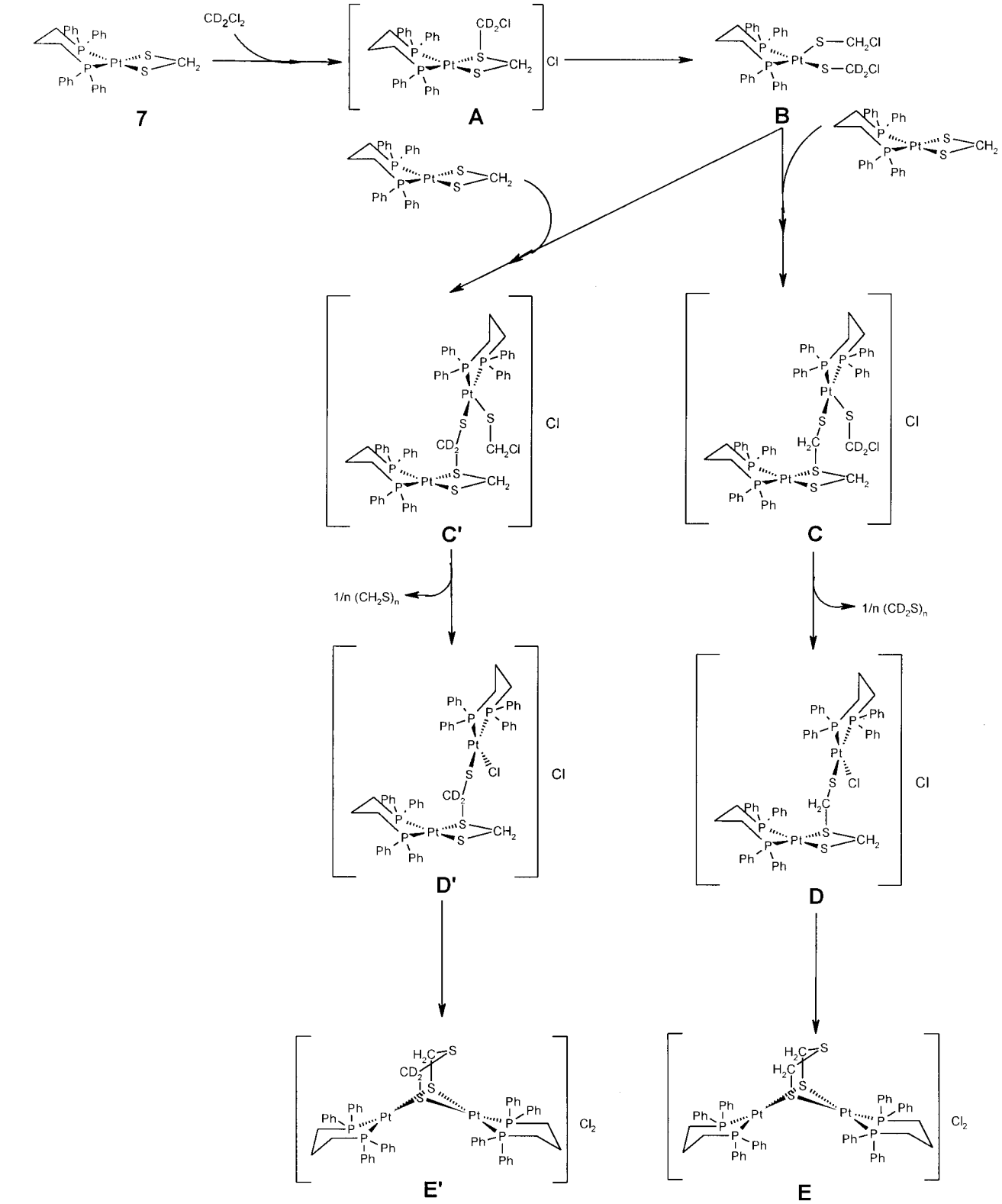

normal van der Waals interactions. Main geometric parameters for **1** (Figure 3) are given in Table 5. Each molecule shows a hinged $\{Pt_2S_2\}$ central ring, dihedral angle θ = 134.8°, with the two platinum atoms bridged by two sulfide anions, coordination being completed by chelating dppp ligands. Ignoring the phenyl rings and the H atoms of the aliphatic carbon chains, the idealized symmetry of the $\{C_3P_2Pt(\mu\text{-}S)_2PtP_2C_3\}$ core is C_{2v}. It can be considered as formed by three rings, the central $\{Pt_2S_2\}$ one fused to two other PtP_2C_3, which give rise to a butterfly structural type. Both PtP_2C_3 rings show a distorted chair conformation. The geometries at the individual Pt sites are approximately square planar, deviations from planarity being less than 0.08 Å, and the Pt−S and Pt−P bond distances agree well with those

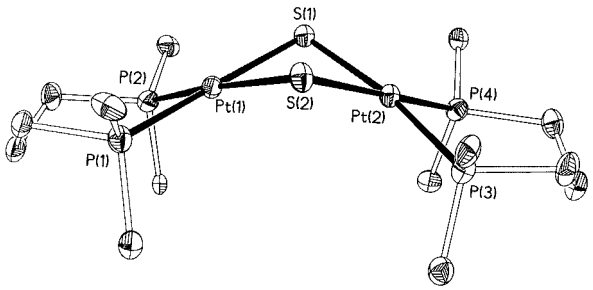

Figure 3. Molecular structure of complex **1** with key atoms labeled and with 50% probability ellipsoids. H atoms, phenyl rings, and the acetone solvent molecule are omitted.

Table 5. Selected Bond Lengths (Å) and Angles (deg) for Complexes **1**, **7**, and **11**

	Complex **1**		
Pt(1)−S(1)	2.3505(13)	Pt(2)−S(1)	2.3318(14)
Pt(1)−S(2)	2.3392(14)	Pt(2)−S(2)	2.3379(14)
Pt(1)−P(1)	2.2704(14)	Pt(2)−P(3)	2.2342(15)
Pt(1)−P(2)	2.2566(15)	Pt(2)−P(4)	2.2546(15)
S(1)−Pt(1)−S(2)	82.80(5)	S(1)−Pt(2)−S(2)	83.24(5)
P(1)−Pt(1)−P(2)	94.77(5)	P(3)−Pt(2)−P(4)	94.59(5)
Pt(1)−S(1)−Pt(2)	87.40(4)	Pt(1)−S(2)−Pt(2)	87.52(4)
	Complex **7**		
Pt(1)−S(1)	2.3214(8)	Pt(1)−S(2)	2.3281(8)
Pt(1)−P(1)	2.2596(8)	Pt(1)−P(2)	2.2558(8)
S(1)−C(30)	1.840(4)	S(2)−C(30)	1.842(4)
S(1)−Pt(1)−S(2)	76.85(3)	P(1)−Pt(1)−P(2)	92.18(3)
Pt(1)−S(1)−C(30)	89.96(12)	Pt(1)−S(2)−C(30)	89.70(11)
S(1)−C(30)−S(2)	103.36(17)		
	Complex **11**		
Pt(1)−S(1)	2.3693(14)	Pt(2)−S(1)	2.3688(14)
Pt(1)−S(2)	2.3791(14)	Pt(2)−S(2)	2.3850(14)
Pt(1)−P(1)	2.2697(16)	Pt(2)−P(3)	2.2738(15)
Pt(1)−P(2)	2.2710(15)	Pt(2)−P(4)	2.2702(14)
S(1)−C(1)	1.843(6)	S(2)−C(2)	1.854(6)
S(3)−C(1)	1.797(7)	S(3)−C(2)	1.783(6)
S(1)−Pt(1)−S(2)	82.56(5)	S(1)−Pt(2)−S(2)	82.45(5)
P(1)−Pt(1)−P(2)	90.44(6)	P(3)−Pt(2)−P(4)	92.39(5)
Pt(1)−S(1)−Pt(2)	86.94(5)	Pt(1)−S(2)−Pt(2)	86.35(5)
Pt(1)−S(1)−C(1)	102.0(2)	Pt(2)−S(1)−C(1)	106.2(2)
Pt(1)−S(2)−C(2)	101.4(2)	Pt(2)−S(2)−C(2)	106.6(2)
S(1)−C(1)−S(3)	117.9(3)	S(2)−C(2)−S(3)	117.2(3)
C(1)−S(3)−C(2)	102.0(3)		

found in dppe analogue **2**.[5] Considering the average values of the angles about the Pt atoms, the more important deviations from the ideal value correspond to P−Pt−P (94.6°) and S−Pt−S (83.0°).

The very few structurally characterized examples with a similar core to that of **1** are the $[Pt_2(dppy)_2(\mu\text{-}S)_2]$ (dppy = 2-diphenylphosphinopyridine)[11] and $[Pt_2(dppe)_2\mu\text{-}S)_2]$ (**2**)[5] complexes and the incompletely determined X-ray structure of $[Pt_2(PMe_2Ph)_4(\mu\text{-}S)_2]$.[1] Comparison of their main geometric parameters (Table 6) indicates that the most significant difference lies in the dihedral angle between the two PtS_2 planes and that a decrease in this angle entails a concomitant shortening of the Pt···Pt and smaller changes in the S···S distances.

Complexes **7** and **8** are structurally related as they both consist of mononuclear $[Pt(P\cap P)(S_2CH_2)]$ (P∩P = dppp (**7**) (Figure 4) or dppe (**8**) discrete molecules devoid of crystallographic symmetry elements. In the case of **7**, there is one

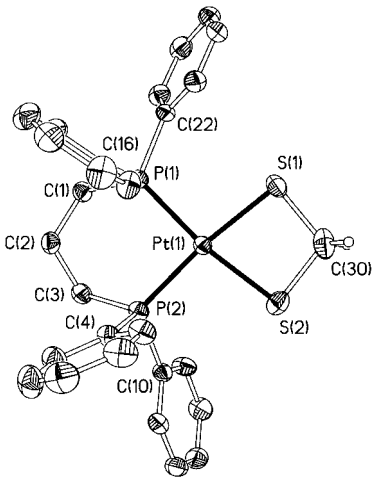

Figure 4. Molecular structure of complex **7** with key atoms labeled and with 50% probability ellipsoids. H atoms and the acetonitrile solvent molecule are omitted.

CH_3CN molecule in each formula unit. The listing of the main geometric parameters for **7** appears in Table 5. The structure can be considered as formed by two fused rings that share a platinum atom. The four-membered PtS_2C ring, which includes the chelating $[SCH_2S]^{2-}$ ligand, is essentially planar, deviations from planarity being less than 0.03 Å. The C_3P_2Pt ring includes six atoms and shows a chair conformation. The platinum atom has square planar coordination, distorted by a significant reduction of the S−Pt−S angle (76.8°) from ideal 90°, and by a twist of 5.0° between the PtS_2 and PtP_2 planes. The bite angle of the diphosphine ligand, 92.1°, dictates the values of the remaining P−Pt−S angles about the platinum atom. The structure of **8**, established qualitatively from a crystal of inferior quality, is similar in its major aspects, having one fewer C atom in the chelate ring.

Complexes of general formula $[L_2Pt(S_2CH_2)]$ with similar structure to **7** and **8** amount to only two examples, $[Pt(PMe_2Ph)_2(S_2CH_2)]$[10] and $[Pt(dppy)_2(S_2CH_2)]$,[11] both with unidentate phosphine ligands. Comparison of these complexes shows remarkable similarities, and particularly, the geometric features of their PtS_2C rings are practically identical (Table 6). Obviously, the structures differ in the P−Pt−P angles, which range from 92.2° to 100.6° (leaving out the smaller angle in **8**), but these differences have no apparent effect on the structural parameters involving the neighboring PtS_2C ring. Concerning the Pt(P∩P) moieties, their geometric features are in good concordance with those observed in **1** and **2**, respectively, as well as in $[Pt(dppp)Cl_2]$ and $[Pt(dppe)Cl_2]$ complexes known[13,25] and related species.[30]

The structure of **11** is totally unprecedented (Figure 5) and consists of dinuclear $[(dppp)Pt(\mu\text{-}SCH_2SCH_2S)Pt(dppp)]^{2+}$ cations and Cl^- counterions, together with toluene solvent molecules. Selected bond angles and distances are given in Table 5. The cation has approximate mirror symmetry. It can be described as formed by a $\{(dppp)Pt(\mu\text{-}S)_2Pt(dppp)\}$ core capped by a CH_2SCH_2 fragment, which lowers the approximate core symmetry from C_{2v} to C_s. The core shows a hinged Pt_2S_2 central ring with the two platinum atoms bridged by two thiolate sulfurs, coordination being completed

Table 6. Main Geometric Parameters[a] of the $\{Pt_2S_2\}$ and $\{PtS_2C\}$ Fragments in Structurally Characterized Complexes

complex	Pt−S	Pt−P	C−S	S−C−S	Pt···Pt	S···S	Pt−S−Pt	S−Pt−S	θ[b]	P−Pt−P	ref
$[Pt_2(dppy)_4(\mu\text{-}S)_2]$	2.33	2.28			3.55	3.01	99.6	80.4	180	102.9	11
$[Pt_2(dppe)_2(\mu\text{-}S)_2]$ (**2**)	2.35	2.24			3.29	3.13	88.9	83.7	140.2	86.2	5
$[Pt_2(dppp)_2(\mu\text{-}S)_2]$ (**1**)	2.34	2.25			3.23	3.10	87.5	83.0	134.8	94.7	*c*
$[Pt_2(PMe_2Ph)_4(\mu\text{-}S)_2]$[d]	2.34	2.26			3.17		85.5	81.6	121		1
$[Pt(dppy)_2(S_2CH_2)]$	2.31	2.27	1.82	103.0				76.2		100.6	11
$[Pt(PMe_2Ph)_2(S_2CH_2)]$	2.30	2.25	1.83	102.1				76.1		94.3	10
$[Pt(dppp)(S_2CH_2)]$ (**7**)	2.32	2.26	1.84	103.4				76.9		92.2	*c*
$[Pt(dppe)(S_2CH_2)]$ (**8**)[d]	2.32	2.27	1.84	102.0				76.2		85.4	*c*

[a] Distances in angstroms; angles in degrees. [b] Dihedral angle between the two PtS_2 planes. [c] This work. [d] Only preliminary crystallographic data.

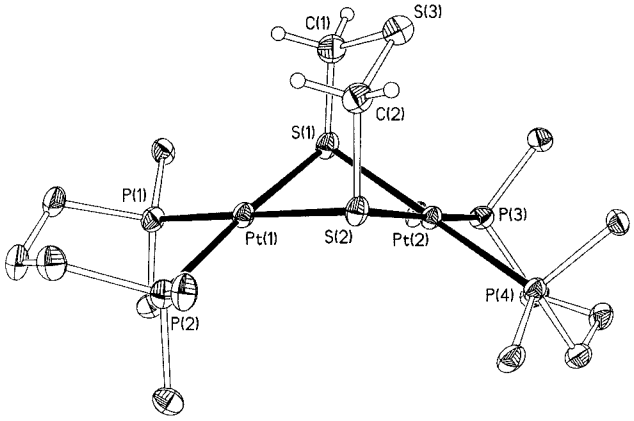

Figure 5. Structure of the cation of complex **11** with key atoms labeled and with 50% probability ellipsoids. H atoms, chloride anions, phenyl rings, and toluene solvent molecules are omitted.

by chelating dppp ligands. The dihedral angle between PtS_2 planes, $\theta = 131.7°$, is smaller than that found in the parent $[(dppp)Pt(\mu\text{-}S)_2Pt(dppp)]$ complex **1** ($\theta = 134.8°$), this reduction being less significant than that experienced by the dppe analogue **2** when acting as a metalloligand.[6] The geometries at the individual Pt sites are essentially square planar, the main distortions being due to the reduction of the S−Pt−S angles from ideal 90° (average 82.5°), and by a twist of 3.6° between the $Pt(1)S_2$ and $Pt(1)P_2$ planes and of 1.3° between $Pt(2)S_2$ and $Pt(2)P_2$. The bite angle of the diphosphine ligand involving Pt(1) (90.4°) and Pt(2) (92.4°) compares well with those found in the parent complex (**1**).

The capping CH_2SCH_2 unit can be considered within the bridging $[SCH_2SCH_2S]^{2-}$ ligand, which, according to the angles about S(1) [Pt(1)−S(1)−C(1) 102.0°; Pt(1)−S(2)−C(2) 101.4°] and S(2) [Pt(2)−S(1)−C(1) 106.2°; Pt(2)−S(2)−C(2) 106.6°], is slightly tilted toward Pt(1) while the thioether S(3) atom is clearly oriented toward Pt(2), the C(1)−S(3)−C(2) angle being 102.0°.

The main novelty of this complex is that no other structure containing the $(SCH_2SCH_2S)^{2-}$ species either as a terminal or bridging ligand has ever been reported. Also, to our knowledge, no dinuclear homometallic platinum complexes with S∩S bridging units have been characterized crystallographically. The closest examples found in the literature are the heterobimetallic bridged dithiolate platinum−rhodium complexes of general formula $[(P-P)Pt\{\mu\text{-}(S-S)\}Rh(COD)]$, where P−P = $(PPh_3)_2$ and S−S = $S(CH_2)_nS$ with $n = 2$, 3, or 4; P−P = dppp and S−S = $S(CH_2)_4S$; P−P = 1,4-bis(diphenylphosphino)butane and S−S = $S(CH_2)_4S$;[27] the homobimetallic bridged dithiolate rhodium−rhodium complexes of general formula $[Rh_2(COD)_2\{\mu\text{-}(S-S)\}]$, where S−S = $S(CH_2)_nS$ with $n = 2$, 3;[28] and a Pt_3 trinuclear complex with two bridging S_2N_2CPh ligands.[32]

The $[SCH_2SCH_2S]^{2-}$ ligand in complex **11** resembles closely the $[SCH_2CH_2CH_2S]^{2-}$ ligand in the previously reported Pd−Rh complex,[27] with the obvious differences in bond lengths (S−C longer than C−C) and angles (C−S−C smaller than C−C−C) produced when the central CH_2 is replaced by S.

Concluding Remarks

A detailed study of the reaction of $[(P\cap P)Pt(\mu\text{-}S)_2Pt(P\cap P)]$, P∩P = dppp or dppe, with CH_2Cl_2 confirms the high nucleophilicity of the sulfide ligand in the $\{Pt_2S_2\}$ core. The experimental results have allowed us to formulate all the steps involved from the initial to the final products. In addition, they show that the nucleophilic behavior is highly dependent on the diphosphine nature. Thus, the $[Pt(dppp)(S_2CH_2)]$ complex reacts further with CH_2Cl_2 and itself to form $[Pt_2(dppp)_2\{\mu\text{-}(SCH_2SCH_2S)\text{-}S,S'\}]Cl_2$ while the dppe analogue does not. Theoretical calculations are consistent with the experimental results showing that complexes with dppp are more nucleophilic than the parent dppe compounds. This enhanced nucleophilicity can be due to a more efficient electron donation from the phosphorus lone pairs of dppp, compared to those from dppe, and it is reasonable to attribute it to the closeness of the bite angle of the dppp ligand to the P−Pt−P angle found in complexes with unidentate unconstrained phosphines. The bite angle also influences the kinetic stability of the different species formed along the reaction. The dppp ligand appears to be more flexible than dppe, and thus, it can better accommodate to the changes in the bite angle required along the reaction pathway. As a consequence, the evolution from $[(P\cap P)Pt(\mu\text{-}S)_2Pt(P\cap P)]$ to $[Pt(P\cap P)(S_2CH_2)]$ and $[Pt[(P\cap P)Cl_2]$ proceeds faster for dppe than for dppp containing complexes. Overall, the observed dependence on the nature of the ligands bound to the $\{Pt_2S_2\}$ core, together with the high number and different nature of the species characterized in this work, gives a reason for the diversity of the compounds reported in the literature as a result of the reaction of $[L_2Pt(\mu\text{-}S)_2PtL_2]$ with weak electrophilic agents.

Acknowledgment. Financial support from the Ministerio de Ciencia y Tecnología of Spain (DGICYT: BQU2001-

(32) Banister, A. J.; Gorrell, I. B.; Lawrence, S. E.; Lehmann, C. W.; May, I.; Tate, Cr.; Blake, A. J.; Rawson, J. M. *Chem. Commun.* **1994**, 1779.

1976 and PB98-0916-CO2-01) and from EPSRC (U.K.) is gratefully acknowledged. C.M. thanks the EU and CESCA/CEPBA for sponsoring her visit to the UAB under the Improving Human Potential Program, Access to Large Scale Facilities (HPRI-1999-CT-00071).

Supporting Information Available: Crystallographic files in CIF format. This material is available free of charge via the Internet at http://pubs.acs.org.

IC0107173

First Evidence of Fast S–H···S Proton Transfer in a Transition Metal Complex**

Gabriel Aullón, Mercè Capdevila, William Clegg, Pilar González-Duarte,* Agustí Lledós,* and Rubén Mas-Ballesté

In the quest to control noncovalent interactions, S–H···S hydrogen bonds are attracting great interest. Despite the prevalence of the thiol group in cysteine residues and the potential importance of S–H···S bridging bonds in biology, little is known about this interaction.[1] Intermolecular S–H···S chains that play an organizing role in the solid state were found in X-ray structures of several compounds containing S–H groups.[2] The S–H···S hydrogen bonds are typically very weak, but may become moderately strong in particular compounds. Resonance[3] and charge[4] assistances have been put forward as being responsible for strong intramolecular S–H···S bonds. The greater acidity of dithiols relative to their monothiol analogues has been attributed to enhanced stabilization of the thiolate anion by an intramolecular $RS^- \cdots HSR$ hydrogen bond.[5] Evidence of S–H···S interactions in transition metal compounds are scarce,[6] although the acidity of the SH group should be enhanced when the sulfur atom is coordinated to a transition metal. Indeed, Sellmann et al. found strong intermolecular S–H···S bridges in the crystal structure of $[Ru(SH_2)(PPh_3)$ "S_4"$]$.[6a] An influence of these bridges on the reactivity of the metal complexes has not been demonstrated, although intramolecular M–SH···hydride interactions have been proposed in the initial stage of the mechanism of hydride protonation.[7] Here we show that a fast S–H···S proton exchange takes place in bimetallic platinum complexes with bridging SH^- and S^{2-} ligands.

Sulfide-bridged aggregates with the Pt_2S_2 core have a rich chemistry.[8, 9] We proved that the reactivity of the Pt_2S_2 core is highly dependent on the nature of the terminal ligands.[9, 10] We have now synthesized of the monoprotonated complexes $[Pt_2\{Ph_2P(CH_2)_nPPh_2\}_2(\mu\text{-S})(\mu\text{-SH})]ClO_4$ ($n=2$, dppe (**1**); $n=3$, dppp (**2**)) by adding $HClO_4$ to a solution of the corresponding $[Pt_2(\mu\text{-S})_2P\cap P)_2]$ ($P\cap P$ = dppe or dppp) complex in benzene. The most remarkable spectroscopic feature of **1** and **2** is the equivalence of the four phosphorus nuclei at room temperature according to the ^{31}P NMR spectrum (Figure 1). The only analogous monoprotonated compound

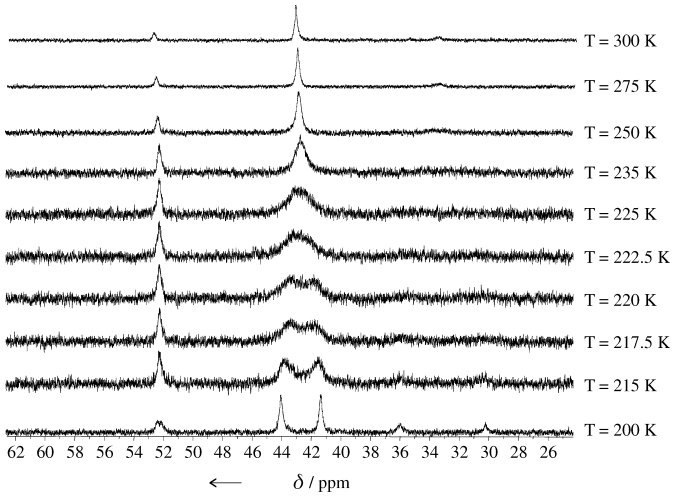

Figure 1. Variable-temperature $^{31}P\{^1H\}$ NMR spectra of **1**.

previously reported, namely, $[Pt_2(\mu\text{-S})(\mu\text{-SH})(PPh_3)_4]PF_6$, has two distinct environments about the P nuclei, as the SH group is *cis* to two phosphorus atoms and *trans* to the other two. Consequently, at room temperature, it shows two ^{31}P NMR signals with two distinct $^1J_{Pt,P}$ coupling constants.[8b, 11] Surprisingly, each of the monoprotonated complexes **1** and **2** shows only one pseudotriplet with the following apparent spectroscopic parameters in [D$_6$]acetone: $\delta_P = 42.8$ ppm and $^1J_{Pt,P} = 3108$ Hz for **1**, and $\delta_P = -3.3$ ppm and $^1J_{Pt,P} = 2960$ Hz for **2**.

We optimized the geometry of the model compounds $[Pt_2\{H_2P(CH_2)_nPH_2\}(\mu\text{-S})(\mu\text{-SH})]^+$ ($n=2$, dhpe (**1t**); $n=3$, dhpp (**2t**)) by B3LYP calculations.[12] Two conformations with a hinged Pt_2S_2 skeleton were found as minima in both complexes; they differ in the *endo* (**e**) or *exo* (**x**) orientation of the thiol proton (see Figure 2). As expected, two different Pt–P and two different Pt–S distances were found in all cases (e.g., in **1t(x)** Pt–P(*trans*-S) 2.338, Pt–P(*trans*-SH) 2.279, Pt–S 2.389, Pt–SH 2.465 Å), and this reflects the different *trans* influences of the sulfide and thiol ligands. The *exo* form is slightly more stable than the *endo* form, although the *exo*/

[*] Prof. Dr. P. González-Duarte, Prof. Dr. A. Lledós, Dr. G. Aullón, Dr. M. Capdevila, Dipl.-Chem. R. Mas-Ballesté
Departament de Química
Universitat Autònoma de Barcelona
08193 Bellaterra, Barcelona (Spain)
Fax: (+34) 935-812-920
E-mail: Pilar.Gonzalez.Duarte§uab.es, agusti@klingon.uab.es
Prof. Dr. W. Clegg
Department of Chemistry
University of Newcastle
Newcastle upon Tyne NE17RU (UK)

  1433-7851/02/4115-2776 $ 20.00+.50/0 *Angew. Chem. Int. Ed.* **2002**, *41*, No. 15

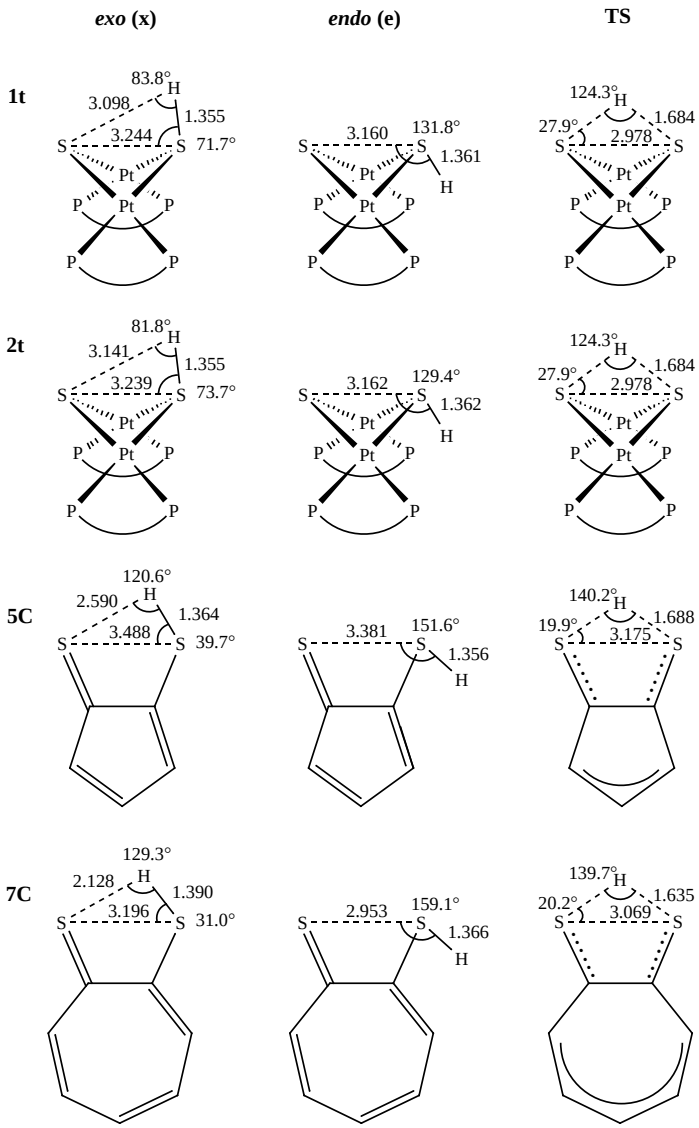

Figure 2. Optimized geometries of the *exo* and *endo* conformations and transition states for proton transfer in **1t**, **2t**, **5C**, and **7C** with bond lengths [Å] and angles [°].

endo interconversion, which takes place through ring inversion,[13] is usually a very fast process. The S–H/S disposition in the *exo* conformations is compatible with the presence of a weak S–H···S hydrogen bond. Comparing the Pt-S-H angle in **1t(x)** (93.3°) with the Pt-S-C angle in the optimized geometry of the methylthiolate analogue (102.1°) reaveals that the S–H proton is tilted towards the sulfide. The energy difference between the *exo* and *endo* forms (Table 1) can be taken as a rough estimate of the hydrogen-bond strength.

Table 1. B3LYP relative energies [kcal mol^{-1}] of the *exo* (**x**) and *endo* (**e**) conformations and the transition states (**TS**) for intramolecular proton transfer. In parentheses: MP2 values.

	Gas phase ($\varepsilon = 1$)			Acetone ($\varepsilon = 20.7$)		
	x	**e**	**TS**	**x**	**e**	**TS**
1t	0.0 (0.0)	0.9 (1.5)	19.7 (17.3)	0.0 (0.0)	−0.4 (−0.3)	19.5 (17.2)
2t	0.0 (0.0)	1.5 (2.3)	19.3 (16.1)	0.0 (0.0)	−0.2 (0.8)	18.0 (13.7)
5C	0.0	2.0	11.3	0.0	1.4	11.4
7C	0.0	2.2	2.3	0.0	1.0	1.6

Similar values (1–2 kcal mol^{-1}) have been reported for weak S–H···S hydrogen bonds.[14]

The X-ray crystal structures[15] of **1** and **2** show that the $Pt_2(\mu\text{-S})(\mu\text{-SH})$ ring is nonplanar, with a dihedral angle between the two PtS_2 planes of 138.3° in **1** and 127.4° in **2** (Figure 3), and it is comparable to that in the singly protonated complex cation $[Pt_2(PPh_3)_4(\mu\text{-S})(\mu\text{-SH})]^+$.[11, 16] The H atom attached to S was not directly located in the structures of **1** and **2**, owing to the presence of heavy atoms and actual or possible disorder. Comparison of the Pt_2S_2 cores in **1** and **2** with those of their deprotonated precursors $[Pt_2(\mu\text{-S})_2(dppe)_2]$[9a] and $[Pt_2(\mu\text{-S})_2(dppp)_2]$,[10] shows that the S···S distance is shorter (by about 0.1 Å) and the dihedral angle smaller (by ca. 2° (**1**) and 7° (**2**)). However, these distortions do not allow a definite proposal for a unequivocal binding situation of the thiol proton in crystals of **1** or **2**. According to theoretical calculations both *endo* or *exo* conformations are possible, and thus weak interactions may determine the prevalence of one orientation over the other. In fact, an *endo* conformation for the thiol proton in **1** and **2** allows S–H···Ph hydrogen bonding.[17] Regarding the acidity of the S–H group in **1** and **2**, NMR data allowed the corresponding pK_a values to be estimated. Both should be within the range 7–9 on the aqueous scale, as they are deprotonated by 4-aminopyridine (pK_a of the conjugated acid 9.11) but not by 2,4-lutidine (pK_a of the conjugated acid 6.99). This represents a decrease of ten pK_a units from the free SH^- ligand (pK_a = 17–19).

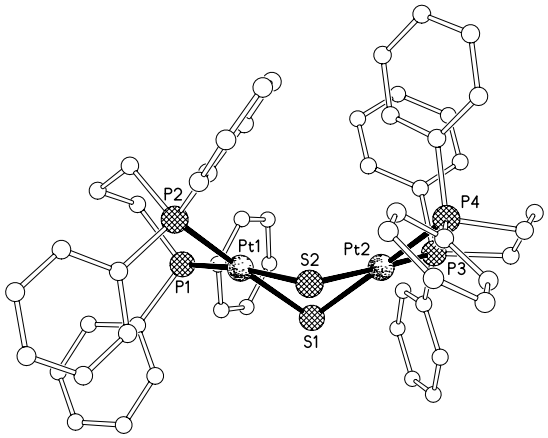

Figure 3. X-ray structure of **2**. Selected bond lengths [Å] and angles [°]: Pt1-S1 2.356(2), Pt1-S2 2.343(2), Pt2-S1 2.350(2), Pt2-S2 2.345(2); S1···S2 3.004, Pt1-S1-Pt2 86.92(7), Pt1-S2-Pt2 87.36(7). Selected bond lengths [Å] and angles [°] for **1**: Pt1-S1 2.374(3), Pt1-S2 2.339(3), Pt2-S1 2.365(3), Pt2-S2 2.343(3); S1···S2 3.057, Pt1-S1-Pt2 89.94(11), Pt1-S2-Pt2 91.37(10).

Hydrogen bonds can be regarded as incipient proton-transfer reactions.[1b] Thus, the equivalence of the phosphorus nuclei in **1** and **2** could be attributed to a fast SH···S proton transfer. To shed light on this process, variable-temperature NMR experiments were carried out (Figure 1). At low temperature, two distinct phosphorus environments were observed for **1** and **2** with the following parameters in [D$_6$]acetone: $\delta_{P(A)} = 44.1$, $\delta_{P(B)} = 41.4$ ppm, $^1J_{Pt,P(A)} = 2626$, $^1J_{Pt,P(B)} = 3608$ Hz for **1**, and $\delta_{P(A)} = -1.8$, $\delta_{P(B)} = -4.9$ ppm, $^1J_{Pt,P(A)} = 3401$, $^1J_{Pt,P(B)} = 2408$ Hz for **2**. Determination of the coalescence temperature allowed an estimation of the energy

  1433-7851/02/4115-2777 $ 20.00+.50/0

barrier of the SH···S proton-transfer process. The values thus obtained are $T_c = 221$ K and $\Delta G^{\neq} = 10.7$ kcal mol^{-1} for **1**, and $T_c = 240$ K and $\Delta G^{\neq} = 10.6$ kcal mol^{-1} for **2**.

We also performed calculations on the intramolecular S–H···S proton-transfer process. The transition state was located and characterized for both complexes (**TS1** and **TS2**, respectively). Both TSs show a trigonal S-H-S arrangement, in which the partial rupture of the S–H bond is compensated by the partial formation of the new S–H bond (Figure 2). The moderate energy barriers found (Table 1) are consistent with the fast process observed on the NMR timescale. We carried out additional calculations to assess the validity of the theoretical values: 1) single-point MP2 calculations on the B3LYP optimized geometries (Table 1, values in parentheses); 2) inclusion of solvent effects by means of the PCM continuum model.[18] The energy barriers are only slightly modified. Thus, theoretical calculations clearly show that intramolecular S–H···S proton transfer can occur in **1** and **2** with a low energy barrier. We also considered the possibility of an intermolecular solvent-assisted proton transfer, as defined in Equation (1). The values obtained for the activation energy of this reaction in acetone (32.2 kcal mol^{-1} for **1t** and 32.0 kcal mol^{-1} for **2t**, respectively) rule out this possibility.

$$exo\text{-}[(P\cap P)_2Pt_2(\mu\text{-}S)(\mu\text{-}SH)]^+ + CH_3COCH_3 \rightarrow [(P\cap P)_2Pt_2(\mu\text{-}S)(\mu\text{-}S)] + (CH_3)_2COH^+ \quad (1)$$

To compare the S–H···S interaction in **1** and **2** with those in other compounds, in which stereochemical constraints place the S-H-S unit in a similar disposition, we performed calculations on dithiotropolone (**7C**) and the parent species with a five-membered ring **5C** (Figure 2, Table 1). The results obtained show that the structural and energetic parameters of the organic systems are similar to those of the platinum complexes, although the magnitude of the SH···S interaction decreases in the order **7C** > **5C** > **1** ≈ **2**.

In conclusion, the combined evidence from experimental and theoretical studies demonstrates the potential of a metal-coordinated thiol ligand to transfer its proton to a metal bound sulfide.

Experimental Section

1: $HClO_4$ (20 μL, 11.6 M) was added to a solution of $[Pt_2(\mu\text{-}S)_2(dppe)_2]$ (200 mg, 0.16 mmol) in benzene (50 mL). After 2 h, a pale yellow solid appeared. The solid product was collected by filtration, washed with benzene and water, and dried with diethyl ether. Yield: 146 mg (68 %). X-ray quality crystals of **1** were obtained by slow evaporation of a solution in methanol. $^{31}P\{^1H\}$ NMR (162.1 MHz, [D$_6$]acetone, 295 K): δ_P(apparent) = 42.8 ppm, $^1J_{Pt,P}$(apparent) = 3108 Hz. ESI-MS: *m*/*z*: 1251.

2: The same procedure as for **1** gave a yellow solid from the reaction of $[Pt_2(\mu\text{-}S)_2(dppp)_2]$ (200 mg) and of $HClO_4$ (20 μL, 11.6 M) Yield: 70 %. Recrystallization of **2** from methanol gave X-ray quality crystals. $^{31}P\{^1H\}$ NMR (162.1 MHz, [D$_6$]acetone, 295 K): δ_P(apparent) = −3.3 ppm, $^1J_{Pt,P}$(apparent) = 2960 Hz. ESI-MS: *m*/*z*: 1280.

Received: February 14, 2002 [Z18715]

[1] a) G. R. Desiraju, T. Steiner, *The Weak Hydrogen Bond in Structural Chemistry and Biology*, Oxford University Press, New York, **1999**, pp. 258–263; b) T. Steiner, *Angew. Chem.* **2002**, *114*, 50; *Angew. Chem. Int. Ed.* **2002**, *41*, 48.

[2] a) J. K. Cockroft, A. N. Fitch, *Z. Kristallogr.* **1990**, *193*, 1; b) C. H. Görbitz, B. Dalhus, *Acta Crystallogr. Sect. C* **1996**, *52*, 1756; c) P. R. Mallinson, D. D. MacNicol, K. L. McCormack, D. S. Yufit, J. H. Gall, R. K. Henderson, *Acta Crystallogr. Sect. C* **1997**, *53*, 90; d) T. Steiner, *Acta Crystallogr. C* **2000**, *56*, 876.

[3] B. Krebs, G. Henkel, W. Stücker, *Z. Naturforsch. B* **1984**, *39*, 43.

[4] P. M. Boorman, X. G. Gao, M. Parvez, *J. Chem. Soc. Chem. Commun.* **1992**, 1656.

[5] J. M. Karty, Y. Wu, J. I. Brauman, *J. Am. Chem. Soc.* **2001**, *123*, 9800.

[6] a) D. Sellmann, P. Lechner, F. Knoch, M. Moll, *J. Am. Chem. Soc.* **1992**, *114*, 922; b) R. J. Pleus, H. Waden, W. Saak, D. Haase, S. Pohl, *J. Chem. Soc. Dalton Trans.* **1999**, 2601.

[7] a) D. Sellmann, J. Käppler, M. Moll, *J. Am. Chem. Soc.* **1993**, *115*, 1830; b) P. G. Jessop, R. H. Morris, *Inorg. Chem.* **1993**, *32*, 2236.

[8] a) S.-W. A. Fong, T. S. A. Hor, *J. Chem. Soc. Dalton Trans.* **1999**, 639, and references therein; b) S.-W. A. Fong, W. T. Yap, J. J. Vittal, T. S. A. Hor, W. Henderson, A. G. Oliver, C. E. F. Rickard, *J. Chem. Soc. Dalton Trans.* **2001**, 1986.

[9] a) M. Capdevila, Y. Carrasco, W. Clegg, R. A. Coxall, P. González-Duarte, A. Lledós, J. Sola, G. Ujaque, *Chem. Commun.* **1998**, 597; b) M. Capdevila, Y. Carrasco, W. Clegg, R. A. Coxall, P. González-Duarte, A. Lledós, J. A. Ramírez, *J. Chem. Soc. Dalton Trans.* **1999**, 3103.

[10] R. Mas-Ballesté, M. Capdevila, P. A. Champkin, W. Clegg, R. A. Coxall, A. Lledós, C. Mégret, P. González-Duarte, *Inorg. Chem.* **2002**, *41*, 3218.

[11] S.-W. A. Fong, J. J. Vittal, W. Henderson, T. S. A. Hor, A. G. Oliver, C. E. F. Rickard, *Chem. Commun.* **2001**, 421.

[12] DFT calculations were carried out with the B3LYP functional. The structures were optimized, and transition states were checked by frequency analysis at the B3LYP level of theory. Single-point MP2 calculations were performed on the optimized B3LYP geometries. Effective core potentials and their related double-zeta basis set LANL2DZ were used for Pt, P, and S atoms, supplemented with polarization functions for the P and S atoms, whereas the 6-31G basis set was used for C and H atoms.

[13] G. Aullón, G. Ujaque, A. Lledós, S. Alvarez, *Chem. Eur. J.* **1999**, *5*, 1391, and references therein.

[14] a) J. E. Lowder, L. A. Kennedy, K. G. P. Sulzmann, S. S. Penner, *J. Quantum Spectr. Radiation Transf.* **1994**, *10*, 17; b) E. L. Woodbridge, T.-L. Tso, M. P. McGrath, W. J. Hehre, E. K. C. Lee, *J. Chem. Phys.* **1986**, *85*, 6991.

[15] Crystal data for **1**: $[C_{52}H_{49}P_4Pt_2S_2]ClO_4$, $M_r = 1351.5$, monoclinic, space group $P2_1$, $a = 9.5504(8)$, $b = 14.9721(12)$, $c = 17.6955(14)$ Å, $\beta = 94.202(2)^\circ$, $V = 2523.5(4)$ Å^3, $Z = 2$, $\rho_{calcd} = 1.779$ g cm^{-3}, $\mu = 5.84$ mm^{-1}, $T = 160$ K, $R = 0.056$ ($F^2 > 2\sigma$), $R_w = 0.152$ (all F^2) for 10719 data and 586 refined parameters. **2**: $[C_{54}H_{53}P_4Pt_2S_2]ClO_4 \cdot 2CH_3OH$, $M_r = 1443.7$, monoclinic, space group $P2_1/c$, $a = 12.5409(8)$, $b = 17.0421(10)$, $c = 26.7036(16)$ Å, $\beta = 98.817(2)^\circ$, $V = 5639.7(6)$ Å^3, $Z = 4$, $\rho_{calcd} = 1.698$ g cm^{-3}, $Mo_{K\alpha}$ radiation ($\lambda = 0.71073$ Å, $\mu = 5.24$ mm^{-1}), $T = 160$ K, $R = 0.053$ ($F^2 > 2\sigma$), $R_w = 0.117$ (all F^2) for 13082 data and 641 refined parameters. CCDC-177519 (**1**) and CCDC 177518 (**2**) contain the supplementary crystallographic data for this paper. These data can be obtained free of charge via www.ccdc.cam.ac.uk/conts/retrieving.html (or from the Cambridge Crystallographic Data Centre, 12, Union Road, Cambridge CB2 1EZ, UK; fax: (+44) 1223-336-033; or deposit@ccdc.cam.ac.uk).

[16] Note that the S^{2-} and SH^- bridging ligands in this complex are disordered and indistinguishable by crystallography, because they are symmetry-equivalent, although this is not explicitly stated in the publication.

[17] a) M. S. Rozenberg, T. Nishio, T. Steiner, *New J. Chem.* **1999**, *23*, 585; b) To test the feasibility of S–H···Ph hydrogen bonding in the *endo* conformer, we took the reported crystal structure of **1** and **2** and located a hydrogen atom on one of the two bridging sulfur atoms with a S–H distance of 1.36 Å and *endo* orientation. Found S–H···C(phenyl ring) distances range between 2.8 and 3.0 Å, which, according to ref. [17a], are consistent with S–H···Ph hydrogen bonding.

[18] a) Solvent effects were taken into account in polarized continuum model (PCM) calculations (acetone: $\varepsilon = 20.70$); b) J. Tomasi, M. Persico, *Chem. Rev.* **1994**, *94*, 2027.

  1433-7851/02/4115-2778 $ 20.00+.50/0

The Evolution of [{$Ph_2P(CH_2)_nPPh_2$}Pt(μ-S)$_2$Pt{$Ph_2P(CH_2)_nPPh_2$}] ($n = 2$, 3) Metalloligands in Protic Acids: A Cascade of Sequential Reactions

Rubén Mas-Ballesté,[a] Gabriel Aullón,[a] Paul A. Champkin,[b] William Clegg,[b] Claire Mégret,[a] Pilar González-Duarte,*[a] and Agustí Lledós*[a]

Abstract: Given the nucleophilicity of the {Pt_2S_2} ring, the evolution of [Pt_2(μ-S)$_2$(P∩P)$_2$] (P∩P = 1,2-bis(diphenylphosphino)ethane (dppe), 1,3-bis(diphenylphosphino)propane (dppp)) metalloligands in the presence of the simplest electrophilic species, the proton, has been studied. Combined use of experimental and theoretical data has allowed the whole set of reactions ensuing the protonation of the {Pt_2S_2} core to be established. The titration of [Pt_2(μ-S)$_2$(P∩P)$_2$] with HCl or $HClO_4$ was monitored mainly by $^{31}P\{^1H\}$ NMR and mass techniques. Characterization of all the species involved was completed with the determination of the crystal structure of [Pt(SH)$_2$(P∩P)], for dppe and dppp, and [Pt_3(μ$_3$-S)$_2$(dppp)$_3$](PF_6)$_2$. The first protonation step of the {Pt_2S_2} core leads to the stable [Pt_2(μ-S)(μ-SH)(P∩P)$_2$]$^+$ complex, but the second step implies disintegration of the ring, thus giving rise to various mononuclear species. The subsequent evolution of some of these species allows regeneration of [Pt_2(μ-S)(μ-SH)(P∩P)$_2$]$^+$, evidencing the cyclic nature of this process. Whereas the reaction pathway is essentially common for both phosphine ligands, dppe and dppp, the different coordinating ability of Cl^- or ClO_4^- determines the nature of the final products, [$PtCl_2$(P∩P)], [Pt_3(μ$_3$-S)$_2$(P∩P)$_3$]Cl_2 or [Pt_3(μ$_3$-S)$_2$(P∩P)$_3$](ClO_4)$_2$. DFT calculations have corroborated the thermodynamic feasibility of the reactions proposed on the basis of experimental data.

Keywords: nucleophilicity · platinum · protonation · S ligands

Introduction

The high nucleophilicity of the bridging sulfido ligands in the {Pt_2S_2} core accounts for the exceptional chemical features of complexes of the formula [$L_2Pt(\mu\text{-}S)_2PtL_2$].[1] In this context, their ability to act as metalloligands in the assembly of a diverse range of sulfido-bridged higher nuclearity aggregates has prompted most of the research into such compounds in recent years.[2] In addition to the reaction of [$L_2Pt(\mu\text{-}S)_2PtL_2$] with metal substrates, that with organic electrophilic agents such as $PhCH_2Br$,[3] CH_3I,[4] and CH_2Cl_2[5] has also been described. As regards the last of these, we recently reported the reaction pathways by which the complexes [Pt_2(μ-S)$_2$(P∩P)$_2$] (P∩P = 1,2-bis(diphenylphosphino)ethane (dppe) **1a**; 1,3-bis(diphenylphosphino)propane (dppp) **1b**) react with CH_2Cl_2.[6] The observed dependence on the nature of the diphosphine ligands, together with the high number and different natures of the species characterized, provided evidence for the rich and diverse chemistry of the {Pt_2S_2} core and encouraged us to extend the nucleophilicity studies to the simplest electron-acceptor species, the proton.

Herein, we explore the reactivity of **1a** and **1b** towards two protic acids, HCl and $HClO_4$, which differ in the coordination ability of the corresponding conjugate bases. Thus, the first and second protonation steps of the {Pt_2S_2} core in the previous complexes and particularly the multistage pathways following cleavage of the {$Pt_2(\mu\text{-}SH)_2$} ring are discussed in detail. Verification of the proposed reaction pathways, shown in Schemes 1 and 2, has required the synthesis and characterization of the mononuclear complexes [Pt(SH)$_2$(P∩P)], (P∩P = dppe **4a**; dppp **4b**), which are transient species resulting from this cleavage. Remarkably, in the presence of HCl and $HClO_4$, **4a** and **4b** spontaneously evolve to the corresponding dinuclear monoprotonated species [Pt_2(μ-S)(μ-SH)(P∩P)$_2$]$^+$ (P∩P = dppe, **2a**, or dppp, **2b**), thus accounting for the cyclic nature of the reactions of **1a** and **1b** with protic acids.

An additional interest in several complex species reported here arises from their relevance to the process of removal of sulfur as SH_2 from petroleum feedstocks, known as hydrodesulfurization (HDS). Thus, the previously characterized complex [$(PPh_3)_2Pt(\mu\text{-}S)_2Pt(PPh_3)_2$] (an analogue of **1a** and **1b**) is obtained as a result of the reaction of [$Pt(PPh_3)_2C_2H_4$] with η^6-coordinated benzothiophene, as a model for homoge-

[a] Prof. Dr. P. González-Duarte, Prof. Dr. A. Lledós, Dipl.-Chem. R. Mas-Ballesté, Dr. G. Aullón, Dipl.-Chem C. Mégret
Departament de Química
Universitat Autònoma de Barcelona
08193 Bellaterra, Barcelona (Spain)
Fax: (+34) 935-813-101
E-mail: Pilar.Gonzalez.Duarte@uab.es

[b] Dr. P. A. Champkin, Prof. Dr. W. Clegg
Department of Chemistry
University of Newcastle, Newcastle upon Tyne, NE1 7RU (UK)

 DOI: 10.1002/chem.200304983

neous HDS of relatively unreactive sulfur-containing species.[7] Moreover, complex species containing the Pt–SH fragment, which is present in complexes $[Pt_2(\mu\text{-}S)(\mu\text{-}SH)(P\cap P)_2]^+$ ($P\cap P$ = dppe, **2a**, or dppp, **2b**), $[Pt_2(\mu\text{-}SH)_2(P\cap P)_2]^{2+}$ ($P\cap P$ = dppe, **3a**, or dppp, **3b**) and $[Pt(SH)_2(P\cap P)]$ ($P\cap P$ = dppe, **4a**, or dppp, **4b**), have been proposed as intermediate species in HDS.[8] The fact that Pt–SH-containing species are scarce[9] and that complexes of formula $[Pt(SH)_2L_2]$ are considered as good potential catalysts in the Claus process (consisting of the oxidation of the SH_2, formed in the HDS process, to elemental sulfur),[10] provide further interest to this study.

Overall, the systematic investigation of the reactions involved in the protonation of the $\{Pt_2S_2\}$ core in the complexes $[Pt_2(\mu\text{-}S)_2(P\cap P)_2]$ (**1a** and **1b**) gives more evidence of the remarkable chemistry of the aforementioned metalloligands in the presence of electrophilic agents and shows the ease of interconversion between apparently unrelated platinum complexes containing the Pt–SH fragment.

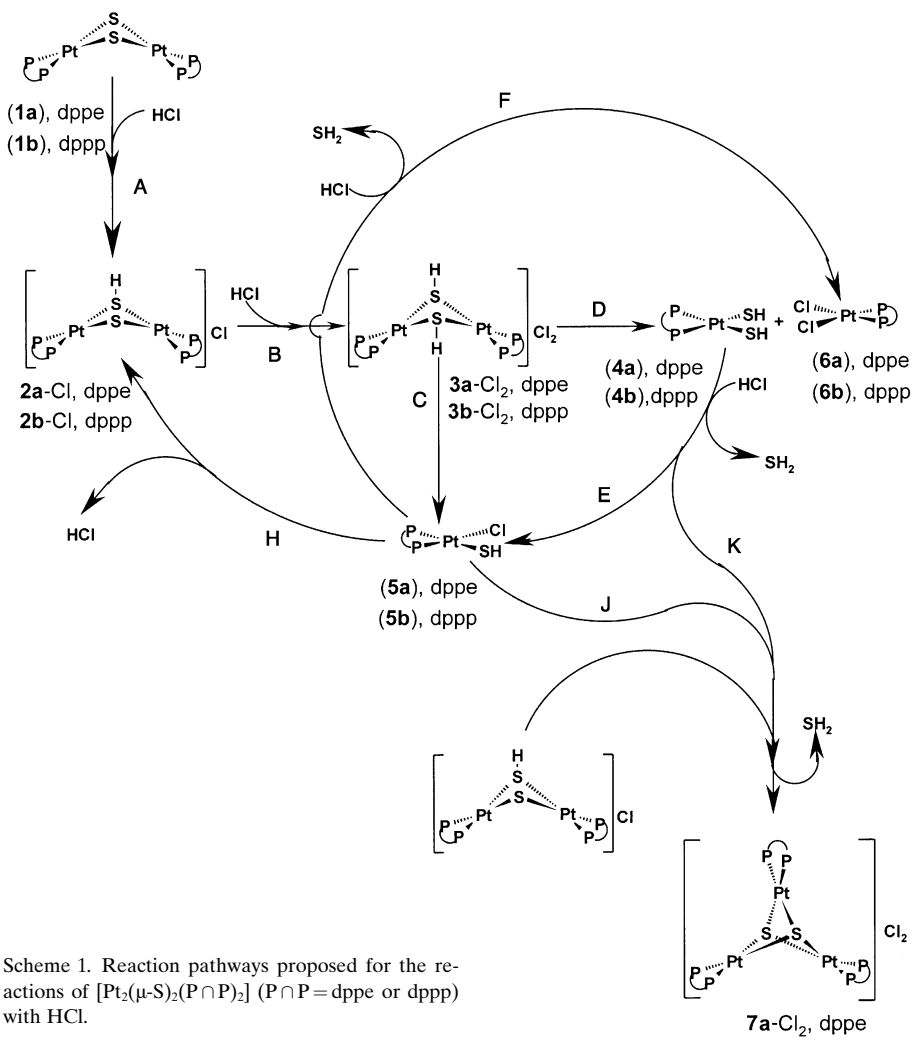

Scheme 1. Reaction pathways proposed for the reactions of $[Pt_2(\mu\text{-}S)_2(P\cap P)_2]$ ($P\cap P$ = dppe or dppp) with HCl.

Abstract in Catalan: *En base a la nucleofilicitat de l'anell $\{Pt_2S_2\}$, s'ha estudiat l'evolució dels metal·lolligands $[Pt_2(\mu\text{-}S)_2(P\cap P)_2]$ ($P\cap P$ = dppe, dppp) envers l'electròfil més senzill, el protó. La combinació de dades experimentals i teòriques ha permès establir el conjunt de reaccions que es deriven de la protonació de l'anell $\{Pt_2S_2\}$. El seguiment de la valoració de $[Pt_2(\mu\text{-}S)_2(P\cap P)_2]$ amb HCl o $HClO_4$ s'ha efectuat essencialment per tècniques de RMN de $^{31}P\{^1H\}$ i d'espectrometria de masses. La caracterització de totes les espècies implicades s'ha completat amb la determinació de l'estructura cristal·lina de $[Pt(SH)_2(P\cap P)]$, per dppe i dppp, i $[Pt_3(\mu_3\text{-}S)_2(dppp)_3](PF_6)_2$. La primera protonació de l'anell $\{Pt_2S_2\}$ dóna lloc a un complex estable, $[Pt_2(\mu\text{-}S)(\mu\text{-}SH)(P\cap P)_2]^+$, però la segona té com a conseqüència la desintegració de l'esmentat anell, originant la formació de diverses espècies mononuclears. L'evolució posterior d'algunes d'aquestes espècies permet la regeneració de $[Pt_2(\mu\text{-}S)(\mu\text{-}SH)(P\cap P)_2]^+$, evidenciant així la naturalesa cíclica del procés. Si bé, qualitativament, el camí de reacció és comú per les dues fosfines, dppe i dppp, la diferent capacitat coordinant de Cl^- o ClO_4^- determina la naturalesa dels productes finals, $[PtCl_2(P\cap P)]$, $[Pt_3(\mu_3\text{-}S)_2(P\cap P)_3]Cl_2$ o $[Pt_3(\mu_3\text{-}S)_2(P\cap P)_3](ClO_4)_2$. Els càlculs teòrics (DFT) han permès establir la viabilitat termodinàmica dels processos proposats en base a les dades experimentals.*

Results and Discussion

General description of the evolution of the complexes $[Pt_2(\mu\text{-}S)_2(P\cap P)_2]$ ($P\cap P$ = dppe, dppp) in the presence of HCl and $HClO_4$: The reaction pathways proposed for the reactions of $[Pt_2(\mu\text{-}S)_2(P\cap P)_2]$ (**1**) with HCl (Scheme 1) and $HClO_4$ (Scheme 2) are based on the experimental data summarized in Tables 1 and 2.

The first information on these reactions was obtained by monitoring the $^{31}P\{^1H\}$ NMR parameters of the species present in solution after controlled addition of HCl to **1** in acetonitrile. Up to one equivalent of protons per mole of $[Pt_2(\mu\text{-}S)_2(P\cap P)_2]$, the addition of HCl led to the immediate formation of $[Pt_2(\mu\text{-}S)(\mu\text{-}SH)(P\cap P)_2]Cl$, **2**-Cl, which are stable in solution and have been structurally characterized in the solid phase as the perchlorate salts, **2**-ClO_4.[11] Subsequent additions of HCl had a small effect, until a significant excess of protons was added with respect to the stoichiometric ratio required to obtain the corresponding diprotonated complexes $[Pt_2(\mu\text{-}SH)_2(P\cap P)_2]^{2+}$ (**3**). After this, the excess of protons produced a decrease in the concentration of **2**-Cl and the concomitant appearance of the corresponding mononuclear species $[PtCl_2(P\cap P)]$ (**6**). For both **1a** and **1b**, the concentration of $[PtCl_2(P\cap P)]$ formed

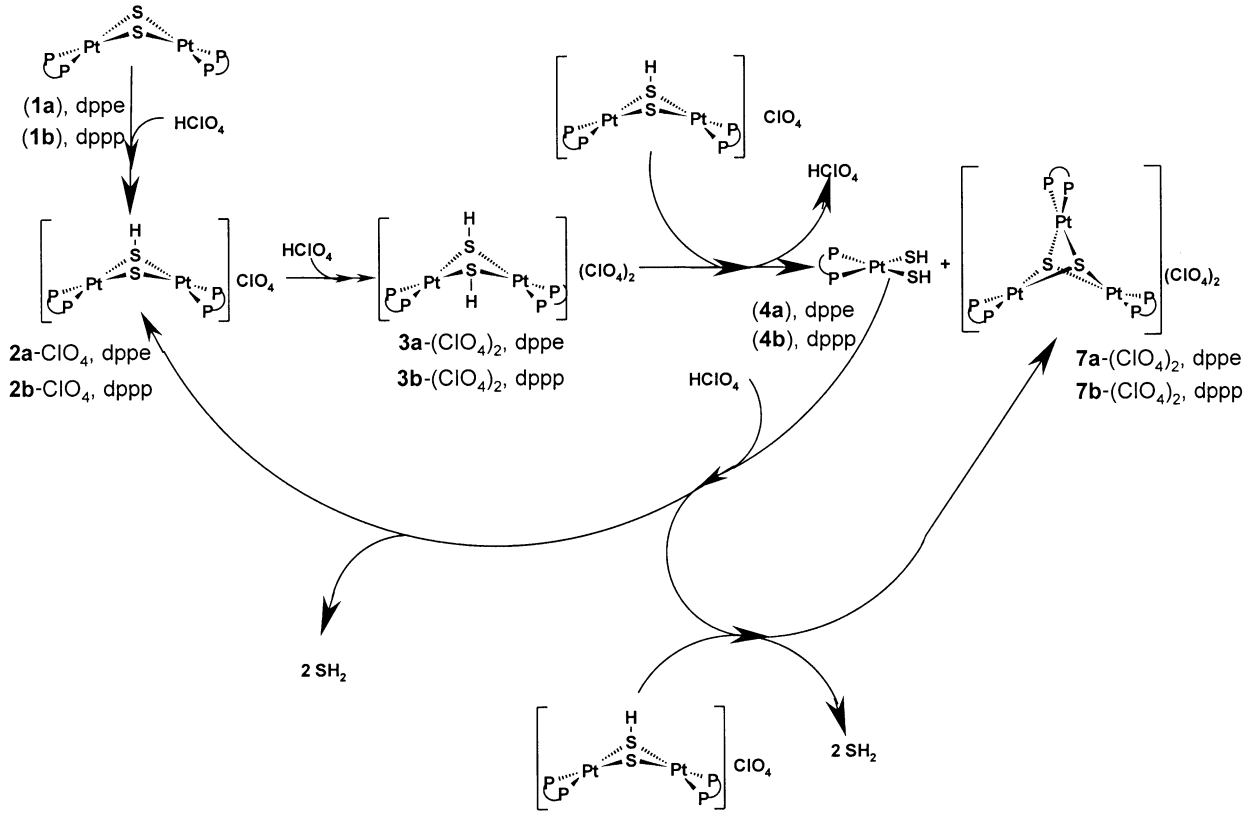

Scheme 2. Reaction pathways proposed for the reactions of $[Pt_2(\mu\text{-}S)_2(P\cap P)_2]$ ($P\cap P$ = dppe or dppp) with $HClO_4$.

Table 1. Identification of the complex species formed throughout different processes as deduced by $^{31}P\{^1H\}$ NMR data.

Experiment	Acid added	Amount of acid added (equiv)	Species detected in solution by $^{31}P\{^1H\}$ NMR	
			$P\cap P$ = dppe	$P\cap P$ = dppp
Titration of **1** with acid	HCl	2	**2a**-Cl + **6a** (minor)	**2b**-Cl + **6b** (minor)
		16	**2a**-Cl + **6a**	**2b**-Cl + **6b** (minor)
		50	**6a**	**2b**-Cl + **6b**
	$HClO_4$	5	**2a**-ClO_4 + (**7a**)$(ClO_4)_2$ (minor)	**2b**-ClO_4
		50	**2a**-ClO_4 + **7a**-$(ClO_4)_2$	**2b**-ClO_4
		75	**7a**-$(ClO_4)_2$	**2b**-ClO_4
		150	**7a**-$(ClO_4)_2$	**2b**-ClO_4 + **7b**-$(ClO_4)_2$ (minor)
Titration of **4** with acid	HCl	25	**2a**-Cl + **7a**-Cl_2 + **6a** (minor)	**2b**-Cl + **6b** (minor)
		50	**6a** + **7a**-Cl_2	**2b**-Cl + **6b**
		75	**6a**	**2b**-Cl + **6b**
	$HClO_4$	2	**2a**-ClO_4 + **7a**-$(ClO_4)_2$ (minor)	**2b**-ClO_4
		5	**2a**-ClO_4 + **7a**-$(ClO_4)_2$	**2b**-ClO_4
		25	**7a**-$(ClO_4)_2$	**2b**-ClO_4
Evolution of **2** in the presence of acid after 1 week	HCl	4	**2a**-Cl + **7a**-Cl_2 + **6a**	**2b**-Cl + **6b**
	$HClO_4$	4	**7a**-$(ClO_4)_2$	no reaction
2 + **6**	–	–	No reaction	no reaction
6 + NaSH (1:1)	–	–	**2a**-Cl + **4a** (minor)	**2b**-(Cl) + **4b** (minor)

was directly related to the amount of HCl added but, for the same amount, the $[PtCl_2(P\cap P)]$ to $[Pt_2(\mu\text{-}S)(\mu\text{-}SH)(P\cap P)_2]Cl$ molar ratio obtained was always greater for dppe than for dppp. After one week, in the case of **2a**-Cl only, the addition of up to approximately four equivalents of acid led to the formation of $[Pt_3(\mu_3\text{-}S)_2(dppe)_3]Cl_2$, **7a**-$Cl_2$, whose X-ray crystal structure and NMR parameters have already been reported.[2e]

Whereas the addition of one equivalent of $HClO_4$ per mole of **1** in acetonitrile caused the immediate formation of **2**-ClO_4, an excess of $HClO_4$ gave rise to the concomitant appearance of the corresponding trinuclear complex $[Pt_3(\mu_3\text{-}S)_2(P\cap P)_3]^{2+}$ (**7**). This occurred in a substantial amount for **7a**-$(ClO_4)_2$, but it required a great excess of acid for **7b**-$(ClO_4)_2$. The crystal structure of **7a**-Cl_2 is known[2e] and that of **7b**-$(PF_6)_2$ is reported here.

Consideration of both sets of data and complementary information (described below) allowed us to deduce that the addition of protons to **2** had caused them to evolve to the corresponding diprotonated complexes **3**, which were of an

Table 2. ESMS and NMR data for complexes **1**, **2**, **4**, **6** and **7**.

Compound	*m*/*z*	Calculated MW	$\delta(^{31}P)$ [ppm][a]	$^{1}J_{Pt,P}$ (Hz)
$[Pt_2(\mu\text{-}S)_2(dppe)_2]$ (**1a**)	1251.7[b]	1251[b]	40.5	2740
$[Pt_2(\mu\text{-}S)_2(dppp)_2]$ (**1b**)	1279.7[b]	1279[b]	−0.1	2615
$[Pt_2(\mu\text{-}S)(\mu\text{-}SH)(dppe)_2]^+$ (**2a**)	1251.7	1251	45.4[c]	3110[c]
$[Pt_2(\mu\text{-}S)(\mu\text{-}SH)(dppp)_2]^+$ (**2b**)	1279.7	1279	−0.8[c]	2965[c]
$[Pt(SH)_2(dppe)]$ (**4a**)[d]	626.2	659	48.5	2883
$[Pt(SH)_2(dppp)]$ (**4b**)[e]	640.1	673	−1.3	2768
$[PtCl_2(dppe)]$ (**6a**)	–		43.4	3610
$[PtCl_2(dppp)]$ (**6b**)	–		−3.7	3408
$[Pt_3(\mu_3\text{-}S)_2(dppe)_3]^{2+}$ (**7a**)	921.4[f]	1844	38.3	3248
$[Pt_3(\mu_3\text{-}S)_2(dppp)_3]^{2+}$ (**7b**)	943.0[f]	1886	−10.8[g]	3016[g]

[a] In $[D_6]$DMSO. [b] $m/e = M+1$. [c] Apparent parameters at room temperature. [d] ^{1}H NMR parameters for **4a**: $\delta(^1H\text{-}S) = -0.82$ ppm; $^2J_{H,Pt} = 51.7$ Hz; $^3J_{H,P(trans)} = 10.8$ Hz, $^3J_{H,P(cis)} = 3.5$ Hz. [e] ^{1}H NMR parameters for **4b**: $\delta(^1H\text{-}S) = -1.00$ ppm; $^2J_{H,Pt} = 48.5$ Hz; $^3J_{H,P(trans)} = 7.2$ Hz. [f] $m/e = M/2$. [g] ^{31}P NMR parameters from the computer simulation for $[Pt_3(\mu_3\text{-}S)_2(dppp)_3]^{2+}$: $\delta(^{31}P) = -10.7$ ppm; $^1J_{Pt,P} = 3016$ Hz; $^2J_{Pt,Pt} = 705$ Hz; $^3J_{Pt,P} < 10$ Hz; $^4J_{P,P} < 10$ Hz.

elusive nature. The sequence of protonation reactions with HCl is given in **A** and **B**.

$$[Pt_2(\mu\text{-}S)_2(P\cap P)_2]\ (\mathbf{1}) + HCl \rightarrow [Pt_2(\mu\text{-}S)(\mu\text{-}SH)(P\cap P)_2]Cl\ (\mathbf{2}\text{-}Cl) \qquad (\mathbf{A})$$

$$[Pt_2(\mu\text{-}S)(\mu\text{-}SH)(P\cap P)_2]Cl\ (\mathbf{2}\text{-}Cl) + HCl \rightarrow [Pt_2(\mu\text{-}SH)_2(P\cap P)_2]Cl_2\ (\mathbf{3}\text{-}Cl_2) \qquad (\mathbf{B})$$

The fact that this second protonation step **B**, unlike the first one **A**, required a significant excess of protons with respect to the stoichiometric ratio indicates that the complexes $[Pt_2(\mu\text{-}S)_2(P\cap P)_2]$ (**1**) are stronger bases than their monoprotonated counterparts $[Pt_2(\mu\text{-}S)(\mu\text{-}SH)(P\cap P)_2]^+$ (**2**), the pK_a values of **2** on the aqueous scale falling in the range 7–9.[11] Moreover, the basicity of **2** is dependent on the nature of the diphosphine ligand, being higher for dppe than for dppp. Overall, the ease of decomposition of **3** impaired their observation in solution, but could account for the different complexes obtained spontaneously as a result of the disintegration of the $\{Pt_2(\mu\text{-}SH)_2\}$ core in these species. The cascade of reactions following this disintegration depends on the nature of the diphosphine ligands and on the coordinating ability of the conjugate base, Cl^- or ClO_4^-, of the acid added. Thus, the sequence of reactions resulting from the addition of HCl to complexes **1** will be described first (Scheme 1), and this will be followed by that involving the addition of $HClO_4$ (Scheme 2).

Following the previous assumption, the reaction between HCl and **2** entails formation of the $\{Pt_2(\mu\text{-}SH)_2\}$ ring, which then cleaves either symmetrically (reaction **C**), affording two equivalents of $[PtCl(SH)(P\cap P)]$ (**5**), or asymmetrically (reaction **D**), leading to a mixture of $[PtCl_2(P\cap P)]$ and $[Pt(SH)_2(P\cap P)]$, that is **4** and **6**.

$$[Pt_2(\mu\text{-}SH)_2(P\cap P)_2]Cl_2\ (\mathbf{3}\text{-}Cl_2) \rightarrow 2\ [PtCl(SH)(P\cap P)]\ (\mathbf{5}) \qquad (\mathbf{C})$$

$$[Pt_2(\mu\text{-}SH)_2(P\cap P)_2]Cl_2\ (\mathbf{3}\text{-}Cl_2) \rightarrow [Pt(SH)_2(P\cap P)]\ (\mathbf{4}) + [PtCl_2(P\cap P)]\ (\mathbf{6}) \qquad (\mathbf{D})$$

The presence of an excess of HCl in solution, which is required for the formation of the diprotonated cations **3**, causes protonation of SH^- and thus its replacement by Cl^- in **4** and **5** (reactions **E** and **F**), as well as the wholesale displacement of these reactions toward the formation of the corresponding compounds **6**, both already known[12] and thus easily identified in solution.[6]

$$[Pt(SH)_2(P\cap P)]\ (\mathbf{4}) + HCl \rightarrow [PtCl(SH)(P\cap P)]\ (\mathbf{5}) + H_2S \qquad (\mathbf{E})$$

$$[PtCl(SH)(P\cap P)]\ (\mathbf{5}) + HCl \rightarrow [PtCl_2(P\cap P)]\ (\mathbf{6}) + H_2S \qquad (\mathbf{F})$$

To verify these reactions we carried out the synthesis and characterization of complexes **4** (described below) and monitored their reactivity towards HCl and $HClO_4$ by a procedure similar to that followed for **1**. Addition of a significant excess of HCl to **4** in acetonitrile yielded **6**, and thus confirmed reactions **E** and **F**. On the other hand, when the amount of HCl added was limited to a smaller excess, complexes **4** spontaneously evolved to **2**, which could occur either directly (reaction **G**) or in two steps (reactions **E** and **H**) through the intermediate species **5**.

$$2\,[Pt(SH)_2(P\cap P)]\ (\mathbf{4}) + HCl \rightarrow [Pt_2(\mu\text{-}S)(\mu\text{-}SH)(P\cap P)_2]Cl\ (\mathbf{2}\text{-}Cl) + 2\,H_2S \qquad (\mathbf{G})$$

$$2\,[PtCl(SH)(P\cap P)]\ (\mathbf{5}) \rightarrow [Pt_2(\mu\text{-}S)(\mu\text{-}SH)(P\cap P)_2]Cl\ (\mathbf{2}\text{-}Cl) + HCl \qquad (\mathbf{H})$$

This last reaction could account for the spontaneous dimerization of **5** and thus for our unsuccessful attempts to detect these species. To obtain evidence for the two-step mechanism, the reaction of $[PtCl_2(P\cap P)]$ (**6**), with $NaSH\cdot H_2O$ in approximately a 1:1 molar ratio was carried out. This resulted in the formation of **2**-Cl in high yield and thus indicated that reaction **H** is feasible under the present experimental conditions. However, theoretical calculations on both processes, **G** and **H**, described below, strongly suggest that reaction **G** is more favorable than **H**.

Overall, the reaction of complexes $[Pt_2(\mu\text{-}S)_2(P\cap P)_2]$ (**1**) with HCl in excess consists of a cyclic process, where the monoprotonated species $[Pt_2(\mu\text{-}S)(\mu\text{-}SH)(P\cap P)_2]^+$ (**2**) initially formed evolves to the new species $[Pt(SH)_2(P\cap P)]$ (**4**), which in turn affords the initial complexes **2**-Cl. However, the concomitant formation of unreactive species, such as $[PtCl_2(P\cap P)]$ (**6**), under the present experimental conditions limits the cyclic process. An additional dead end, for $P\cap P =$ dppe only, is the formation of the trinuclear complex $[Pt_3(\mu_3\text{-}S)_2(dppe)_3]^{2+}$ (**7a**). It was also observed that the formation of **7a**-Cl_2, as well as **7a**-$(ClO_4)_2$, is solvent-dependent and, in both cases, the amount formed follows the order: acetonitrile > acetone ≈ methanol > methylene chloride.

There are several possible ways for the formation of the trimetallic compound **7a**-Cl_2 to occur. According to experimental data, complexes **2a**-Cl and **6a** do not react with themselves, and thus their combination (reaction **I**) cannot be a possible source for complex **7a**-Cl_2.

$$[PtCl_2(P\cap P)]\ (\mathbf{6}) + [Pt_2(\mu\text{-}S)(\mu\text{-}SH)(P\cap P)_2]Cl\ (\mathbf{2}\text{-}Cl) \rightarrow [Pt_3(\mu_3\text{-}S)_2(P\cap P)_3]Cl_2\ (\mathbf{7}\text{-}Cl_2) + HCl \qquad (\mathbf{I})$$

Two alternative reaction pathways for the formation of **7a**-Cl_2 are given in chemical equations **J** and **K**, in which the

binuclear complexes **2** react with their mononuclear counterparts **4** or **5**.

$$[Pt(SH)_2(P\cap P)]\ (\mathbf{4}) + [Pt_2(\mu\text{-}S)(\mu\text{-}SH)(P\cap P)_2]Cl\ (\mathbf{2}\text{-}Cl) + HCl \rightarrow [Pt_3(\mu_3\text{-}S)_2(P\cap P)_3]Cl_2\ (\mathbf{7}\text{-}Cl_2) + 2\,H_2S \quad (\mathbf{J})$$

$$[PtCl(SH)(P\cap P)]\ (\mathbf{5}) + [Pt_2(\mu\text{-}S)(\mu\text{-}SH)(P\cap P)_2]Cl\ (\mathbf{2}\text{-}Cl) \rightarrow [Pt_3(\mu_3\text{-}S)_2(P\cap P)_3]Cl_2\ (\mathbf{7}\text{-}Cl_2) + H_2S \quad (\mathbf{K})$$

Another possible pathway arises from the self-combination of two equivalents of $[Pt_2(\mu\text{-}SH)_2(P\cap P)_2]Cl_2$ (**3**) (reaction **L**), which affords not only **7**-Cl_2 but also the mononuclear $[Pt(SH)_2(P\cap P)]$ (**4**) complex and HCl as a byproduct. These two latter compounds react further, thus generating the binuclear complex **2** (by means of reaction **G**) and confirming the cyclic process proposed above.

$$2\,[Pt_2(\mu\text{-}SH)_2(P\cap P)_2]Cl_2\ (\mathbf{3}\text{-}Cl_2) \rightarrow [Pt_3(\mu_3\text{-}S)_2(P\cap P)_3]Cl_2\ (\mathbf{7}\text{-}Cl_2) + [Pt(SH)_2(P\cap P)]\ (\mathbf{4}) + 2\,HCl \quad (\mathbf{L})$$

The experimental data obtained in the titration of **1**, as well as **4**, with $HClO_4$ (Table 1) compare very well with those obtained with HCl, the only differences being due to the lower coordinating ability of the ClO_4^- counterion. As shown in Scheme 2, the addition of the first equivalent of $HClO_4$ to **1** leads to the immediate formation of the monoprotonated species **2**-ClO_4. Subsequent additions of $HClO_4$ cause the latter species to evolve to **4**, with the concomitant formation of the corresponding trinuclear complexes **7**-$(ClO_4)_2$, which, unlike **4**, do not react further under the present experimental conditions. As with the titration with HCl, it has not been possible to detect the transient diprotonated complexes **3**-$(ClO_4)_2$. Direct titration of **4** with $HClO_4$, has allowed us to verify that they evolve into the initial complexes **2**-ClO_4, and thus to reconfirm the cyclic nature of the protonation process of the $\{Pt_2S_2\}$ core in **1**. However, as the ClO_4^- counterion prevents the generation of analogues of **6**, the only dead end of the cycle is the formation of **7**-$(ClO_4)_2$. Detection of **7b**-$(ClO_4)_2$ requires a greater excess of acid than **7a**-$(ClO_4)_2$, which is easily observed in the titration of either **1a** or **4a** with $HClO_4$. The dependence of the ease of formation of the trinuclear species with the phosphine ligand, (greater stability for dppe than for dppp), compares well with the results obtained in the titration with HCl.

Theoretical study of the reaction pathway followed by the $[Pt_2(\mu\text{-}S)_2(P\cap P)_2]$ ($P\cap P$ = dppe, dppp) complexes in the presence of HCl: We have performed theoretical calculations to evaluate the thermodynamic feasibility of the proposed reactions (**A** – **L**) corresponding to the evolution of the $\{Pt_2S_2\}$ core in the presence of HCl. In addition to the energetic picture of the aforementioned reactions, and to the relative stabilities of the species involved, this study provides an insight into the structural features of the compounds involved, some of them not well characterized. In the calculations, we have modeled dppe and dppp real ligands by $H_2P(CH_2)_2PH_2$ (dhpe) and $H_2P(CH_2)_3PH_2$ (dhpp), respectively. To obtain realistic values of the reaction energies, the solvent has been taken into account in the calculations. The reason for proceeding in this way is that in some of the considered reactions the charges of reactants and products are not the same, the process entailing a net charge creation or annihilation. In these cases solvent effects on the thermodynamics of the reaction are dramatic. For instance, reaction **A** (charge of reactants 0, charge of products +1 and −1) is computed to be slightly exothermic in solution (~ -4.5 kcal mol^{-1}) but it is extremely endothermic in the gas phase ($\sim +82$ kcal mol^{-1}). The effect is much lower when the charges of reactants and products remain the same. For instance, ΔE values of approximately -7.5 kcal mol^{-1} and -9.5 kcal mol^{-1} are computed for reaction **E** in the gas phase and solution, respectively. To obtain a global picture of all the processes considered, solvent effects have been included in all the reactions. Thus, all the reported values have been obtained in acetonitrile as solvent ($\varepsilon = 36.64$) by means of the polarizable continuum model (PCM). Accordingly, the reaction energies (ΔE) for reactions **A** – **L** have been calculated (Table 3). From these values, it is possible to obtain the relative energy per "$\{Pt_2\}$" unit for all the species involved from $[Pt_2(\mu\text{-}S)_2(P\cap P)_2]$ (taken as the zero of energy) to $[Pt_3(\mu_3\text{-}S)_2(P\cap P)_3]^{2+}$ (Table 4), and to establish the energy profile for the whole process (Figure 1). Energies obtained with dhpe and dhpp ligands are very similar (see Table 3), and thus, only the values for dhpe are represented in Figure 1.

Table 3. Theoretical evaluation of energetic changes (ΔE) accompanying the proposed reactions pathways **A** – **L**. All energies are in kcal mol^{-1}.

	Reactions	ΔE	
		dhpe	dhpp
A	**1** + HCl → **2**-Cl	−4.7	−4.5
B	**2**-Cl + HCl → **3**-Cl_2	+17.2	+15.9
C	**3**-Cl_2 → 2 **5**	−41.5	−41.2
D	**3**-Cl_2 → **4** + **6**	−39.5	−39.1
E	**4** + HCl → **5** + H_2S	−9.1	−9.8
F	**5** + HCl → **6** + H_2S	−7.1	−7.7
G	2 **4** + HCl → **2**-Cl + 2 H_2S	+6.1	+5.6
H	2 **5** → **2**-Cl + HCl	+24.3	+25.2
I	**2**-Cl + **6** → **7**-Cl_2 + HCl	+17.8	+18.8
J	**2**-Cl + **5** → **7**-Cl_2 + H_2S	+10.7	+11.1
K	**2**-Cl + **4** + HCl → **7**-Cl_2 + 2 H_2S	+1.6	+1.4
L	2 **3**-Cl_2 → **7**-Cl_2 + **4** + 2 HCl	−38.9	−36.2

The overall process depicted in Scheme 1 can be considered as being formed by three steps: 1) protonation of the

Table 4. Relative energy per dimer $\{Pt_2\}$ for compounds involved in the proposed reactions. The energy for complexes $[Pt_2(\mu\text{-}S)_2(P\cap P)_2]$ is arbitrarily taken to zero. All energies are in kcal mol^{-1}.

Compounds	Relative energy	
	dhpe	dhpp
1	0.0	0.0
2-Cl	−4.7	−4.5
3-Cl_2	+12.5	+11.4
2 **5**	−29.0	−29.7
4 + **6**	−27.0	−27.6
5 + **6**	−36.1	−37.4
2 **6**	−43.2	−45.1
5 + **4**	−19.9	−19.9
2 **4**	−10.8	−10.2
1/2 **4** + 1/2 **7**-Cl_2	−6.9	−6.7

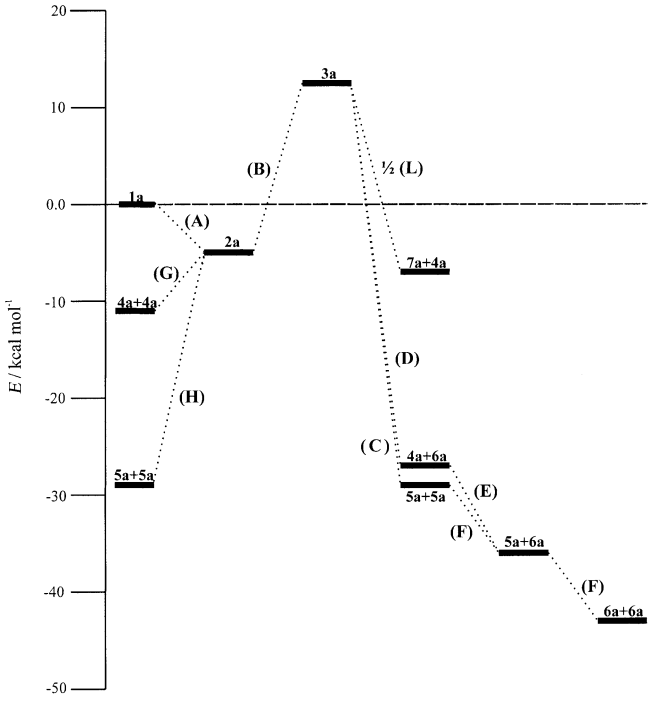

Figure 1. Energy profile for the reaction pathway of $[Pt_2(\mu\text{-}S)_2(dhpe)_2]$ with HCl in acetonitrile as solvent. Reactions are shown from left (reagents) to right (products).

bimetallic $\{Pt_2S_2\}$ core, which includes the addition of the first and second proton to the sulfido bridges; 2) cleavage of the bimetallic $\{Pt_2S_2\}$ core yielding various monometallic species, and their subsequent evolution by reaction with HCl; and 3) formation of trimetallic species either from dinuclear species alone or from a combination of mononuclear and dinuclear complexes.

1) Protonation of the $\{Pt_2S_2\}$ core: The two consecutive additions of H^+ to the sulfido bridges of $[Pt_2(\mu\text{-}S)_2(P\cap P)_2]$ have very different consequences. In the first protonation (reaction **A**), stable mixed (μ-S)(μ-SH)-bridged complexes are formed in a slightly exothermic ($\sim$5 kcal mol^{-1}) reaction, in agreement with the isolation, and in some cases X-ray characterization, of such compounds with Pt[11],[13] and Ni.[14] In contrast, the second protonation step (reaction **B**) is highly endothermic, indicating very unstable diprotonated complexes. We have checked the true minimum nature of the highly unstable diprotonated species by means of vibrational analysis. No imaginary frequencies are found for species **3**, thus confirming their nature as unstable reaction intermediates. Accordingly, the diprotonated complex could only be synthesized by using a large excess of protic acid. Notwithstanding this, owing to the cleavage of the $\{Pt_2(SH)_2\}$ ring (see below), no $[Pt_2(\mu\text{-}SH)_2(P\cap P)_2]^{2+}$ species has been isolated or detected in solution. The very difficult diprotonation of $[Pt_2(\mu\text{-}S)_2(P\cap P)_2]$, also found in $[Ni_2(\mu\text{-}S)_2(P\cap P)_2]$ complexes,[14] is consistent with the acidic nature of the sulfhydryl proton-sulfur bond. The thermodynamic instability of the diprotonated species is a key factor that justifies the sequence of reactions taking place in steps 2 and 3, leading to far more stable compounds.

The main structural parameters of optimized binuclear complexes, together with the X-ray structure of the parent experimental compounds, are given in Table 5.

Structural trends in edge-sharing binuclear d^8 complexes with X and XR bridges have recently been analyzed.[15] A characteristic structural parameter for complexes having $\{M_2(\mu\text{-}X)_2\}$ cores is the dihedral angle θ that describes the degree of folding of the M_2X_2 ring. This angle is $\sim$135° in compounds $[Pt_2(\mu\text{-}S)_2(P\cap P)_2]$, and small variations, of less than 2°, are found for all isomers of $[Pt_2(\mu\text{-}S)(\mu\text{-}SH)(P\cap P)_2]^+$.

Table 5. Calculated and X-ray-determined parameters for bimetallic and trimetallic complexes with $\{(P_2Pt)_n(\mu\text{-}S)_2\}$ cores.

Compound[a]	Pt···Pt	S···S	Pt–S	Pt–S_H	Pt-P_S	Pt–P_{SH}	S-Pt-S	Pt-S-Pt	Pt-S_H-Pt	P-Pt-P	θ	Reference[b]
$[(dhpe)_2Pt_2(\mu\text{-}S)_2]$	3.307	3.213	2.399	–	2.299	–	84.1	87.1	–	86.6	136.3	calcd
$[(dhpp)_2Pt_2(\mu\text{-}S)_2]$	3.293	3.222	2.406	–	2.294	–	84.1	86.4	–	95.6	134.4	calcd
$[(dppe)_2Pt_2(\mu\text{-}S)_2]$ (NILDAN)	3.292	3.134	2.350	–	2.245	–	83.7	88.9	–	86.2	140.2	[2f]
$[(dppp)_2Pt_2(\mu\text{-}S)_2]$	3.235	3.101	2.340	–	2.254	–	83.0	87.5	–	94.7	134.8	[6]
$[(Ph_2pyP)_2Pt_2(\mu\text{-}S)_2]$ (YIJNEK)	3.355	3.004	2.327	–	2.277	–	80.4	99.6	–	103.0	180.0	[5d]
$[(dhpe)_2Pt_2(\mu\text{-}S)(\mu\text{-}SH)]^+$	3.326	3.244	2.389	2.465	2.338	2.279	83.8	88.2	84.8	86.1	134.2	calcd: *exo*
$[(dhpe)_2Pt_2(\mu\text{-}S)(\mu\text{-}SH)]^+$	3.351	3.160	2.394	2.449	2.336	2.279	81.5	88.8	86.3	86.1	132.0	calcd: *endo*
$[(dhpp)_2Pt_2(\mu\text{-}S)(\mu\text{-}SH)]^+$	3.375	3.239	2.394	2.468	2.335	2.283	83.5	89.6	86.2	94.1	137.1	calcd: *exo*
$[(dhpp)_2Pt_2(\mu\text{-}S)(\mu\text{-}SH)]^+$	3.409	3.162	2.399	2.452	2.333	2.285	81.4	90.6	88.1	93.9	136.0	calcd: *endo*
$[(dppe)_2Pt_2(\mu\text{-}S)(\mu\text{-}SH)]^+$	3.350	3.057	2.341	2.371	2.261	2.244	80.9	91.4	89.9	85.7	138.3	[11]
$[(dppp)_2Pt_2(\mu\text{-}S)(\mu\text{-}SH)]^+$	3.237	3.004	2.344	2.353	2.262	2.260	79.5	87.4	86.9	93.3	127.4	[11]
$[(Ph_3P)_4Pt_2(\mu\text{-}S)(\mu\text{-}SH)]^+$ (QIDPUO)[c]	3.340	2.976	2.342	2.342	2.284	2.284	78.9	91.0	91.0	99.0	135.0	[13b]
$[(dhpe)_2Pt_2(\mu\text{-}SH)_2]^{2+}$	3.519	3.331	–	2.468	–	2.318	84.9	–	91.0	85.2	150.2	calcd: *exo*
$[(dhpe)_2Pt_2(\mu\text{-}SH)_2]^{2+}$	3.550	3.285	–	2.463	–	2.319	83.6	–	92.2	85.0	150.3	calcd: *anti*
$[(dhpp)_2Pt_2(\mu\text{-}SH)_2]^{2+}$	3.536	3.319	–	2.472	–	2.319	84.3	–	91.3	92.2	149.7	calcd: *exo*
$[(dhpp)_2Pt_2(\mu\text{-}SH)_2]^{2+}$	3.558	3.281	–	2.468	–	2.320	83.3	–	93.2	91.4	153.2	calcd: *anti*
$[(dhpe)_3Pt_3(\mu\text{-}S)_2]^{2+}$	3.257	3.118	2.443	–	2.312	–	78.3	83.6	–	85.5	120.0	calcd
$[(dhpp)_3Pt_3(\mu\text{-}S)_2]^{2+}$	3.272	3.112	2.448	–	2.312	–	78.9	83.9	–	92.9	120.0	calcd
$[(dppe)_3Pt_3(\mu\text{-}S)_2]^{2+}$ (CENRAO)	3.118	3.063	2.364	–	2.248	–	80.8	82.6	–	86.1	120.0	[2e]
$[(dppe)_3Pt_3(\mu\text{-}S)_2]^{2+}$ (PAHSOQ)	3.121	3.064	2.365	–	2.248	–	80.8	82.6	–	85.8	120.0	[18a]
$[(dppp)_3Pt_3(\mu\text{-}S)_2]^{2+}$ (**7b**)	3.130	3.024	2.357	–	2.301	–	79.8	83.2	–	93.1	120.0	*this work*
$[(PhMe_2P)_6Pt_3(\mu\text{-}S)_2]^{2+}$ (CIXRUW)	3.157	3.016	2.366	–	2.269	–	79.2	83.7	–	98.9	120.0	[18b]

[a] S and S_H indicate the sulfur atoms of sulfido and thiol groups, Pt–P_S are Pt–P lengths *trans* to SH groups. [b] For experimental compounds, if available, refcode of Cambridge Structural Database is given. [c] Hydrogen atoms are disordered between the two *endo* bridging sulfur atoms.

However, when both bridges are thiol groups, $[Pt_2(\mu\text{-}SH)_2(P\cap P)_2]^{2+}$, more planar rings are obtained ($\theta = 150^\circ$), with the concomitant lengthening of the Pt···Pt distance. These changes in the degree of bending are responsible for the variations on the bond angles about the sulfur bridges.[16] Two conformations, which differ in the *endo* or *exo* orientation of the thiol proton with respect the hinged Pt_2S_2 ring,[16] have been calculated for $[Pt_2(\mu\text{-}S)(\mu\text{-}SH)(P\cap P)_2]^+$. Isomer *endo* becomes most stable when the solvent effect is introduced, but with an energy difference of only 0.4 kcal mol^{-1}. Unfortunately, hydrogen atoms have not been located in the crystal structures, precluding a comparison with the calculated structures. For complexes $[Pt_2(\mu\text{-}SH)_2(P\cap P)_2]^{2+}$, the *syn-exo* conformation is found to be $\sim$1 kcal mol^{-1} more stable than the *bent-anti* one. Protonation of sulfido bridges lengthens Pt–S bonds, and Pt–S_H lengths (thiol bridge, $\sim$2.47 Å) are always longer than those of the Pt–S (sulfido bridge, $\sim$2.40 Å). The difference can be also observed in experimental compounds.[6] These variations in Pt–S/S_H lengths are reflected in the Pt–P lengths by a *trans* influence, and values of 2.28 Å and 2.32 Å are obtained for Pt–P_{SH} and Pt–P_S, *trans* to the thiol and sulfido group, respectively. The very elongated Pt–S_H bond in the diprotonated species is worth mentioning as it is consistent with the presence of weakened Pt–S bonds, a factor that facilitates its cleavage.

A major difference between the dhpe and dhpp phosphines is found in the bite P-Pt-P angle of the complexes. Despite the diversity of compounds calculated, dhpp complexes always have P-Pt-P angles greater than those with dhpe, with differences varying between 6° and 9° for analogous compounds. Whereas calculated dhpe complexes present bite angles in a range of 85 – 87°, compounds having dhpp ligand appear more flexible, with values of 91 – 96°. Experimental complexes with related chelating diphosphines show the same tendency.[6] We conclude that the presence of dppe or dppp terminal diphosphine does not significantly affect the thermodynamics of the protonation steps.

An interesting point for $[Pt_2(\mu\text{-}S)(\mu\text{-}SH)(P\cap P)_2]^+$ complexes, related to the acidic character of the SH proton, is the possibility of SH···S hydrogen bonding. We studied this aspect in a recent communication. In addition to the presence of weak hydrogen bonding, for **2a** and **2b** we reported the first evidence of a fast S–H···S proton transfer in a transition metal system.[11]

2) Cleavage of the {Pt_2S_2} core: Two processes, which lead to different monometallic compounds, can be envisaged for the disintegration of the $\{Pt_2(\mu\text{-}SH)_2\}$ skeleton. If the two Pt–S bonds of the same platinum atom are broken, two different products, $[PtCl_2(P\cap P)]$ and $[Pt(SH)_2(P\cap P)]$ are formed (reaction **D**). In contrast to this, the rupture of one Pt–S bond from each moiety affords two mononuclear $[PtCl(SH)(P\cap P)]$ complexes (reaction **C**). Both processes are very exothermic and have similar reaction energies (around -40 kcal mol^{-1}). It can be expected that both processes take place simultaneously, and thus that species **4** – **6** are all present in solution. It is clear from Figure 1 that the driving force for the disintegration of the bimetallic species is the thermodynamic stability of the mononuclear compounds formed from the cleavage of the $\{Pt_2S_2\}$ core.

The experimental study shows that protonation of the SH ligands in **4** and **5** is followed by their subsequent replacement by Cl^- anions, leading to **6** as the final products. The substitution of the first SH^- by one Cl^- is favored by $\sim$9 kcal mol^{-1} (reaction **E**), and the second replacement by $\sim$7 kcal mol^{-1} (reaction **F**). The monometallic dichloride compounds are very stable, unreactive species, and their formation appears as a dead end in Figure 1. When $HClO_4$ is used as the source of protons, only dithiol complexes can be formed, due to the non-coordinating nature of the perchlorate anions.

Experimental data evidencing formation of bimetallic $[Pt_2(\mu\text{-}S)(\mu\text{-}SH)(P\cap P)_2]^+$ complexes from monometallic species show that the disintegration/formation of the $\{Pt_2S_2\}$ core is a cyclic process. Calculations indicate that the presence of $[Pt(SH)_2(P\cap P)]$ compounds is crucial for the cyclic character of this process. Such species are the less stable monometallic compounds, and $[Pt_2(\mu\text{-}S)(\mu\text{-}SH)(P\cap P)_2]^+$ complexes are found to be only 6 kcal mol^{-1} above two $[Pt(SH)_2(P\cap P)]$ molecules (reaction **G**). Formation of **2** from the direct dimerization of two $[PtCl(SH)(P\cap P)]$ monomers (reaction **H**) appears less plausible, given the high endothermicity of the reaction ($\sim$24 kcal mol^{-1}). As this process involves the formation of HCl, its removal with a base should facilitate the thermodynamically unfavored reaction **H**, as reported for related compounds in the presence of ternary amines.[5d] Consequently, the presence of NaSH, and its reaction with HCl, probably accounts for the experimental evolution of **6** to **2**. In an acidic medium, a more favorable pathway from **5** to **2** would probably require prior exchange of Cl^- by SH^- ligands in **5** to afford **6** and **4**, the latter evolving to **2** (reaction **G**).

Structural data for optimized monometallic complexes and related experimental compounds are presented in Table 6. As for the bimetallic complexes, a good agreement with the X-ray determined data is found. It is worth mentioning that the SH^- ligands have a stronger *trans* influence than Cl^- on the Pt–P bonds, as reflected in the Pt–P_S bonds, which are 0.05 Å longer than the Pt–P_{Cl}. The S···S distance in monometallic dithiol complexes is longer than in bimetallic or trimetallic due to greater S-Pt-S angles (Table 5 and Table 6). The optimized geometries show an increase in the P-Pt-P angles for the monometallic compounds when SH^- is replaced by Cl^-.

3) Generation of trimetallic species: Several possible pathways can be proposed to account for the generation of trimetallic complexes, among which trimolecular reactions can be excluded for kinetic reasons. Accordingly, on the basis of a bimolecular reaction, the following reaction mechanisms are possible: i) combination of two bimetallic complexes to give one trimetallic and one monometallic species and, ii) one bimetallic species reacts with a monometallic complex.

The reaction of two diprotonated dimers $[Pt_2(\mu\text{-}SH)_2(P\cap P)_2]^{2+}$ (**3**) to afford $[Pt_3(\mu_3\text{-}S)_2(P\cap P)_3]^{2+}$ (**7**) and $[Pt(SH)_2(P\cap P)]$ (**4**) (reaction **L**) is highly favored, mainly because of the diprotonated dimer's high energy. The mononuclear complex **4** can regenerate the $\{Pt_2S_2\}$ core by reaction

Table 6. Calculated and X-ray-determined geometrical parameters for $[PtX_2(P\cap P)]$ (X = Cl or SH) complexes. Some selected experimental compounds retrieved from Cambridge Structural Database are also shown.

Compound[a]	Pt–Cl	Pt–S	$Pt–P_{Cl}$[b]	$Pt–P_S$[b]	P-Pt-P	X-Pt-X	Reference[b]
[(dhpe)$PtCl_2$]	2.399	–	2.253	–	88.4	96.2	calcd
[(dhpp)$PtCl_2$]	2.408	–	2.257	–	98.5	95.9	calcd
[(dppe)$PtCl_2$] (BOFVIB)	2.348	–	2.208	–	86.2	90.2	[29]
[(dpype)$PtCl_2$] (WIXGIT)	2.354	–	2.210	–	86.2	90.8	[30]
[(dppe)$PtCl_2$] (DEBXUD)	2.355	–	2.227	–	86.8	89.1	[31]
[(dcype)$PtCl_2$] (WANHOI)	2.366	–	2.223	–	87.7	89.2	[32]
[(dtbpe)$PtCl_2$] (CBPTCB)	2.366	–	2.261	–	89.4	86.7	[33]
[(dtbpe)$PtCl_2$] (CBPEPT)	2.369	–	2.264	–	89.4	86.3	[33]
[(dppp)$PtCl_2$] (FONKOI)	2.362	–	2.232	–	91.6	88.4	[34]
[(dtbpp)$PtCl_2$] (BUPRPT)	2.360	–	2.282	–	99.1	83.2	[35]
mean values[c]	*2.352 ± 14*	–	*2.229 ± 23*	–	*94.6 ± 6.1*	*88.4 ± 1.8*	
[(dhpe)PtCl(SH)]	2.400	2.388	2.255	2.308	87.0	92.3	calcd
[(dhpp)PtCl(SH)]	2.407	2.395	2.256	2.313	95.4	91.8	calcd
[$(Ph_3P)_2$PtCl(SAr)$_2$] (PINDAR)	2.334	2.320	2.249	2.286	96.6	90.5	[36]
[(dhpe)$Pt(SH)_2$]	–	2.404	–	2.305	86.2	92.8	calcd
[(dhpp)$Pt(SH)_2$]	–	2.412	–	2.304	94.0	92.0	calcd
[(dppe)$Pt(SH)_2$] (**4a**)	–	2.350	–	2.251	86.2	87.6	this work
[(dppp)$Pt(SH)_2$] (**4b**)	–	2.356	–	2.270	91.2	86.2	this work
[(dppe)$Pt(SPh)_2$] (KIXGUT)	–	2.350	–	2.249	86.1	99.2	[37]
[(dppe)$Pt(SPy)_2$] (FOQPOQ)	–	2.358	–	2.263	85.7	82.7	[38]
[(dppe)$Pt(SPip)_2$] (KURMIT)	–	2.373	–	2.260	86.0	93.5	[39]
[$(Ph_3P)_2$Pt$(SH)_2$] (DTHLPT01)	–	2.343	–	2.255	97.0	86.8	[9b]
[$(Ph_3P)_2$Pt$(SAr)_2$] (PINDEV)	–	2.361	–	2.323	97.7	93.7	[36]

[a] For experimental compounds, phosphine (R = 2-py for dpype, R = Cy for dcype, R = *t*Bu for dtbpe, dtbpp) and monodentate ligands (SPy = 2-thiopyridinato, SPip = 4-thio-2-methyl-pyperidine, SAr = 2,4,6-tris(isopropyl)phenylthiolate anions) are as indicated; in most cases the refcode for the compound in the Cambridge Structural Database is provided. [b] $Pt–P_{Cl}$ and $Pt–P_S$ are Pt–P lengths *trans* to Cl and SH groups. [c] Mean and standard deviation of sample for 178 fragments of 166 refcodes found in a search on Cambridge Structural Database.

G, as shown above, although this reaction is competitive with the substitution of SH^- by Cl^- if the acid added is HCl. Complexes **3** are very unstable species, having two different ways of evolving towards stable products: disintegration (reactions **C** and **D**) or recombination (reaction **L**). Thus, it is not surprising that different behavior is observed, depending on factors such as the presence or absence of coordinating conjugate bases or the nature of the solvent.

Alternatively, $[Pt_2(\mu\text{-}S)(\mu\text{-}SH)(P\cap P)_2]^+$ may react with a monometallic complex (**4**, **5** or **6**) to form $[Pt_3(\mu_3\text{-}S)_2(P\cap P)_3]^{2+}$. This reaction is very plausible for **4** (reaction **K**), with a reaction energy of less than 2 kcal mol^{-1}, but the energy increases when the chloro complexes [PtCl(SH)(P∩P)] (**5**) or $[PtCl_2(P\cap P)]$ (**6**) are considered (~11 and ~18 kcal mol^{-1}, respectively). So reactions **I** and **J** are far less probable for the formation of the trimetallic complex (**7**) in acidic medium.

The high value calculated for the energy of reaction **I** agrees with the experimental data that complexes **2a**-Cl and **6a** do not react among themselves, and thus their combination cannot be a possible source of complex **7a**-Cl_2. It is clear that while the evolution of **2** in the presence of $HClO_4$ leads exclusively to the trimer **7**, in the presence of HCl, the formation of **7** competes with that of highly stable and inactive chloro complexes **6**.

One aspect of the formation of trimetallic $[Pt_3(\mu_3\text{-}S)_2(P\cap P)_3]^{2+}$ complexes that is not well reproduced by our calculations is the effect of the diphosphine ligand. Formation of these species is easier with dppe than with dppp. Our calculations give very similar ΔE values for both dhpe and dhpp throughout the corresponding reaction pathways. It seems reasonable to propose that the observed experimental differences are due to kinetic rather than thermodynamic factors.[17]

Structural data for $[Pt_3(\mu_3\text{-}S)_2(P\cap P)_3]^{2+}$ complexes have been presented in Table 5, where bimetallic compounds have been included for the sake of comparison. The Pt–S distances in the trimetallic species show similar values, which are intermediate between the Pt–SH and Pt–S distances found in dinuclear complexes with a $\{Pt_2S_2\}$ core. Furthermore, the bending angles of 120° in the trinuclear species imply shorter Pt···Pt distances than in the dinuclear analogues.[1]

Spectroscopic and structural characterization of the platinum complexes formed during the acid titration of $[Pt_2(\mu\text{-}S)_2P\cap P_2]$ (P∩P = dppe, dppp): The identification of the complexes formed in the evolution of $[Pt_2(\mu\text{-}S)_2(P\cap P)_2]$ (P∩P = dppe (**1a**), dppp (**1b**)) in the presence of HCl and $HClO_4$, which was monitored by $^{31}P\{^1H\}$ NMR data, required knowledge of the spectroscopic features of the species involved in this process. To this end, the synthesis and structural and spectroscopic characterization of complexes **4a**, **4b** and **7b**-$(PF_6)_2$ was undertaken; that of **1a** and **1b**,[2f,6] as well as their corresponding precursors, **6a** and **6b**,[12] and of **7a**-Cl_2,[2e] were already known. Within this context, the synthesis and X-ray crystal structures of **2a**-ClO_4 and **2b**-ClO_4 were also achieved. As variable-temperature $^{31}P\{^1H\}$ NMR studies in solutions containing **2a** or **2b** were indicative of an unprecedented intramolecular SH···S proton transfer in both cations, all these results have been anticipated in the form of a communication.[11] Main NMR and ESI MS parameters for complexes **1**, **2**, **4**, **6** and **7** are summarized in Table 2. Our unsuccessful attempts to isolate the doubly-protonated spe-

cies, **3a** and **3b**, are consistent with the absence of fully characterized sulfide-bridged analogous platinum complexes with other phosphine ligands.

As regards the monoprotonated complexes **2**, they were easily identified on the basis of the $^{31}P\{^{1}H\}$ NMR parameters at room temperature, where the four phosphorus nuclei become equivalent in solution, and easily characterized by ESI MS (Table 2). On the other hand, the ESI MS-monitored reaction of the isolated **2a**-ClO_4 and **2b**-ClO_4 with acid gave peaks at *m*/*z* 626.3 and 640.0, respectively, which could be initially assigned as $[\mathbf{2a}+H]^{2+}$ and $[\mathbf{2b}+H]^{2+}$. These observations, together with the fact that the intensity of both peaks increased when more acid was added to these mixtures, would be consistent with the formation of the corresponding doubly-protonated species, **3a** and **3b**, despite their elusive nature under usual laboratory conditions. Interestingly, we have observed peaks with the same *m*/*z* values (626.2 and 640.1) in the ESI MS spectra of **4a** and **4b**. In these species, the loss of one SH^- ligand accounts for the formation of the $[Pt(SH)(P\cap P)]^+$ fragment, whose mass exactly coincides with half of that of $[Pt_2(\mu\text{-}SH)_2(P\cap P)_2]^{2+}$. Accordingly, the mass spectral data obtained after adding acid to **2a**-ClO_4 and **2b**-ClO_4 would also be compatible with the formation of the corresponding $[Pt(SH)(P\cap P)]^+$ fragment, and thus the existence of the diprotonated cations, **3a** and **3b**, under ESI MS conditions is inconclusive evidence.

Complexes **4** have been characterized in the solid state by X-ray diffraction, as well as in solution. The $^{31}P\{^{1}H\}$ NMR spectra of **4**, unlike all the dinuclear and trinuclear platinum complexes involved in the evolution of **1** in the presence of acid, display a first-order pattern (Table 2). Concerning the signal corresponding to the protons of the SH groups in **4a** and **4b**, it appears as a false triplet, due to $^{2}J_{H,Pt}$ coupling, in both $^{1}H\{^{31}P\}$ NMR spectra, but it shows different patterns in the ^{1}H NMR spectra. Thus, for complex **4b**, containing the dppp ligand, it shows the $^{3}J_{H,P}$ coupling involving only the phosphorus atom *trans* to hydrogen, while for **4a**, with dppe, both $^{3}J_{H,P}$ couplings to P_{trans} and P_{cis} can be observed (Figure 2). These variations could be attributed to the different geometric constraints imposed by the diphosphine ligands, as the average P-Pt-S angle for adjacent P and S atoms is about 2° greater in **4a** than in **4b** (see below).

In addition, complex **7b**-$(PF_6)_2$ has been characterized in the solid state by X-ray diffraction, as well as in solution. Although it has been obtained by a different procedure from that followed for its analogue **7a**-Cl_2,[2e] the structures of **7a** and **7b** in the solid state compare well, as described below. Similarly, interpretation of the $^{31}P\{^{1}H\}$ NMR spectra of **7b** in solution requires consideration of second-order effects, as already reported for **7a**,[2e] whose spin system has facilitated the computer simulation and thus determination of the $^{1}J_{P,Pt}$, $^{2}J_{Pt,Pt}$ $^{3}J_{P,Pt}$ and $^{4}J_{P,P}$ coupling constants given in Table 2.

Molecular structures: Complexes **4a** and **4b** are structurally related as they both consist of mononuclear $[Pt(SH)_2(P\cap P)]$ discrete molecules ($P\cap P$ = dppe (**4a**), Figure 3, or dppp (**4b**), Figure 4), devoid of crystallographic symmetry elements. In the case of **4a**, there is also one CH_2Cl_2 molecule for each formula unit. The listing of the main geometric parameters for **4a** and **4b** appears in Table 7. In both **4a** and **4b**, the platinum atom has square planar coordination; the twist between the PtS_2 and PtP_2 planes is 7.2° (**4a**) or 3.4° (**4b**). In neither case could the hydrogen atoms of the SH groups be located, probably because they are rotationally disordered, having no hydrogen bond interactions.

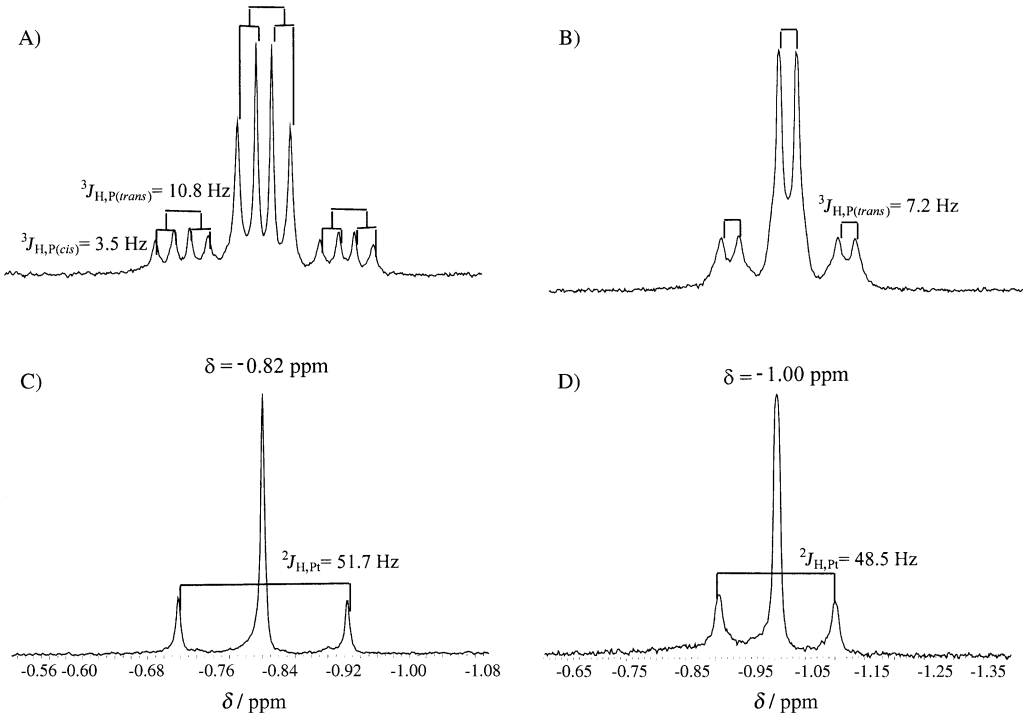

Figure 2. ^{1}H NMR signals corresponding to the SH groups in **4a** (A) and **4b** (C). $^{1}H\{^{31}P\}$ NMR signals corresponding to the SH groups in **4a** (B) and **4b** (D).

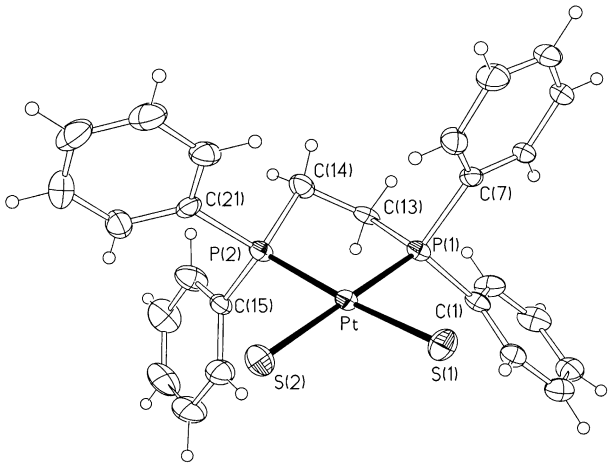

Figure 3. Structure of complex **4a**, with 50% probability displacement ellipsoids and selected atom labels.

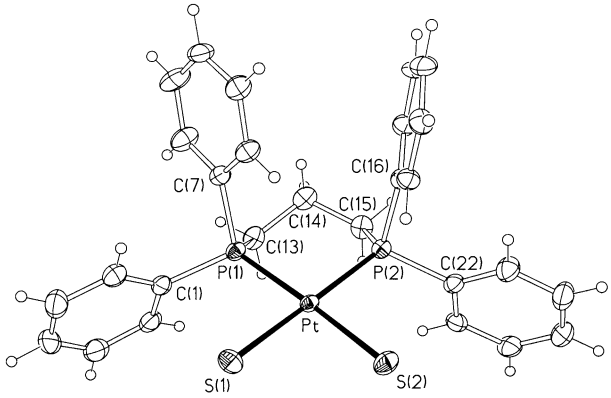

Figure 4. Structure of complex **4b**, with 50% probability displacement ellipsoids and selected atom labels.

Table 7. Selected bond lengths [Å] and angles [°] for compounds **4a** and **4b**.

	4a	**4b**
P–S(1)	2.3528(12)	2.3561(10)
Pt–S(2)	2.3469(14)	2.3553(10)
Pt–P(1)	2.2545(12)	2.2668(10)
Pt–P(2)	2.2478(12)	2.2730(10)
S(1)-Pt-S(2)	87.60(5)	86.16(4)
P(1)-Pt-P(2)	86.16(5)	91.16(4)
Pt-P(1)-C(13)	107.89(18)	114.08(13)
Pt-P(2)-C(14/15)	105.3(3)	117.02(14)

Comparison of **4a** and **4b** with the only other reported analogue for which structural parameters are available, $[Pt(SH)_2(PPh_3)_2]$,[9b] shows that the three structures have remarkable similarities. Obviously, they differ in the P-Pt-P angles (86.2 (**4a**), 91.2 (**4b**), and 97.0° for PPh_3 ligands), but these differences have no significant effect on the structural parameters involving the $Pt(SH)_2$ fragment (S-Pt-S angles are 87.6, 86.2, and 86.8°, respectively). Concerning the Pt(P∩P) moieties in **4a** and **4b**, their geometric features are in good concordance with those observed, respectively, in $[PtCl_2(dppe)]$ (**6a**) and $[PtCl_2(dppp)]$ (**6b**)[12] as well as in related species such as $[Pt_2(\mu\text{-}S)_2(P\cap P)_2]$ (P∩P = dppe (**1a**) or dppp (**1b**)),[2d,6] $[Pt_2(\mu\text{-}S)(\mu\text{-}SH)(P\cap P)_2]^+$ (P∩P = dppe (**2a**) or dppp (**2b**)),[11] and $[Pt_3(\mu_3\text{-}S)_2(P\cap P)_3]^{2+}$ (P∩P = dppe (**7a**)[2e] or dppp (**7b**)). As expected, the S-Pt-S angle, and thus the S–S length, in the $Pt(SH)_2$ fragment of the three mononuclear species are greater than those in the $\{Pt_2S_2\}$ rings of the dinuclear (**2**) or trinuclear complexes (**7**).

Complex **7b**-$(PF_6)_2$ consists of discrete trinuclear $[Pt_3(\mu_3\text{-}S)_2(dppp)_3]^{2+}$ cations (Figure 5) and PF_6^- anions, held together by electrostatic interactions. Main geometric parameters for **7b** are given in Table 8. The C_{3h} crystallographic

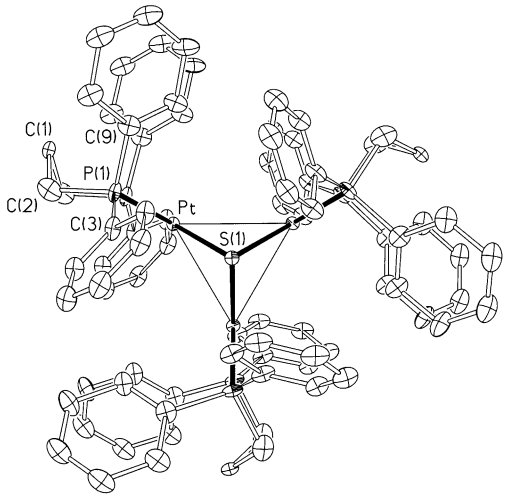

Figure 5. Structure of the complex cation **7b**, viewed along the threefold rotation axis, with 10% probability displacement ellipsoids and selected atom labels.

Table 8. Selected bond lengths [Å] and angles [°] for compound **7b**-$(PF_6)_2$.

Pt(1)–S(1)	2.357(7)	Pt(1)–P(1)	2.301(8)
S(1)-Pt(1)-S(1A)	79.8(4)	S(1)-Pt(1)-P(1)	93.5(3)
S(1)-Pt(1)-P(1A)	173.7(3)	P(1)-Pt(1)-P(1A)	93.1(5)
Pt(1)-S(1)-Pt(1B)	83.2(3)	Pt(1)-P(1)-C(2)	121(2)
Pt(1)···Pt(1A)	3.131(3)	θ	120.0

Symmetry operations for equivalent atoms: A: $x, y, 1-z$; B: $1-y, x-y, z$.

symmetry of the cation, the regular trigonal bipyramid geometry of the central Pt_3S_2 unit, and the square planar coordination of the platinum atoms in the three sulfur-linked PtS_2P_2 units are the main features of this structure, and compare well with those of the $[Pt_3(\mu_3\text{-}S)_2(dppe)_3]^{2+}$ (**7a**) analogue, already reported.[2e] By extending the structural comparison not only to the three other examples containing a $\{Pt_3(\mu_3\text{-}S)_2\}$ core,[2e,18] but also to complexes with a $\{Pt_3(\mu_3\text{-}X)_2\}$ core (X = Se, Te),[19] it is noteworthy that they all show significant similarities and that, among them all, the Pt_3S_2 core in complex **7b** has the highest crystallographic symmetry.

Concluding Remarks

Detailed study of the evolution of $[Pt_2(\mu\text{-}S)_2(P\cap P)_2]$ (P∩P = dppe or dppp) in the presence of protic acids, HCl or $HClO_4$,

confirms the outstanding nucleophilicity of the sulfide ligands in the $\{Pt_2S_2\}$ core. Experimental observations and theoretical calculations have allowed us to propose a cascade of sequential reactions triggered by the protonation of the stable monoprotonated $[Pt_2(\mu\text{-}S)(\mu\text{-}SH)(P\cap P)_2]^+$ complexes. This second protonation first involves disintegration of the $\{Pt_2S_2\}$ ring, and, eventually, regeneration of the monoprotonated dinuclear complex. Formation of complexes $[Pt(SH)_2(P\cap P)]$ is the keystone for the cyclical nature of the overall processes. The complexes $[PtCl_2(P\cap P)]$ and $[Pt_3(\mu_3\text{-}S)_2(P\cap P)_3]^{2+}$ do not react any further and thus are responsible for the cycles' dead end. Remarkably, the reaction pathways can be directed by controlling i) the concentration and nature of the protic acid (ie, the coordinative features of the conjugate anion); ii) the chelating diphosphine ligands, each having a particular bite angle; and iii) the polarity of the solvent used. Overall, while the richness of the chemistry of $[Pt_2(\mu\text{-}S)_2(P\cap P)_2]$ metalloligands was not unexpected, their tremendous versatility in the presence of protic acids had not been known up to that point. The cyclical nature of the latter processes, as well as the relevance of complexes containing the metal-SH fragment in the hydrodesulfurization processes, provides additional interest to the present findings with respect to their potential catalytic applications.

Experimental Section

Materials and methods: All manipulations were carried out at room temperature under an atmosphere of pure dinitrogen, and conventionally dried and degassed solvents were used throughout. These were Purex Analytical Grade from SDS. Metal complexes of formula $[PtCl_2(P\cap P)]$, $P\cap P$ = dppe (**6a**) or dppp (**6b**), were prepared according to published methods.[12] The synthesis of $[(P\cap P)Pt(\mu\text{-}S)_2Pt(P\cap P)]$, $P\cap P$ = dppe (**1a**) or dppp (**1b**), has already been reported.[2f,6]

Elemental analyses were performed on a Carlo-Erba CHNS EA-1108 analyzer. Analytical data for the carbon content in **4a** and **7b**-$(PF_6)_2$ deviate from calculated values, as already found in related complexes.[6],[11] Notwithstanding this, both complexes have been fully characterized by NMR, ESI MS and X-ray diffraction data. ^{1}H, ^{13}C{^{1}H} and ^{31}P{^{1}H} NMR spectra were recorded from samples in $(CD_3)_2SO$ solution at room temperature, using a Bruker AC250 spectrometer. ^{13}C and ^{1}H chemical shifts are relative to $SiMe_4$, and ^{31}P chemical shifts to external 85 % H_3PO_4. The ^{31}P{^{1}H} NMR spectrum of $[Pt_3(\mu_3\text{-}S)_2(dppp)_3]^{2+}$ was simulated on a Pentium-200 computer using the gNMR V4.0.1 program by P. H. M. Budzelaar from Cherwell Scientific Publishing.[20] The ESI MS measurements were performed on a VG Quattro Micromass Instrument. Experimental conditions were as follows: 10 μL of sample was injected at 15 μL min^{-1}; capillary-counter electrode voltage, 4.5 kV; lens-counter electrode voltage, 1.0 kV; cone potential, 55 V; source temperature, 90 °C; *m*/*z* range, 300 to 1600. The carrier was a 1:1 mixture of acetonitrile and water containing 1 % formic acid. In the case of the $[Pt_2(\mu\text{-}S)(\mu\text{-}SH)(P\cap P)_2]^+$ cations, **2a** and **2b**, the ESI MS measurements were carried out at different concentrations of formic acid (1 %, 10 % and 20 %).

Titration of $[Pt_2(\mu\text{-}S)_2(P\cap P)_2]$ ($P\cap P$ = dppe, 1a, or dppp, 1b) and $[Pt(SH)_2P\cap P]$ ($P\cap P$ = dppe, 4a or dppp, 4b) with HCl or $HClO_4$: In order to analyze the course of the reaction of **1a**, **1b**, **4a** and **4b** with HCl or $HClO_4$, controlled amounts of a concentrated or 2 M solution of acid were added to a solution of 10 mg of the corresponding pure compound in 5 mL of CH_3CN. The different solutions were evaporated to dryness, and the ^{31}P NMR spectra in $[D_6]$DMSO were recorded. When the amount of acid added impaired the evaporation to dryness, adding water to the previously concentrated solution precipitated the product.

Evolution with time of a solution of $[Pt_2(\mu\text{-}S)(\mu\text{-}SH)(P\cap P)_2]ClO_4$ ($P\cap P$ = dppe, 2a-ClO_4, or dppp, 2b-ClO_4) in the presence of HCl or $HClO_4$: $HClO_4$ (conc., 30 μL, 0.34 mmol) or HCl (conc., 25 μL, 0.30 mmol) was added to a solution of **2a**-ClO_4 or **2b**-ClO_4 (100 mg, 0.074 mmol **2a**-ClO_4, 0.072 mmol **2b**-ClO_4) in 50 mL of CH_3CN, CH_3OH, $(CH_3)_2CO$ or CH_2Cl_2. This solution was monitored for one week by taking one aliquot every 24 h, evaporating it to dryness and recording the ^{31}P NMR spectrum in $[D_6]$DMSO.

Reaction between $[Pt_2(\mu\text{-}S)(\mu\text{-}SH)(P\cap P)_2]ClO_4$ ($P\cap P$ = dppe, 2a-ClO_4, or dppp, 2b-ClO_4) and $[PtCl_2(P\cap P)]$ ($P\cap P$ = dppe, 6a or dppp, 6b): Solid **6a** or **6b** (50 mg, 0.075 mmol) was added to a solution of **2a**-ClO_4 or **2b**-ClO_4 (100 mg, 0.074 mmol **2a**-ClO_4, 0.072 mmol **2b**-ClO_4) in CH_3CN (50 mL), with stirring. The resulting suspension was stirred for one week and monitored by taking one aliquot every 24 h, evaporating it to dryness and recording the ^{31}P NMR spectrum in $[D_6]$DMSO. These data revealed that the reaction of **2a** with **6a**, as well as that of **2b** with **6b**, does not proceed under these experimental conditions.

Reaction between $[PtCl_2(P\cap P)]$ ($P\cap P$ = dppe, 6a or dppp, 6b) and $NaSH\cdot H_2O$ at a 1:1 molar ratio: $NaSH\cdot H_2O$ (11 mg, 0.150 mmol) was added to a suspension of **6a** or **6b** (100 mg, 0.150 mmol **6a**, 0.147 mmol **6b**) in benzene (50 mL). After 8 h of stirring, the final suspension was evaporated to dryness. The ^{31}P{^{1}H} NMR spectrum in $[D_6]$DMSO of the solid thus obtained showed the presence of the corresponding complexes of formulae $[Pt_2(\mu\text{-}S)(\mu\text{-}SH)(P\cap P)_2]Cl$ (**2a**-Cl or **2b**-Cl), and $[Pt(SH)_2(P\cap P)]$ (**4a** or **4b**) as a minor component. Alternatively, when the experiment was carried out using a fivefold excess of $NaSH\cdot H_2O$ (50 mg, 0.68 mmol), complexes **4a** or **4b** were obtained as major products and **1a** and **1b** as minor components. Formation of the latter can be attributed to the presence of sulfide as a minor impurity in commercial $NaSH\cdot H_2O$.

Synthesis of $[Pt(SH)_2(dppe)]$ (4a): $[PtCl_2(dppe)]$ (**6a**) (500 mg, 0.73 mmol) was added to a benzene solution (250 mL) of $NaSH\cdot H_2O$ (200 mg, 2.7 mmol) and the mixture stirred at room temperature for 8 h. The excess $NaSH\cdot H_2O$, the formed NaCl and the unreacted $[PtCl_2(dppp)]$ were filtered off. The filtrate was concentrated to 5 mL and the yellow solid was filtered and washed with diethyl ether. Yield 63 %; elemental analysis calcd (%) for $C_{26}H_{26}P_2PtS_2$: C 47.34, H 3.97, S 9.72; found: C 46.55, H 4.00, S 9.48. X-ray quality crystals of this compound were obtained by slow evaporation of a solution in CH_2Cl_2.

Synthesis of $[Pt(SH)_2(dppp)]$ (4b): Using the same procedure as that indicated for the previous compound, a yellow solid was obtained from the reaction of $[PtCl_2(dppp)]$ (**6b**) (500 mg, 0.75 mmol) with $NaSH\cdot H_2O$ (200 mg, 2.7 mmol) in a benzene solution (250 mL). Yield 59 %; elemental analysis calcd (%) for $C_{27}H_{28}P_2PtS_2\cdot C_6H_6$: C 52.72, H 4.56, S 8.53; found: C 52.93, H 4.84, S 7.93. Recrystallization in CH_2Cl_2 allowed isolation of yellow crystals.

Synthesis of $[Pt_3(\mu_3\text{-}S)_2(dppp)_3](PF_6)_2$, 7b-$(PF_6)_2$: $Na_2S\cdot 9H_2O$ (50 mg, 0.21 mmol) was added to a CH_3CN solution (25 mL) of $[PtCl_2(dppp)]$ (**6b**) (192 mg, 0.28 mmol) and KPF_6 (36 mg, 0.21 mmol) and the mixture stirred at room temperature for 24 h. These reaction conditions were chosen after monitoring the reaction by means of ^{31}P NMR, which allowed determination of the most appropriate reaction time for maximum yield. The NaCl and KCl formed were filtered off. The solvent was removed from the filtrate under vacuum, to yield the title compound as a yellow solid. Yield 75.0 %; elemental analysis calcd (%) for $C_{81}H_{78}F_{12}P_8Pt_3S_2$: C 44.70, H 3.61, S 2.95; found: C 43.89, H 3.60, S 2.94. Recrystallization of this compound from methanol gave colorless crystals suitable for X-ray diffraction.

CAUTION: The concentrated solutions of $HClO_4$ can give rise to explosive reactions. Concentrated $HClO_4$ should not make contact with dmso, because the reaction is very violent and exothermic.

X-ray crystallographic characterization: Crystal data for complexes **4a**, **4b** and **7b**-$(PF_6)_2$ are given in Table 9. All measurements were made at 160 K on a Bruker AXS SMART CCD diffractometer, with graphite-monochromated $Mo_{K\alpha}$ radiation (λ = 0.71073 Å). Cell parameters were refined from the observed positions of all strong reflections in the complete data sets. Absorption corrections were applied by inter-frame scaling procedures, based on redundant and symmetry-equivalent reflections.[21] The structures were solved by direct methods, and refined on all unique F^2 values, with anisotropic displacement parameters and constrained isotropic hydrogen atoms.[21] Hydrogen atoms could not be located on the SH ligands, and are probably rotationally disordered. Satisfactory refinement of the structure of **7b**-$(PF_6)_2$ was hampered by extensive disorder of the anions (modeled approximately by partial-occupancy sites for F atoms, the sum of the

Table 9. Crystallographic data for complexes **4a**, **4b** and **7b**-$(PF_6)_2$.

Complex	**4a** · CH_2Cl_2	**4b**	**7b**-$(PF_6)_2$
formula	$C_{26}H_{26}P_2PtS_2 \cdot CH_2Cl_2$	$C_{27}H_{28}P_2PtS_2$	$C_{81}H_{78}P_6Pt_3S_2(PF_6)_2$
M	744.5	673.6	2176.6
crystal system	orthorhombic	monoclinic	hexagonal
space group	$P2_12_12_1$	$P2_1/n$	$P62c$
a [Å]	9.7477(4)	12.9935(5)	16.774(5)
b [Å]	13.4951(6)	9.1308(4)	
c [Å]	21.0737(9)	21.2394(9)	19.025(4)
β [°]		91.997(2)	
V [Å^{-3}]	2772.2(2)	2518.33(18)	4636(2)
Z	4	4	2
ρ_{calcd} [g cm^{-3}]	1.784	1.777	1.559
μ [mm^{-1}]	5.54	5.88	4.76
reflections measured	22357	20755	23387
unique reflections	6412	5873	2101
R_{int}	0.037	0.039	0.097
parameters	308	290	186
R (F, $F^2 > 2\sigma$)	0.030	0.027	0.128
R_w (F^2, all data)	0.064	0.059	0.334
goodness of fit on F^2	1.10	1.04	1.22
max., min. electron density [e Å^{-3}]	1.80, −1.59	1.33, −1.35	6.04, −2.31

occupancies being constrained to 6 per anion; all P–F lengths are reasonable, but the angles are essentially meaningless and the anions are probably extensively rotationally disordered). An ambiguous space group assignment (many candidate space groups could fit the observed diffraction data approximately equally well, but no sensible ordered structure could be obtained in any lower-symmetry space group), and partial racemic twinning; the refinement was assisted by restraints on ligand geometry and atomic displacement parameters, and the gross structure of the trinuclear cation is unambiguously established.

CCDC-206306 (**4a**), CCDC-206307 (**4b**), and CCDC-206305 (**7b**-$(PF_6)_2$) contain the supplementary crystallographic data for this paper. These data can be obtained free of charge at www.ccdc.cam.ac.uk/conts/retrieving.html (or from the Cambridge Crystallographic Data Centre, 12 Union Road, Cambridge CB21EZ, UK; fax: (+44) 1223-336-033; or e-mail: deposit@ccdc.cam.ac.uk).

Computational details: Calculations were performed using the GAUSSIAN98 series of programmes.[22] Geometry optimizations were done in the full potential energy surface, without restrictions, using density functional theory (DFT) with the hybrid B3LYP functional.[23]. In the case of the most unstable species, vibrational analysis were performed to characterize them as minima. Effective core potentials (ECP) and their associated double-ξLANL2DZ basis set were used for the platinum, phosphorus, sulfur and chlorine atoms,[24] supplemented by an extra *d*-polarization in the case of P, S and Cl.[25] The 6–31G basis set was used for the C and H atoms.[26] Solvent effects were taken into account by means of PCM calculations,[27] using standard options of PCM and cavity keywords.[22] Energies were calculated with acetonitrile ($\varepsilon = 36.64$) as solvent, keeping the geometry optimized for the isolated species (single-point calculations). We have already used this approach in the study of the reactions of $[L_2Pt(\mu\text{-}S)_2PtL_2]$ with CH_2Cl_2.[6]

Structural analysis: Collection of structural data was carried out using the Cambridge Structural Database (Version 5.23).[28]

Acknowledgement

Financial support from the Ministerio de Ciencia y Tecnología of Spain (projects BQU2001–1976 and BQU2002–04110-CO2–02) is gratefully acknowledged. This research was partially supported by the Improving Human Potential Programme, Access to Research Infrastructures under contract HPRI-1999-CT-000071, Access to CESCA and CEPBA Large-Scale Facilities established between the European Community and CESCA-CEPBA. RMB is indebted to the Universitat Autònoma de Barcelona for a pre-doctoral scholarship.

[1] S.-W. A. Fong, T. S. A. Hor, *J. Chem. Soc. Dalton Trans.* **1999**, 639, and references therein.
[2] Selected recent references: a) S.-W. A. Fong, W. T. Yap, W. Teck, J. J. Vittal, W. Henderson, T. S. A. Hor, *J. Chem. Soc. Dalton Trans.* **2002**, 1826; b) Z. Li, Z.-H. Loh, K. F. Mok T. S. A. Hor, *Inorg. Chem.* **2000**, *39*, 5299; c) Z. Li, X. Xu, S. Khoo, K. F. Mok, T. S. A. Hor, *J. Chem. Soc. Dalton Trans.* **2000**, 2901; d) H. Liu, C. Jiang, J. S. L. Yeo, K. F. Mok, L. K. Liu, T. S. A. Hor, Y. K. Yan, *J. Organomet. Chem*. **2000**, *595*, 276; e) M. Capdevila, Y. Carrasco, W. Clegg, R. A. Coxall, P. González-Duarte, A. Lledós, J. A. Ramírez, *J. Chem. Soc. Dalton Trans.* **1999**, 3103; f) M. Capdevila, Y. Carrasco, W. Clegg, P. González-Duarte, A. Lledós, J. Sola, G. Ujaque, *Chem. Commun.* **1998**, 597.
[3] J. Chatt, D. M. P. Mingos, *J. Chem. Soc. A* **1970**, 1243.
[4] R. Ugo, G. La Monica, S. Cenini, A. Segre, F. Conti, *J. Chem. Soc. A* **1971**, 522.
[5] a) R. R. Gukathasan, R. H. Morris, A. Walker, *Can. J. Chem*. **1983**, *61*, 2490; b) M. Zhou, C. F. Lam, K. F. Mok, P.-H. Leung, T. S. A. Hor, *J. Organomet. Chem.* **1994**, *476*, C32; c) A. Shaver, R. D. Lai, P. H. Bird, W. Wickramasinghe, *Can. J. Chem*. **1985**, *63*, 2555; d) V. W.-W. Yam, P. Kok-Yan, K.-K. Cheung, *J. Chem. Soc. Chem. Commun.* **1995**, 267; e) M. Zhou, P.-H. Leung, K. F. Mok, T. S. A. Hor, *Polyhedron* **1996**, *15*, 1737.
[6] R. Mas-Ballesté, M. Capdevila, P. A. Champkin, W. Clegg, R. A. Coxall, A. Lledós, C. Mégret, P. González-Duarte, *Inorg. Chem.* **2002**, *41*, 3218.
[7] H. Li, G. B. Carpenter, D. A. Sweigart, *Organometallics* **2000**, *19*, 1823.
[8] R. J. Angelici, *Acc. Chem. Res.* **1988**, *21,* 391.
[9] a) M. S. Morton, R. N. Lachicotte, D. A. Vicic, W. D. Jones, *Organometallics* **1999**, *18*, 227; b) R. Vicente, J. Ribas, X. Solans, G. Germain, *An. Quim. Ser. B* **1986**, *82*, 47.
[10] A. Shaver, M. El-Khateeb, A.-M. Lebuis, *Angew. Chem.* **1996**, *108*, 2510; *Angew. Chem. Int. Ed. Engl*. **1996**, *35*, 2362.
[11] G. Aullón, M. Capdevila, W. Clegg, P. González-Duarte, A. Lledós, R. Mas-Ballesté, *Angew. Chem.* **2002**, *114*, 2900; *Angew. Chem. Int. Ed.* **2002**, *41*, 2776.
[12] M. P. Brown, R. J. Puddephatt, M. Rashidi, K. R. Seddon, *J. Chem. Soc. Dalton Trans.* **1977**, 951.
[13] a) S.-W. A. Fong, W. T. Yap, J. J. Vittal, T. S. A. Hor, W. Henderson, A. G. Oliver, C. E. F. Rickard, *J. Chem. Soc. Dalton Trans.* **2001**, 1986; b) S.-W. A. Fong, J. J. Vittal, W. Henderson, T. S. A. Hor, A. G. Oliver, C. E. F. Rickard, *Chem. Commun.* **2001**, 421.
[14] S. S. Oster, R. J. Lachicotte, W. D. Jones, *Inorg. Chim. Acta* **2002**, *330*, 118.

[15] G. Aullón, G. Ujaque, A. Lledós, S. Alvarez, *Chem. Eur. J.* **1999**, *5*, 1391.
[16] G. Aullón, A. Lledós, S. Alvarez, *Inorg. Chem.* **2000**, *39*, 906.
[17] The effect of the bite angle on reactivity has been recently reviewed: a) P. Dierkes, P. W. N. M. van Leeuwen, *J. Chem. Soc., Dalton Trans.* **1999**, 1519; b) P. W. N. M. van Leeuwen, P. C. J. Kamer, J. N. H. Reek, P. Dierkes, *Chem. Rev.* **2000**, *100*, 2741; c) P. C. J. Kamer, P. W. N. M. van Leeuwen, J. N. H. Reek, *Acc. Chem. Res.* **2001**, *34*, 895.
[18] a) M. J. Pilkington, A. M. Z. Slawin, D. J. Williams, J. D. Woollins, *J. Chem. Soc. Dalton Trans.* **1992**, 2425; b) G. W. Bushnell, K. R. Dixon, R. Ono, A. Pidcock, *Can. J. Chem.* **1984**, *62*, 696; c) Z. Li, H. F. Mok, A. S. Batsanov, J. A. K. Howard, T. S. A. Hor, *J. Organomet. Chem.* **1999**, *575*, 223.
[19] a) A. L. Ma, J. B. Thoden, L. F. Dahl, *J. Chem. Soc. Chem. Commun.* **1992**, 1516; b) K. Matsumoto, M. Ikuzawa, S. Ooi, *Inorg. Chim. Acta* **1994**, *217*, 129; c) R. Oliunkaniem, R. S. Laitinen, M. Ahlgren, *J. Organomet. Chem.* **2000**, *595*, 232.
[20] P. H. M. Budzelaar, *gNMR (V4.01)*; Cherwell Scientific Publishing Ldt.: Oxford, 1997.
[21] SMART, SAINT, SADABS and SHELXTL software; Bruker AXS Inc.: Madison, WI, 2001.
[22] M. J. Frisch, G. W. Trucks, H. B. Schlegel, G. E. Scuseria, M. A. Robb, J. R. Cheeseman, V. G. Zakrzewski, J. A. Montgomery, R. E. Stratmann, J. C. Burant, S. Dapprich, J. M. Millam, A. D. Daniels, K. N. Kudin, M. C. Strain, O. Farkas, J. Tomasi, V. Barone, M. Cossi, R. Cammi, B. Mennucci, C. Pomelli, C. Adamo, S. Clifford, J. Ochterski, G. A. Petersson, P. Y. Ayala, Q. Cui, K. Morokuma, D. K. Malick, A. D. Rabuck, K. Raghavachari, J. B. Foresman, J. Cioslowski, J. V. Ortiz, B. B. Stefanov, G. Liu, A. Liashenko, P. Piskorz, I. Komaromi, R. Gomperts, R. L. Martin, D. J. Fox, T. Keith, M. A. Al-Laham, C. Y. Peng, A. Nanayakkara, M. Challacombe, P. M. W. Gill, B. Johnson, W. Chen, M. W. Wong, J. L. Andres, C. Gonzalez, M. Head-Gordon, E. S. Replogle, J. A. Pople, Gaussian98 (Revision A.7), Gaussian Inc., Pittsburgh, PA, **1998**.
[23] a) A. D. Becke, *J. Chem. Phys.* **1993**, *98*, 5648; b) C. Lee, W. Yang, R. G. Parr, *Phys. Rev. B* **1988**, *37*, 785.
[24] a) P. J. Hay, W. R. Wadt, *J. Chem. Phys.* **1985**, *82*, 299; b) P. J. Hay, W. R. Wadt, *J. Chem. Phys.* **1985**, *82*, 270.
[25] A. Höllwarth, M. Böhme, S. Dapprich, A. W. Ehlers, A. Gobbi, V. Jonas, K. F. Köhler, R. Stegman, A. Veldkamp, G. Frenking, *Chem. Phys. Lett.* **1993**, *208*, 237.
[26] W. J. Hehre, R. Ditchfield, J. A. Pople, *J. Chem. Phys.* **1972**, *56*, 2257.
[27] a) J. Tomasi, M. Persico, *Chem. Rev.* **1994**, *94*, 2027; b) C. Amovilli, V. Barone, R. Cammi, E. Cancès, M. Cossi, B. Mennucci, C. S. Pomelli, J. Tomasi, *Adv. Quantum Chem.* **1998**, *32*, 227.
[28] F. H. Allen, O. Kennard, *Chem. Des. Autom. News* **1993**, *8*, 31.
[29] D. H. Farrar, G. Ferguson, *J. Cryst. Spectrosc. Res.* **1982**, *12*, 465; B. Bovio, F. Bonati, G. Banditelli, *Gazz. Chim. Ital.* **1985**, *115*, 613.
[30] N. D. Jones, K. S. MacFarlane, M. B. Smith, R. P. Schutte, S. J. Rettig, B. R. James, *Inorg. Chem.* **1999**, *38*, 3956.
[31] L. M. Engelhardt, J. M. Patrick, C. L. Raston, P. Twiss, A. H. White, *Aust. J. Chem.* **1984**, *37*, 2193.
[32] J. T. Mague, M. J. Fink, C. A. Recatto, *Acta Crystallogr. Sect. C* **1993**, *49*, 1176.
[33] M. Harada, Y. Kai, N. Yasuoka, N. Kasai, *Bull. Chem. Soc. Jpn.* **1976**, *49*, 3472.
[34] G. B. Robertson, W. A. Wickramasinghe, *Acta Crystallogr. Sect. C* **1987**, *43*, 1694.
[35] M. Harada, Y. Kai, N. Yasuoka, N. Kasai, *Bull. Chem. Soc. Jpn.* **1979**, *52*, 390.
[36] Q. Chen, F. Boeheim, J. Dabrowiak, J. Zubieta, *Inorg. Chim. Acta* **1994**, *216*, 83.
[37] W. Gou-Wei, H. Zhi-Ying, H. Mao-Chun, L. Han-Qin, *Jiegou Huaxue J. Struct. Chem.* **1991**, *10*, 159.
[38] T. S. Lobana, R. Verma, G. Hundal, A. Castiñeiras, *Polyhedron* **2000**, *19*, 899.
[39] M. Capdevila, W. Clegg, P. González-Duarte, B. Harris, I. Mira, J. Sola, I. C. Taylor, *J. Chem. Soc. Dalton Trans.* **1992**, 2817.

Received: March 24, 2003 [F4983]

Electrochemical and theoretical study of the redox properties of transition metal complexes with $\{Pt_2S_2\}$ core

Rubén Mas-Ballesté,[a] Mercé Capdevila,[a] Pilar González-Duarte,*[,a] Mohamed Hamidi,[a,b] Agustí Lledós,*[,a] Claire Mégret,[a] and Dominique de Montauzon[c†]

[a] *Departament de Química, Universitat Autònoma de Barcelona, E-08193 Bellaterra, Barcelona, Spain. Fax: (+34)935811363; Tel: (+34)935813101; E-mail: Pilar.Gonzalez.Duarte@uab.es agusti@klingon.uab.es*
[b] *Département de Chimie, Faculté des Scineces et Techniques, Université Moulay Ismaïl, P.B. 509, Er-Rachidia (Morocco)*
[c] *Laboratoire de Chimie de Coordination du CNRS, 205 Route de Narbone, 31077 Toulouse Cedex 4, France.*
† Dominique de Montauzon passed away on August 13th, 2001.

***This submission was created using the RSC Article Template* (*DO NOT DELETE THIS TEXT*)**
(*LINE INCLUDED FOR SPACING ONLY - DO NOT DELETE THIS TEXT*)

The oxidation processes undergone by the $\{Pt_2(\mu\text{-}S)_2\}$ core in $[Pt_2(P\cap P)_2(\mu\text{-}S)_2]$ ($P\cap P = Ph_2P(CH_2)_nPPh_2$, n = 2, 3) complexes have been analysed on the basis of electrochemical measurements. The experimental results are indicative of two consecutive monoelectronic oxidations after which the $\{Pt_2(\mu\text{-}S)_2\}$ core evolves into $\{Pt_2(\mu\text{-}S_2)\}^{2+}$, containing a bridging disulfide ligand. However, the instability of the monoxidised $[Pt_2(P\cap P)_2(\mu\text{-}S)_2]^+$ species formed initially, which converts into $[Pt_3(P\cap P)_3(\mu\text{-}S)_2]^{2+}$, hampered the synthesis and characterisation of the mono and dioxidised species. These drawbacks have been surpassed by means of DFT calculations which have also allowed the elucidation of the structural features of the species obtained from the oxidation of $[Pt_2(P\cap P)_2(\mu\text{-}S)_2]$ compounds. The calculated redox potentials corresponding to the oxidation processes are consistent with the experimental data obtained. In addition, calculations on the thermodynamics of possible processes following the degradation of $[Pt_2(P\cap P)_2(\mu\text{-}S)_2]^+$ are fully consistent with the concomitant formation of monometallic $[Pt(P\cap P)S_2)]$ and trimetallic $[Pt_3(P\cap P)_3(\mu\text{-}S)_2]^{2+}$ compounds. Extension of the theoretical study on the $\{Pt_2Te_2\}$ core and comparisons with the results obtained for $\{Pt_2S_2\}$ have given a more general picture of the behaviour of $\{Pt_2X_2\}$ (X= chalcogenide) cores subject to oxidation processes.

Introduction

The redox chemistry of bimetallic complexes containing a $\{M_2X_2\}$ (X = O, S) core has attracted great interest due to the relevance of these bimetallic complexes in essential biological redox processes such as electron transport[1] or oxygen activation.[2,3] For this reason compounds containing $\{Cu_2O_2\}$,[4] $\{Mn_2O_2\}$[5], $\{Fe_2O_2\}$[6], $\{Cu_2S_2\}$[7], $\{Mn_2S_2\}$[8] or $\{Fe_2S_2\}$[9] cores have been extensively investigated. Often, redox processes involving the $\{M_2X_2\}$ ring provoke significant structural changes as a result of bond-breaking or bond-forming across the ring.

From theoretical analysis it has been established that bonding between antipodal atoms in binuclear complexes obeys qualitative rules based on the occupation of framework molecular orbitals.[10,11] The absence of a through-ring bond is found for eight framework electrons, corresponding to four M-X bonds, whereas the presence of X-X or M-M bonding is anticipated for less than eight framework electrons. From these rules, it can be deduced that an electrochemical oxidation of a $\{M_2X_2\}$ (M = d^8-metal) core induces formation of X-X or M-M bonds by changing the number of electrons in the framework molecular orbitals. Indeed, both M-M and X-X bond forming have been observed upon oxidation of $\{Pt_2X_2\}$ rings. Thus, chemical oxidation of $[NBu_4]_2[Pt_2(\mu\text{-}PPh_2)_2(C_6F_5)_4]$ results in a considerable decrease in the Pt-Pt distance (from 3.621 Å to 2.7245 Å) in accordance with the formation of the binuclear Pt(III) compound with a Pt-Pt bond.[12] Analogously, chemical oxidation of $[Pt_2(PEt)_3)_4(\mu\text{-}Te)_2]$ causes a decrease in the Te-Te distance from a nonbonding length (3.263 Å) to a bonding length (2.695 Å), indicating the formation of a Te-Te bond in the dication.[13]

Significant advances in the chemistry of $[L_2Pt(\mu\text{-}S)_2PtL_2]$ complexes have been made in recent years. The ability to bridge sulfide ligands in the $\{Pt_2S_2\}$ core to act as electron-donors accounts for the unusual richness of the chemistry shown by $[L_2Pt(\mu\text{-}S)_2PtL_2]$ complexes.[14] This feature has allowed the synthesis of a wide range of homo- and heterometallic sulfide-bridged aggregates where compounds containing the $\{Pt_2S_2\}$ fragment play the role of metalloligand.[15] Recently, efforts have been focused on understanding the reactivity of $[L_2Pt(\mu\text{-}S)_2PtL_2]$ (L_2 = chelating diphosphine) towards non-metallic electron-acceptor species such as CH_2Cl_2[16] or the simplest electron-acceptor species, *i.e.* the proton.[17] These reactivities, that involve disintegration of the $\{Pt_2S_2\}$ core, consist in multi-step chemical processes that depend on the nature of the terminal phosphine ligand. Only recently has there been interest in studying the catalytic potential of such complexes in organic transformations.[18] However, the redox chemistry of $[L_2Pt(\mu\text{-}S)_2PtL_2]$ complexes still remains almost unexplored. The only available data refers to trimetallic aggregates. Electrochemical studies of the trimetallic clusters $[Pt_3S_2(P\cap P)_3]^{2+}$ ($P\cap P$ = dppm, dppe, dppp, dppb) have shown that the cyclic voltammograms depend on the chelate ring size and that the reversibility of the redox processes varies in the order dppe>dppp>dppb=dppm.[19] In addition, the role of the sulfide ligand in monoelectronic electrochemical oxidation of the $\{Pt_2S_2Hg\}$ core has been demonstrated recently.[20]

In this work the energetic and structural consequences of the successive removal of two electrons from the $\{Pt_2S_2\}$ core will be studied for the complexes $[Pt_2(P\cap P)_2(\mu\text{-}S)_2]$ ($P\cap P$ = 1,2-bis(diphenylphosphino)ethane (dppe) **1**, and 1,3-bis(diphenylphosphino)propane (dppp) **2**, by combining electrochemical measurements and DFT calculations. The structural assignment of the cyclic voltammogram peaks will rely on theoretical calculations, which have recently shown to be very useful for studying the redox properties of bimetallic complexes.[21] To asses the validity of our results, and also to extend the scope of this work, a theoretical study of the redox processes in the experimentally studied[13] $[Pt_2(PEt)_3)_4(\mu\text{-}Te)_2]$ (complex **3**) has also been undertaken.

Experimental

Electrochemical measurements. Complexes **1** and **2** were obtained according to published procedures.[16,22] Cyclic voltammograms and controlled potential coulometries of solutions of **1** and **2** in acetonitrile were recorded at 293 ± 1 K in a homemade potentiostat interfaced with a microcomputer. The former were recorded in 2 mmol L^{-1} with platinum wires as the working and counter electrodes. The latter were recorded in a 0.4 mmol L^{-1} solution with a gold disk (125μm of diameter) and a platinum wire as the working and counter electrodes, respectively. Throughout all the electrochemical measurements NBu_4BF_4 (0.1 mol L^{-1}) was used as the supporting electrolyte and the saturated calomel electrode as the reference electrode. All potentials are reported as reduction potentials with respect to this electrode.

EPR measurements of a 20 mmol L^{-1} solution of **2** in THF were carried out at 230 K in a Bruker ER 200D-SRC spectrometer in parallel with the controlled potential coulometry at 70 mV, using a glassy carbon rod and a platinum wire as the working and counter electrodes, respectively.

Computational details. Calculations were performed with the GAUSSIAN 98 series of programs.[23] Density Functional Theory (DFT) was applied with the B3LYP functional.[24] Effective core potentials (ECP) were used to represent the innermost electrons of the platinum atom[25a] as well as the electron core of P, S and Te atoms.[25b] The basis set for Pt was that associated with the pseudopotential, with a standard double-ζ LANL2DZ contraction.[23] The basis set for the P S and Te atoms was that associated with the pseudopotential, with a standard double-ζ LANL2DZ contraction[23] supplemented with a set of d-polarization functions.[26] A 6-31G basis set was used for the C and H atoms.[27] Solvent effects were taken into account by means of PCM calculations [28] using standard options of PCM and cavity keywords. [23] Free solvation energies were calculated with CH_2Cl_2 (ε = 8.93) or CH_3CN (ε = 36.64) as the solvent, keeping the geometry optimised for the isolated species (single-point calculations).

Results and discution

Experimental study of the electrochemical behaviour of $[Pt(dppe)_2(\mu\text{-}S)_2]$(1) and $[Pt(dppp)_2(\mu\text{-}S)_2]$(2) complexes

In order to investigate the oxidation processes of complexes **1** and **2**, electrochemical studies were carried out. Numerical data corresponding to the cyclic voltammograms (CV) recorded on a positive scan at 100 mV s^{-1} are summarised in Table 1. All potentials are reported with respect to the saturated calomel electrode (SCE).

The CV of **1** displays two oxidation waves, evidencing the monoelectronic oxidations at 960 and 56 mV, the former quasi-reversible and the latter irreversible (Figure 1A). An additional oxidation can be inferred from the quasi-reversible oxidation process at 293 mV. Complex **2** exhibits similar electrochemical behaviour, with two quasi-reversible oxidation waves with peak potentials of 875 and –45 mV (Figure 1B), whose separation with the corresponding reduction peaks (Table 1) could be indicative of two monoelectronic oxidation processes. In addition, there is a low intensity signal at approximately 200 mV that disappears at higher scan rates. In both complexes, an increase in the scan rate is accompanied by an increase in the reversibility of the first oxidation wave (E_a = 56 (**1**), -45 (**2**) mV) and a decrease in the intensity of the second wave (E_a = 293 (**1**), E_a ≈ 200 (**2**) mV). These data give evidence that the oxidation of the $[Pt_2(P\cap P)_2(\mu\text{-}S)_2]$ complexes (**1**, **2**) to yield $[Pt_2(P\cap P)_2(\mu\text{-}S)_2]^+$ ($\mathbf{1}^+$, $\mathbf{2}^+$) is followed by decomposition, one of the new species formed being responsible for the second oxidation wave. The stability of the oxidised $[Pt_2(P\cap P)_2(\mu\text{-}S)_2]^+$ form, which has been evaluated on the basis of the dependence of the reversibility of the oxidation wave (E_a = 56 (**1**), -45 (**2**) mV) with the scan rate,[29] being greater for dppp (mean life time *ca.*10 s) than for dppe (mean life time *ca.* 0.5 ms).

Controlled-potential coulometry for **1** in acetonitrile at 120 mV as well as for **2** in the same solvent at 70 and 1000 mV

Table 1 Numerical data from cyclic voltammograms of complexes **1** and **2** ($4x10^{-4}$ mol L^{-1}) in acetonitrile containing 0.1 mol L^{-1} NBu_4BF_4 at scan rate of 100 mV s^{-1} at 293 K

	E_{pa}(V)	E_{pc}(V)	$E_{1/2}$(V)	I_a/I_c
$[Pt_2(dppe)_2(\mu\text{-}S)_2]$ (**1**)	0.06	-	0.02	-
	0.29	0.22	0.25	0.87
	0.96	0.85	0.92	0.68
$[Pt_2(dppp)_2(\mu\text{-}S)_2]$ (**2**)	-0.04	-0.12	-0.08	0.69
	0.87	0.77	0.83	0.71

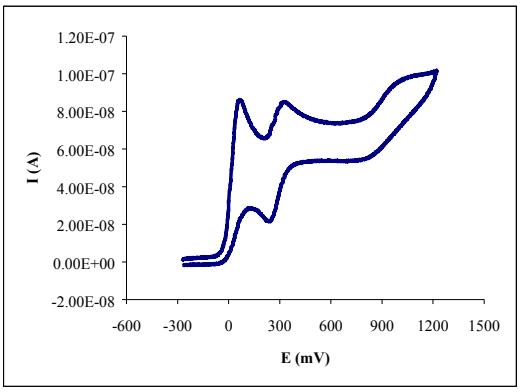

A

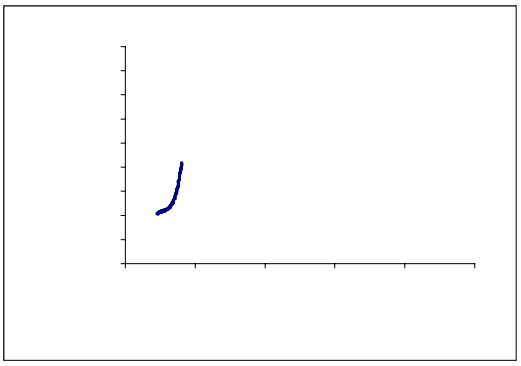

B

Fig.1 Cyclic voltammograms recorded on a positive scan at a scan rate of 100 mV s^{-1} ($4x10^{-4}$ mol L^{-1} in Acetonitrile Containing 0.1 mol L^{-1} NBu_4BF_4) at 293 K for complexes**1** (A) and **2** (B).

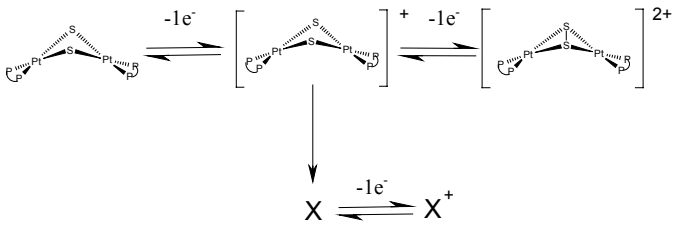

Scheme 1

indicates that the processes involved are one-electron oxidations. In addition, ^{31}P NMR spectra of the solutions containing the species obtained by electrolysis of **1** and **2** show the presence of the structurally characterised trinuclear $[Pt_3(P\cap P)_3(\mu_3\text{-}S)_2]^{2+}$ complex, P∩P= dppe,[15e] P∩P= dppp.[17a] This chemical evolution involves, at some stage, the breaking of the $\{Pt_2S_2\}$ central ring in $[Pt_2(P\cap P)_2(\mu\text{-}S)_2]^{+}$ to give $[Pt_3(P\cap P)_3(\mu_3\text{-}S)_2]^{2+}$. The greater mean life time of $[Pt_2(dppp)_2(\mu\text{-}S)_2]^{+}$ compared to that of the dppe analogue concords well with previous findings on the dependence of the reactivity of the $\{Pt_2S_2\}$ core in $[Pt_2(P\cap P)_2(\mu\text{-}S)_2]$ metalloligands with the diphosphine nature.[16,17] The electrochemical behaviour of **1** and **2** is summarised in Scheme 1, where X denotes the set of products resulting from the decomposition of $[Pt_2(P\cap P)_2(\mu\text{-}S)_2]^{+}$. X and X^{+} include the corresponding trinuclear $[Pt_3(P\cap P)_3(\mu_3\text{-}S)_2]^{2+}$ complex. This easy decomposition hampered the synthesis of $[Pt_2(P\cap P)_2(\mu\text{-}S_2)]^{2+}$ ($\mathbf{1}^{2+}$, $\mathbf{2}^{2+}$) via chemical oxidation of $[Pt_2(P\cap P)_2(\mu\text{-}S)_2]$.

In order to corroborate that the oxidation of **1** and **2** mainly affects the electronic density around the sulfur atoms, EPR measurements of **2** were run in parallel with the controlled potential coulometry at 70 mV (*vs* SCE) and 230 K. The EPR measurements show clearly that the spectrum of the oxidized $[Pt_2(dppp)_2(\mu\text{-}S)_2]^{+}$ species consists of only one singlet (3370G, g = 2.006). The absence of coupling with neighbouring nuclei indicates that the unpaired electron in $\mathbf{2}^{+}$ is highly localised in the sulfur atoms, suggesting that the electrochemical oxidation at 70 mV can be attributed to the oxidation of S^{2-} to S^{-} and therefore discounting the involvement of platinum ($Pt^{II} \rightarrow Pt^{III}$) or phosphorus ($P^{III} \rightarrow P^{IV}$) in the oxidation process. In the case of **1** no EPR signals were recorded in the analogous experiment, probably due to the ease of decomposition of the oxidised $[Pt_2(dppe)_2(\mu\text{-}S)_2]^{+}$ complex to yield diamagnetic species.

Theoretical study of the redox behaviour of $[Pt(P\cap P)_2(\mu\text{-}S)_2]$ (P∩P = dppe or dppp) complexes

Experimental evidences from circular voltammetry and EPR measurements show that the reversible oxidation of $[Pt_2(P\cap P)_2(\mu\text{-}S)_2]$ (P∩P = dppe or dppp) complexes results in the abstraction of two electrons from the bridging sulfide ligands. However, the easy disintegration of the bimetallic $\{Pt_2S_2\}$ core in the monocationic $[Pt_2(P\cap P)_2(\mu\text{-}S)_2]^{+}$ species, yielding the trimetallic $[Pt_3(P\cap P)_3(\mu_3\text{-}S)_2]^{2+}$ compound, makes it impossible to isolate and characterise the mono- or dicationic oxidised products. The experimental difficulty of characterising the bimetallic oxidised species has been overcome by means of DFT calculations. The study of molecular and electronic structures of the species involved in the redox process has been completed by the theoretical calculation of their redox potentials. Comparisons between experimental and calculated values of redox potentials can be used as criterion to determine the agreement of theoretical results with experimental data. In addition, this theoretical work includes a thermodynamic assessment of the decomposition reaction of $[Pt_2(P\cap P)_2(\mu\text{-}S)_2]^{+}$ to yield $[Pt_3(P\cap P)_3(\mu_3\text{-}S)_2]^{2+}$. Also, in order to widen the scope of this work towards a more general knowledge about the redox properties of $\{Pt_2X_2\}$ (X = Chalcogenide) rings, the theoretical study has been extended to $\{Pt_2Te_2\}$ compounds for which experimental data of their redox behaviour is known.

Molecular and electronic structures. The geometries of the $[Pt_2(P\cap P)_2(\mu\text{-}S)_2]^{n+}$ (n = 0, 1, 2; P∩P = dppp or dppe) compounds have been optimised by modelling dppe and dppp real ligands with $H_2P(CH_2)_2PH_2$ (dhpe) or $H_2P(CH_2)_3PH_2$ (dhpp), respectively. The main geometric parameters obtained are given in Table 2. The optimised geometries of the neutral and oxidised forms of the P∩P = dhpp complex are presented in Figure 2.

The B3LYP calculated geometries of neutral $[Pt_2(P\cap P)_2(\mu\text{-}S)_2]$ (P∩P = dhpe or dhpp) compounds have already been reported,[17a] and match well with the X-ray structures of **1**[22] and **2**.[16] Structural trends in edge-sharing binuclear d^8 complexes with $\{M_2(\mu\text{-}X)_2\}$ cores have recently been analysed.[30] A characteristic structural parameter for these complexes is the flexible dihedral angle between the two MX_2 planes (θ) that describes the degree of folding of the M_2X_2 ring.

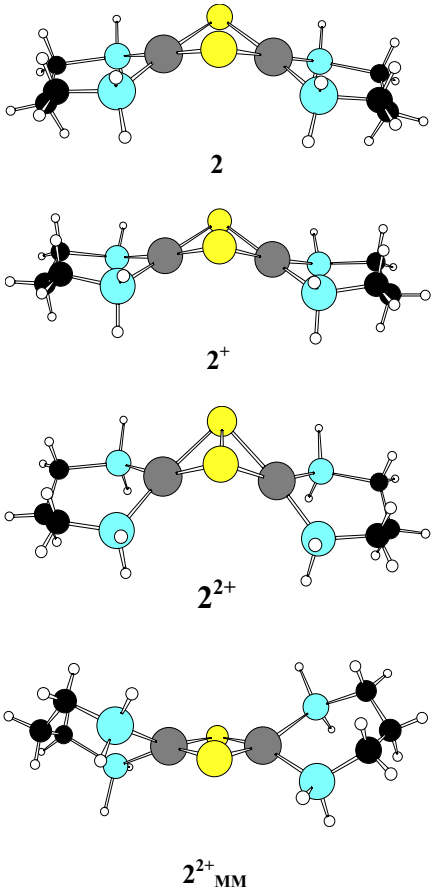

Fig. 2 Optimised structures for neutral and oxidised forms of $[Pt_2(H_2P(CH_2)_3PH_2)_2(\mu\text{-}S)_2]$.

Table 2 Optimised structural parameters for $[Pt_2(H_2P(CH_2)_nPH_2)_2(\mu\text{-}S)_2]^{z+}$ (n = 2, 3; z = 0, 1, 2). Bond lengths in Å, and angles in degrees.

	Pt···Pt	S···S	Pt-S	Pt-P	Pt-S-Pt	S-Pt-S	P-Pt-P	θ
1	3.301 *(3.292)*	3.216 *(3.134)*	2.399 *(2.341)*	2.299 *(2.238)*	86.1 *(87.4)*	84.2 *(83.0)*	95.7 *(94.6)*	134.0 *(134.8)*
$\mathbf{1}^{+}$	3.392	2.973	2.387	2.316	90.7	77.1	92.7	130.9
$\mathbf{1}^{2+}$	3.501	2.113	2.457	2.306	90.7	50.3	92.1	104.0
$\mathbf{1}^{2+}{}_{MM}$	2.824	3.811	2.371	2.348	73.1	106.9	85.4	179.8
2	3.286 *(3.235)*	3.228 *(3.101)*	2.406 *(2.332)*	2.293 *(2.255)*	86.9 *(88.9)*	84.1 *(83.6)*	86.5 *(86.2)*	136.0 *(140.2)*
$\mathbf{2}^{+}$	3.401	32.972	2.390	2.313	90.5	77.1	85.6	130.6
$\mathbf{2}^{2+}$	3.505	2.112	2.462	2.306	90.9	50.9	85.64	104.2
$\mathbf{2}^{2+}{}_{MM}$	2.876	3.771	2.381	2.351	74.6	105.3	91.6	176.1

[a] Experimental values in brackets and italic font-style.

Neutral $[Pt_2(P\cap P)_2(\mu\text{-}S)_2]$ complexes have a hinged $\{Pt_2S_2\}$ core ($\theta \sim 135$) (Figure 2). The values of the Pt···Pt and S···S distances clearly indicate the non-existence of through-ring bonds (see Table 2). Despite the structure of the $\{Pt_2S_2\}$ core being essentially preserved by the abstraction of one electron from the neutral compounds, some significant structural changes accompany the oxidation process. The main changes when going from **1** and **2** to the monocations $\mathbf{1}^+$ and $\mathbf{2}^+$ are: a slight decrease of the S···S distances and S-Pt-S angles, and the lengthening of the Pt···Pt distances. With these changes the central ring is squeezed, in such a way that the sulfur atoms approach each other, and the process can be interpreted as the formation of an incipient S-S bond. The structures of $\mathbf{1}^+$ and $\mathbf{2}^+$ described above have been obtained starting from the fully optimised neutral geometries and defining a positive charge for the system. We have looked for alternative structures of the monoxidised species, starting the optimisation from the two geometries of the dications (see below). In all the cases the optimisation has converged to the same geometry, thus confirming that $\mathbf{1}^+$ and $\mathbf{2}^+$ are the only stable structures for the $[Pt_2(P\cap P)_2(\mu\text{-}S)_2]^+$ species. The abstraction of a second electron from the $\{Pt_2S_2\}$ core enhances the structural tendencies found in the monoxidised complexes, with major consequences in the $\{Pt_2S_2\}$ ring: a S-S bond is formed (S-S = 2.113 Å in $\mathbf{1}^{2+}$ and S-S = 2.112 in $\mathbf{2}^{2+}$), with the concomitant lengthening of the Pt···Pt distance (Pt···Pt *ca.* 3.50 Å) and closing of the S-Pt-S angle. Another major change in the $\{Pt_2S_2\}$ framework upon oxidation is a large folding of the two PtS_2 planes along the S-S axis to give a highly bent geometry ($\theta = 104^o$ in $\mathbf{1}^{2+}$ and $\mathbf{2}^{2+}$). Thus, the dicationic species consist in a disulfide S_2^{2-} ligand bridging the two metallic centres, with a very hinged $\{Pt_2S_2\}$ ring (Figure 2). The same structural trends were found in the X-ray structure of the $[Pt_2(PEt)_3)_4(\mu\text{-}Te)_2]^{2+}$ complex.[13] A Hartree-Fock calculation of the $[Pt_2(PH_3)_4(\mu\text{-}Se)_2]^{n+}$ (n = 0, 2) complex also pointed out the formation of a Se-Se bond with the oxidation.[31]

We have considered the possible existence of isomeric forms of the dications, obtained by Pt oxidation. The optimisation of $[Pt_2(P\cap P)_2(\mu\text{-}S)_2]^+$ starting from a geometry with a short Pt-Pt distance leads to two new minima ($\mathbf{1}^{2+}_{\mathbf{MM}}$ and $\mathbf{2}^{2+}_{\mathbf{MM}}$) characterised by short Pt-Pt distances (Pt-Pt = 2.824 Å in $\mathbf{1}^{2+}_{\mathbf{MM}}$ and Pt-Pt = 2.876 in $\mathbf{2}^{2+}_{\mathbf{MM}}$), and long S···S distances (> 3.8 Å). These species present a planar $\{Pt_2S_2\}$ core (θ *ca.* 180º) and coordination geometry around the platinum atoms halfway between square-planar and tetrahedral (P-Pt-P-S dihedral angles of about 160º) (Figure 2). The same Pt-Pt distance has been found in the B3LYP optimised geometry of the oxidised $[Pt_2(C_6F_5)_4(\mu\text{-}PH_2)_2]$, calculated as a model of $[Pt_2(C_6F_5)_4(\mu\text{-}PPh_2)_2]$ and described as a Pt(III)-Pt(III) compound.[12b] The structural data of $\mathbf{1}^{2+}_{\mathbf{MM}}$ and $\mathbf{2}^{2+}_{\mathbf{MM}}$ indicates the oxidation of the metallic centres and the resulting formation of a Pt-Pt bond. However the products of the metal oxidation lie more than 140 kJ/mol above those of the sulfide oxidation (147.9 kJ/mol for $\mathbf{1}^{2+}_{\mathbf{MM}}$ and 151.4 kJ/mol for $\mathbf{2}^{2+}_{\mathbf{MM}}$). The greater stability of the disulfide containing $[Pt_2(P\cap P)_2(\mu\text{-}S_2)]^{2+}$ complexes suggests that this isomer is the final product for the abstraction of two electrons from the neutral $[Pt_2(dppp)_2(\mu\text{-}S)_2]$ compound. This hypothesis will be confirmed by the comparison of the calculated and experimental redox potentials (see below).

Figure 3 shows 3-D plots of the $[Pt_2(dhpp)_2(\mu\text{-}S)_2]^{n+}$ (n = 0, 1, 2) orbitals directly involved in the redox process. The HOMO of the neutral $[Pt_2(dhpp)_2(\mu\text{-}S)_2]$ complex consists in an antibonding combination of p_π orbitals of the sulfur atoms perpendicular to the $\{Pt_2S_2\}$ core (p_z). The Semi Occupied Molecular Orbital (SOMO) of the monocationic species is essentially the same combination of p_π orbitals, localised in the S atoms in agreement with the EPR measurements. Thus, it is clear that the electron is removed from the non-bonding electron pairs in the p_π orbitals of sulfide ligands. The structural changes, as a consequence of the oxidation of the $\{Pt_2S_2\}$ core, provoke an increase in the participation of d orbitals of the metallic centre

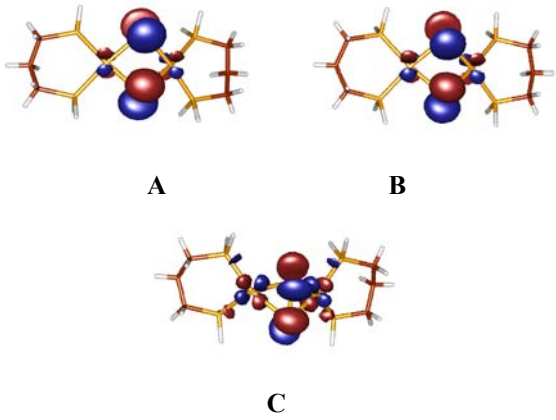

Fig. 3 HOMO (A), SOMO (B) and LUMO (B) of $[Pt_2(dhpp)_2(\mu\text{-}S)_2]$ $[Pt_2(dhpp)_2(\mu\text{-}S)_2]^+$ and $[Pt_2(dhpp)_2(\mu\text{-}S_2)]^{2+}$.

and an increased contribution of sulfur p_y orbitals in the LUMO of the dication. This qualitative orbital analysis shows that the molecular orbitals implied in the electrochemical oxidation of the complexes studied correspond to the sulfide ligands. The redox behaviour of the sulfide ligands in $[Pt_2(P\cap P)_2(\mu\text{-}S)_2]$ complexes is in strong accordance with the widely reported nucleophilicity of the bridging sulfur atoms of complexes containing a $\{Pt_2S_2\}$ core.[14-18]

The analysis of the evolution of NPA charges throughout the oxidation process gives an indication of how the positive charge is distributed. The atomic charges in the neutral $[Pt_2(dhpe)_2(\mu\text{-}S)_2]$ complex are –0.66e, + 0.11e and +0.56e, for the S, Pt and P atoms, respectively. In the monooxidised $\mathbf{1}^+$ the negative charge on each sulfur atom has decreased by 0.27e, whereas the positive charges in Pt and P atoms have only increased by 0.01e. In $\mathbf{1}^{2+}$ the atomic charges in each S, Pt and P atom are –0.11e, +0.11e and +0.60e. The remainder of the positive charge goes to the rest of the P-P ligands, which are mainly localised in the H atoms of these ligands. A very similar evolution of the atomic charges is found in the $[Pt_2(dhpp)_2(\mu\text{-}S)_2]$ system. So the NPA charges are fully consistent with the oxidation of the sulfur ligands. It is worth mentioning that in the $\mathbf{1}^{2+}_{\mathbf{MM}}$ isomer the positive charge increases in the platinum centre in accordance with the fact that the oxidation takes place in metal atoms.

Redox potentials. The theoretical data reported above indicates that the electrochemical oxidation of $[Pt(P\cap P)_2(\mu\text{-}S)_2]$ binuclear complexes results in the oxidation of sulfide ligands in the $\{Pt_2S_2\}$ core yielding the disulfide containing $[Pt(P\cap P)_2(\mu\text{-}S_2)]^{2+}$ products. However, the main experimental data obtained in this work are the potentials of electrochemical oxidation, which remain at this point without a theoretical estimation. Thus, with the aim of verifying that the theoretical and experimental data are fully consistent, the redox potentials of the oxidation processes have been calculated.

In order to obtain a realistic energetic approximation of reactions where charged species are generated, is necessary to take into account the solvent effects. With this aim we have calculated the free energy changes, (ΔG_{ox}) for the oxidation reactions in acetonitrile, following the approach based on continuum solvent models that can be found in recent literature.[21,32] An accurate calculation of the redox potentials is a very demanding problem. Only very recently has it been possible to calculate reduction potentials for the cyclooctatetraene and nitrobenze that are highly consistent with the experimental values.[33] We are aware of the difficulties of such calculations in large systems, with transition metal atoms, and that only semi-

Table 3 Calculated and experimental electrochemical potentials for the oxidation of $[Pt_2(P\cap P)_2(\mu\text{-}S)_2]$ complexes

P∩P			$(\Delta G_{ox})_{sol}$ (kJ/mol)	Calculated absolute potential (V)	Calculated potential *vs* ECS (V)	Experimental redox potential (V)
$H_2P(CH_2)_2PH_2$	$M\rightarrow M^+$		+430.9	4.47	-0.20	+0.02
	$M^+\rightarrow M^{2+}$	$\mathbf{1}^{2+}$	+507.0	5.26	+0.59	+0.92
		$\mathbf{1}^{2+}_{MM}$	+636.2	6.60	+1.93	
$H_2P(CH_2)_3PH_2$	$M\rightarrow M^+$		+428.8	4.45	-0.22	-0.08
	$M^+\rightarrow M^{2+}$	$\mathbf{2}^{2+}$	+504.9	5.24	+0.57	+0.83
		$\mathbf{2}^{2+}_{MM}$	+637.8	6.62	+1.95	

quantitative results can be expected. From the $(\Delta G_{ox})_{sol}$, the absolute redox potential can be calculated according to the following expression:

$$E_{ox} = (\Delta G_{ox})_{sol}/nF$$

Experimental data are always reported relative to a reference electrode. To obtain the values referenced with respect to the potential of the saturated calomel electrode (SCE) it is necessary to calculate the difference between the absolute potential obtained from the considered complex and the absolute potential of the reference electrode. The value of the absolute reduction potential of the hydrogen electrode appears in literature as +4.43 V.[34] From this value, and considering that the well-known reduction potential of SCE with respect to the hydrogen electrode is +0.24 V, the values of the potentials of the studied complexes, taking the SCE as a reference, can be calculated. The calculated redox potentials are given in Table 3. Despite these kinds of calculations only having semi-quantitative significance, the accordance between the experimental and theoretical values is remarkable. The experimental differences between the redox potentials corresponding to the first and second oxidations are 0.90V in **1** and 0.91V in **2**. The calculated differences in the theoretical models of **1** and **2** are both 0.79V. Depending on the considered isomer of the dicationic species two different values of the redox potential are obtained for the process $M^+\rightarrow M^{2+}$. However, while the calculated values corresponding to the process of obtaining the most stable isomers ($\mathbf{1}^{2+}$ and $\mathbf{2}^{2+}$) are close to the experimental redox potentials, the values for the $\mathbf{1}^{2+}_{MM}$ and $\mathbf{2}^{2+}_{MM}$ isomers are in marked disaccord with the experimental data. The closeness between the electrochemical data and DFT calculations confirms that the experimentally observed abstraction of two electrons from $[Pt_2(P\cap P)_2(\mu\text{-}S_2)]$ results in the formation of the disulfide containing complexes $[Pt_2(P\cap P)_2(\mu\text{-}S_2)]^{2+}$.

Reaction of degradation of monocationic complexes. According to the CV data, the experimental difficulty to determine all species implied in the oxidation of the $\{Pt_2S_2\}$ core arises from the disintegration of the monocationic species. Thus, both experiments of electrochemical or chemical oxidation have as a result the formation of several species, the main product being the well-known trimetallic $[Pt_3(P\cap P)_3(\mu_3\text{-}S)_2]$[2+,15e,17a] compounds. Probably, the evolution of the system is the result of a complex process where kinetic and thermodynamic factors have an important role. However, to get some ideas on how the disintegration of the monocationic complexes can proceed, we have considered several pathways for the degradation of the bimetallic monocationic species. In order to study the thermodynamic viability of the processes in acetonitrile as the solvent, single point PCM calculations on the optimised structures were performed and their ΔG in acetonitrile were calculated. We do not consider the kinetics of these processes, which probably include several steps. Notwithstanding, a thermodynamic estimation of the disintegration processes can give an additional insight into the chemical systems presented here.

The first reaction considered is the recombination of two monocations to give the trimetallic complexes and a neutral mononuclear complex:

$$2\,[Pt_2(P\cap P)_2(\mu\text{-}S)_2]^+ \rightarrow [Pt_3(P\cap P)_3(\mu_3\text{-}S)_2]^{2+} + [Pt(P\cap P)(S_2)] \quad \text{(Reaction 1)}$$

For both the complexes considered this reaction appears as very favourable, with ΔG values of –41.8 kJ per mol of $[Pt_2(dhpe)_2(\mu\text{-}S)_2]^+$ and –45.1 kJ per mol of $[Pt_2(dhpp)_2(\mu\text{-}S)_2]^+$. We have calculated the redox potentials for the oxidation of the mononuclear species:

$$[Pt(P\cap P)S_2)] \rightarrow [Pt(P\cap P)(S_2)]^+$$

The calculated redox potentials, with reference to the SCE, are 0.16 V and 0.13V, for P∩P = dhpe and dhpp, respectively. During the CV experiments we measured an oxidation potential of 0.25V for a disintegration product of $[Pt_2(dppe)_2(\mu\text{-}S)_2]^+$. Comparing the theoretical and experimental values, it is likely that $[Pt(dppe)(S_2)]$ is the detected disintegration product. In the optimised structure of this complex an S-S distance of 2.117 Å and a S-Pt-S of 52.2 were found, indicating the presence of a η^2-disulfide ligand. The only example found in literature, recently reported, of a complex structurally characterized containing the $\{PtS_2\}$ ring, shows similar structural features.[35]

We have also calculated the energetics of the reaction:

$$3\,[Pt_2(P\cap P)_2(\mu\text{-}S)_2]^+ \rightarrow 2\,[Pt_3(P\cap P)_3(\mu_3\text{-}S)_2]^{2+} + \tfrac{1}{2}\,S_4^{2-} \quad \text{(Reaction 2)}$$

The calculated ΔG in acetonitrile, which are similar for both diphosphine ligands, are indicative that this process is also favoured (ΔG = -19.2 kJ per mol of $[Pt_2(dhpe)_2(\mu\text{-}S)_2]^+$ and ΔG = –22.1 kJ per mol of $[Pt_2(dhpp)_2(\mu\text{-}S)_2]^+$), although it is less exothermic than reaction 1. As for reaction 1, we have calculated the redox potential for the oxidation of the reaction product:

$$S_4^{2-} \rightarrow S_4^-$$

Comparison of the value obtained (-2.52V) with the measured oxidation potential of the disintegration product (0.25V) led us to discard the S_4^{2-} anion as the CV detected species from the degradation of the monocationic species. Thus, from the theoretical results it is reasonable to conclude that reaction 1 is, probably, the source of the experimental difficulty to characterise the oxidised forms of the $\{Pt_2S_2\}$ compounds. It must be pointed out that despite the experimentally observed different stabilities of the monocationic species depending on the terminal diphosphine ligand, no thermodynamic differentiation is found by DFT calculations. This fact can be attributed to kinetic reasons that have already been reported in the literature for the formation of the trimetallic species from the reaction of $\{Pt_2S_2\}$ compounds with protic acids.[17a]

Comparison with telluride analogues. The closest work, found in literature, to the study presented here consists in the isolation and characterisation of $[Pt_2(PEt_3)_4(\mu\text{-}Te)_2]$ (**3**) and

Table 4 Optimised structural parameters for $[Pt_2(P(CH_3)_3)_4(\mu\text{-}S)_2]^{z+}$ (z = 0, 1, 2). Bond lengths in Å, and angles in degrees.

	Pt···Pt	Te···Te	Pt-Te	Pt-P	Pt-Te-Pt	Te-Pt-Te	P-Pt-P	θ
3	4.177 *(4.100)*	3.390 *(3.263)*	2.706 *(2.618)*	2.346*(2.286)*	101.0 *(103.0)*	77.6 *(77.0)*	105.4 *(106.3)*	164.0 *(180.0)*
$\mathbf{3}^{+}$	3.889	3.099	2.705	2.356	94.6	71.5	98.1	129.8
$\mathbf{3}^{2+}$	3.831 *(3.648)*	2.713 *(2.697)*	2.741 *(2.634)*	2.343*(2.273)*	*88.6 (87.5)*	*59.3 (61.5)*	*98.5 (98.3)*	*107.0 (107.4)*

[a] Experimental values for the complex with phosphine = $P(Et)_3$ in brackets and italic font-style.

$$[Pt_2(\mu\text{-}Te)_2(P(CH_3)_3)_4] \xrightarrow{-0.73\ V} [Pt_2(\mu\text{-}Te)_2(P(CH_3)_3)_4]^{+} \underset{(+0.40\ V)}{\xrightarrow{+0.23\ V}} [Pt_2(\mu\text{-}Te_2)(P(CH_3)_3)_4]^{2+}$$

Scheme 2

$[Pt_2(PEt)_3)_4(\mu\text{-}Te_2)]^{2+}$ ($\mathbf{3}^{2+}$).[13] Taking advantage of the existence of electrochemical and structural experimental data corresponding to these $\{Pt_2Te_2\}$ compounds, this work has been completed by the theoretical study of the oxidation processes of these complexes. Comparisons between the results obtained for $\{Pt_2Te_2\}$ and $\{Pt_2S_2\}$ complexes can improve the understanding of factors that modulate the redox activity of bimetallic $\{M_2X_2\}$ (X = Chalcogenide) systems.

The structures of neutral, monocationic and dicationic $\{Pt_2Te_2\}$ species have been optimised by taking PMe_3 as the terminal ligand. The main optimised geometrical parameters are given in Table 4, together with the X-ray determined values for **3** and $\mathbf{3}^{2+}$.[13] The structure of the monooxidised species has never been reported. The B3LYP structures of $[Pt_2(PMe)_4(\mu\text{-}Te)_2]$ and $[Pt_2(PMe)_3)_4(\mu\text{-}Te_2)]^{2+}$ are highly consistent with their experimental analogues. The neutral compound has a flat $\{Pt_2Te_2\}$ central ring without through-ring bonds (Te···Te = 3.390 Å). The removal of one electron causes the hinging of the $\{Pt_2Te_2\}$ core (θ = 129.8º) and the incipient formation of a Te-Te bond (Te···Te = 3.099 Å). The removal of the second electron essentially results in the enhancement of the folding of the core (θ = 107.0º) and the complete formation of the Te-Te bond (Te···Te = 2.713 Å). Therefore, a bridging ditelluride is present in the dication. We have also looked for a $\mathbf{3}^{2+}_{\mathbf{MM}}$ isomer, with a short Pt-Pt distance. However in this case only the isomer of the dicationic complex with a short Te-Te distance was found.

The orbital analysis of the $\{Pt_2Te_2\}$ compounds gives the same qualitative results as the previous study of sulfide analogues: the molecular orbitals involved in the oxidation of bimetallic $\{Pt_2X_2\}$(X= Chalcogenide) species correspond to the chalcogenide anion. The energy of the HOMO of $[Pt_2(PMe_3)_4(\mu\text{-}Te)_2]$ (-3.46eV) is approximately 0.43 eV above the HOMO of the $[Pt_2(\mu\text{-}S)_2(P\cap P)_2]$ complexes. This fact is in strong accordance with the lower electronegativity of tellurium compared with that of sulfur and indicates that the lone electron-pairs in chalcogenide anions are more accessible in $\{Pt_2Te_2\}$ compounds than in their sulfide-containing analogues. This effect is also observed in the calculated values of redox potentials. The evolution of the NPA charges throughout the oxidation is consistent with the process taking place in the telluride ligands. Charges on each Te atom are –0.49e, -0.18e and +0.06e, in the neutral, monocationic and dicationic complexes, respectively.

In order to obtain the redox potentials and the ΔG of the process of degradation of the monocationic species, single point PCM calculations in CH_2Cl_2 (the solvent used in the experiments reported in literature) were performed. The calculated redox potentials are presented in the Latimer diagram shown in Scheme 2. The results obtained show that **3** exhibits two monoelectronic oxidations. Our value of the redox potential for the second monooxidation (0.22V) is not far from that of the irreversible oxidation wave measured for $[Pt_2(PEt_3)_4(\mu\text{-}Te)_2]$[13] The calculated difference between the potential values corresponding to the first and second electrochemical oxidations of **3** (0.96V) is comparable to that observed in the study of $\{Pt_2S_2\}$ compounds. Nevertheless, the values of redox potentials found for $\{Pt_2Te_2\}$ complexes are significantly lower than those observed for compounds containing $\{Pt_2S_2\}$. This observation is highly consistent with the higher energy of the HOMO of $[Pt_2(PMe_3)_4(\mu\text{-}Te)_2]$ complex compared with that of $\{Pt_2S_2\}$ compounds and with the lower electronegativity of the tellurium atom.

The process to obtain the trimetallic complex $[Pt_3(PEt_3)_6(\mu_3\text{-}Te)_2]^{2+}$ accompanying the formation of the oxidised $\mathbf{3}^{2+}$ has been reported.[13] We have also analysed the viability of the formation of the trimetallic complex from the degradation of the monocation, by calculating the energetics of the following reactions in dichloromethane:

$$2\ [Pt_2(PMe_3)_4(\mu\text{-}Te)_2]^{+} \rightarrow [Pt_3(PMe_3)_6(\mu_3\text{-}Te)_2]^{2+} + [Pt(PMe_3)_2Te_2)] \qquad \text{(Reaction 3)}$$

$$3\ [Pt_2(PMe_3)_4(\mu\text{-}Te)_2]^{+} \rightarrow 2\ [Pt_3(PMe_3)_6(\mu_3\text{-}Te)_2]^{2+} + \tfrac{1}{2}\ Te_4^{2-} \qquad \text{(Reaction 4)}$$

These two processes are analogous to reactions 1 and 2 which are considered for the degradation of the $\{Pt_2S_2\}$ monooxidised species in acetonitrile. The theoretical results indicate that reaction 3 is slightly exothermic (-8.3 kJ per mol of $[Pt_2(PMe_3)_4(\mu\text{-}Te)_2]^{+}$) whereas reaction 4 is endothermic (ΔG = +32.2 kJ per mol of $[Pt_2(P(CH_3)_3)_4(\mu\text{-}Te)_2]^{+}$). Matching well with the reported results, the cleavage of $\{Pt_2Te_2\}^{+}$ is significantly less favourable than that of $\{Pt_2S_2\}^{+}$. Consequently, although the formation of $[Pt_3(PEt_3)_6(\mu_3\text{-}Te)_2]^{2+}$ is also a competitive reaction with the process to obtain $\mathbf{3}^{2+}$, it has been possible to isolate and characterise $[Pt_2(PEt_3)_4(\mu\text{-}Te_2)]^{2+}$ in contrast with the results obtained with the $\{Pt_2S_2\}$ compounds.

Concluding Remarks

Experimental and theoretical data reported here demonstrate the potentiality of $\{Pt_2(\mu\text{-}X)_2\}$ (X = chalcogenide) systems to show reversible redox processes comparable to those observed in several metalloenzimes. The oxidation induces major structural changes in the $\{Pt_2X_2\}$ ring and entails formation of a through-ring X-X bond and a large folding of the two Pt_2X planes along the X-X axis. The oxidised species can be described as containing a bridging dichalcogenide ligand. The reversible oxidation reaction $\{Pt_2(\mu\text{-}X)_2\} \rightarrow \{Pt_2(\mu\text{-}X_2)\}^{2+}$ appears plausible, considering that, in all cases studied, the potential of this process is less than 1V (*vs.* SCE). The experimental data reported here also demonstrate that the redox properties of the $\{Pt_2(\mu\text{-}S)_2\}$ are tuneable by means of subtle parameters such as changing the P-Pt-P bite angle caused by replacing dppe by dppp as the terminal ligands.

Nevertheless, the decomposition of monooxidised $\{Pt_2(\mu\text{-}X)_2\}^{+}$ species to yield $\{Pt_3(\mu_3\text{-}X)_2\}^{2+}$ appears as a

competitive reaction with the formation of dichalcogenide containing $\{Pt_2(\mu\text{-}X_2)\}^{2+}$ species. Fortunately, as shown in the literature, the ability of bimetallic species $\{Pt_2(\mu\text{-}X)_2\}$ to form trimetallic $\{Pt_3(\mu_3\text{-}S)_2\}^{2+}$ complexes can be tuned by controlling, for example, the nature of terminal ligands. Future works in this field could be addressed to the study of $\{M_2(\mu\text{-}X)_2\}$ complexes where the formation of $\{M_3(\mu_3\text{-}X)_2\}^{2+}$ compounds is disfavoured. The use of bulky terminal ligands preventing the formation of the dead end $\{M_3(\mu_3\text{-}X)_2\}^{2+}$ species could be one of the possible strategies.

In conclusion, this work shows that the redox chemistry of $\{M_2(\mu\text{-}X)_2\}$ has the characteristic subtlety found in biological systems, where several electronic and structural parameters play an important role. New insights on the factors that allow control over the redox properties of systems containing biological and synthetic $\{M_2(\mu\text{-}X)_2\}$ seems to be a promising area, which deserves further development.

Acknowledgments

Financial support from the *Ministerio de Ciencia y Tecnología* of Spain (projects BQU2001-1976 and BQU2002-04110-CO2-02) is gratefully acknowledged. RMB is indebted to the *Universitat Autònoma de Barcelona* for a pre-doctoral scholarship. The use of the computational facilities of the Centre de Supercomputació de Catalunya (CESCA) is also gratefully appreciated.

References

1 (a) J. W. Peteres, W. N. Lanzilotta, L. Brian and L. Seefeldt, *Science*, 1998, **282**, 1858. (b) S. J. Lippard and J. M. Berg, *Principles of Bioinorganic Chemistry*, University Science Books: Mill valley, California, 1994.

2 (a) G. Aullón E. Ruiz and S. Alvarez, *Chem. Eur. J.,* 2002, **8**, 2508. (b) E. I. Solomon, T. C. Brunold, M. I. Davis, J. N. Kemsley, S.-K. Lee, F. Lehnert, F. R. Neese, A. J. Skulan, Y.-S. Yang and J. Zhou, *Chem Rev.,* 2000, **100**, 235. (c) J. Stubbe and van der W. A. Donk, *Chem Rev.,* 1998, **98**, 705.

3 L.Que Jr. and W. B. Tollman, *Angew. Chem. Int. Ed.,* 2002, **41**, 1114.

4 (a) S. Itoh, M. Taki, H. Nakao, P. L. Holland, W. B. Tolman, L. Que Jr. and S. Fukuzumi, *Angew. Chem Int. Ed. Engl.*, 2000, **39**, 398. (b) J. A. Halfen, S. Mahapatra, E. C. Wilkinson, G. Pan, X. Wang, V. G. Young Jr., L. Que Jr. and W. B. Tolman, *Science*,1996, **271**, 1397.

5 (a) R. Manchada, G. V. Burdvig and R. H. Crabtree, *Coord. Chem. Rev.*, 1995, **144**, 1. (b) K. Wieghardt, *Angew. Chem Int. Ed. Engl.*, 1989, **28**, 1153.

6 Y. Zang, Y. Dong, L. Que Jr., K. Kauffmann and E. Münk, *J. Am. Chem. Soc.*, 1995, **117**, 1169.

7 K. Fujisawa, Y. Moro-oka and N. Kitajima, *J. Chem. Soc., Chem. Commun.,* 1994, 623.

8 R. D. Adams, O.-S. Kwon and M. D. Smith, *Inorg. Chem.*, 2002, **41**, 1658.

9 (a) N. Ueyama, Y. Yamada, T.-A. Okamura, S. Kimura and A. Nakamura, *Inorg. Chem.*, 1996, **35**, 6475. (b) N. Ueyama, S. Ueno, T. Sugawara, K. Tatsumi, N. Nakamura and N. Yasuoka, *J. Chem. Soc., Dalton Trans*., 1991, 2723. (c) A. Salifoglou, M. G. Kanatzidis and D. Coucouvanis, *Inorg. Chem.*, 1988, **27**, 3394.

10 S. Alvarez, A. A. Palacios and G. Aullón, *Coord. Chem. Rev.,* 1999, **185-186**, 431.

11 (a) A. A. Palacios, P. Alemany and S. Alvarez, *J. Chem. Soc., Dalton Trans*., 2002, 2235. (b) A. A. Palacios, G. Aullón, P. Alemany and S. Alvarez, *Inorg. Chem.*, 2000, **39**, 3166. (c) X.-Y. Liu, A. A. Palacios, J. J. Novoa and S. Alvarez, *Inorg. Chem*., 1998, **37**, 1202. (d) G. Aullón, P. Alemany and S. Alvarez, *J. Organomet. Chem.*, 1994, **478**, 75. (e) P. Alemany and S. Alvarez, *Inorg. Chem.*, 1992, **31**, 4266.

12 (a) E. Alonso, J. M. Casas, J. Forniés, C. Fortuño, A. Martín, A. G. Orpen, C. A. Tsipis and A. C. Tsipis, *Organometallics*, 2001, **20**, 5571. (b) E. Alonso, J. M. Casas, F. A. Cotton, X. Feng, J. Forniés, C. Fortuño and M. Tomas, *Inorg. Chem.*, 1999, **38**, 5034.

13 A. L. Ma, J.B. Thoden and L. F. Dahl, *J. Chem. Soc., Chem. Commun.,* 1992, 1516.

14 S.-W. A. Fong and T. S. A. Hor, *J. Chem. Soc., Dalton Trans*., 1999, 639, and references therein.

15 Selected recent references: (*a*) S.-W. A. Fong, W. T. Yap, W. Teck, J. J. Vittal, W. Henderson and T. S. A. Hor, *J. Chem. Soc., Dalton Trans*., 2002, 1826. (*b*) Z. Li, Z.-H. Loh, K. F. Mok and T. S. A. Hor, *Inorg. Chem.,* 2000, **39**, 5299. (*c*) Z. Li, X. Xu, S. Khoo, K. F. Mok and T. S. A. Hor, *J. Chem. Soc., Dalton Trans*., 2000, 2901. (*d*) H. Liu, C. Jiang, J. S. L. Yeo, K. F. Mok, L. K. Liu, T. S. A. Hor and Y. K. Yan, *J. Organomet. Chem*., 2000, **595**, 276. (*e*) M. Capdevila, Y. Carrasco, W. Clegg, R. A. Coxall, P. González-Duarte, A. Lledós and J. A. Ramírez, *J. Chem. Soc., Dalton Trans*., 1999, 3103.

16 R. Mas-Ballesté, M. Capdevila, P. A. Champkin, W. Clegg, R. A. Coxall, A. Lledós, C. Mégret and P. González-Duarte, *Inorg. Chem.,* 2002, **41**, 3218.

17 (a) R. Mas-Ballesté, G. Aullón, P. A. Champkin, W. Clegg, C. Megret, P. González-Duarte and A. Lledós, *Chem. Eur. J.,* 2003, **9**, 5023. (b) G. Aullón, M. Capdevila, W. Clegg, P. González-Duarte, A. Lledós and R. Mas-Ballesté, *Angew. Chem. Int. Ed. Engl.* 2002, **41**, 2776.

18 (a) S. H. Chong, A. Tjindrawan and T. S. A. Hor, *J. Mol. Cat. A*, 2003, **204**, 267. (b) H. Brunner, M. Weber and M. Zabel, *J. Organomet. Chem.*, 2003, **684**, 6.

19 (a) K. Matsumoto, K. Takahashi, M. Ikuzawa, H. Kimoto and S. Okeya, *Inorg. Chim. Acta*, 1998, **281**, 174. (b) K. Matsumoto, M. Ikuzawa, M. Kamikubo and S. Ooi, *Inorg. Chim. Acta*, 1994, **217**, 129. (c) K. Matsumoto, N. Saiga, S. Tanaka and S. Ooi, *J. Chem. soc., Dalton Trans.*, **1991**, 1265.

20 X. Xu, S-W. A. Fong, Z. Li, Z.-H. Loh, J. J. Vittal, W. Henderson, S-B. Khoo and T. S. A. Hor, *Inorg. Chem.* 2002, **41**, 6838.

21 (a) S. Blasco, I. Demachy, Y. Jean and A. Lledós, *New J. Chem.*, 2001, **25**, 611. (b) M.-H. Baik, T. Ziegler and C. K. Schauer, *J. Am. Chem. Soc.*, 2000, **122**, 9143.

22 M. Capdevila, Y. Carrasco, W. Clegg, P. González-Duarte, A. Lledós, J. Sola and G. Ujaque, *Chem. Commun.,* 1998, 597.

23 M. J. Frisch, G. W. Trucks, H. B. Schlegel, G. E. Scuseria, M. A. Robb, J. R. Cheeseman, V. G. Zakrzewski, J. A. Montgomery, R. E. Stratmann, J. C. Burant, S. Dapprich, J. M. Millam, A. D. Daniels, K. N. Kudin, M. C. Strain, O. Farkas, J. Tomasi, V. Barone, M. Cossi, R. Cammi, B. Mennucci, C. Pomelli, C. Adamo, S. Clifford, J. Ochterski, G. A. Petersson, P. Y. Ayala, Q. Cui, K. Morokuma, D. K. Malick, A. D. Rabuck, K. Raghavachari, J. B. Foresman, J. Cioslowski, J. V. Ortiz, B. B. Stefanov, G. Liu, A. Liashenko, P. Piskorz, I. Komaromi, R. Gomperts, R. L. Martin, D. J. Fox, T. Keith, M. A. Al-Laham, C. Y. Peng, A. Nanayakkara, C. Gonzalez, M. Challacombe, P. M. W. Gill, B. Johnson, W. Chen, M. W. Wong, J. L. Andres, C. Gonzalez, M. Head-Gordon, E. S. Replogle and J. A. Pople, *Gaussian98 (Revission A.7)*; Gaussian Inc.: Pittsburgh, PA, 1998.

24 (a) C. Lee, W. Yang and R. G. Parr, *Phys. Rev. B*, 1988, **37**, 785. (b) A. D. Becke, *J. Chem. Phys*., 1993, **98**, 5648. (c) P. J. Stephens, F. J. Delvin, C. F. Chabalowski and M. J. Frisch, *J. Phys. Chem*., 1994, **98**, 11623.

25 (a) P. J. Hay and W. R. Wadt, *J. Chem. Phys*., 1985, **82**, 299. (b) W. R. Wadt and P. J. Hay, *J. Chem. Phys*., 1985, **82**, 284.

26 A. Höllwarth, M. Böhme, S. Dapprich, A. W. Ehlers, A. Gobbi, V. Jonas, K. F. Köhler, R. Stegman, A. Veldkamp and G. Frenking, *Chem. Phys. Lett*., 1993, **208**, 237.

27 W. J. Hehre, R. Ditchfield and J. Pople, A. *J. Chem. Phys*., 1972, **56**, 2257.

28 (a) C. Amovilli, V. Barone, R. Cammi, E. Cancès, M. Cossi, B. Mennucci, C. S. Pomelli and J. Tomasi, *Adv. Quantum Chem.,* 1998, **32**, 227. (b) J. Tomasi and M. Persico, *Chem. Rev.,* 1994, **94**, 2027.

29 R. S. Nicholson and I. Shain, *Anal. Chem.,* 1964, **36**, 706.

30 G. Aullón, G. Ujaque, A. Lledós and S. Alvarez, *Inorg. Chem.*, 1998, **37**, 804.

31 A. Bencini, M. di Vaira, R. Morassi and P. Stoppioni, *Polyhedron*, 1996, **15**, 2079.

32 (a) P. Winget, E. J. Weber, C. J. Cramer and D. G. Truhlar, *Phys. Chem. Chem. Phys.*, 2000, **2**, 1231. (b) L. J. Kette, S. P. Bates and A. R. Mount, *Phys. Chem. Chem. Phys.*, 2000, **2**, 195. (c) L. Li, C. L. Fisher, R. Konecny, D. Bashford and L. Noodleman, *Inorg. Chem.*, 1999, **38**, 929. (d) J. Li, M. R. Nelson, C. Y. Peng, D. Bashford and L. Noodleman, *J. Phys Chem.*, 1998, **102**, 6311. (e) S. A. Macgregor and K. K. Moock, *Inorg. Chem.*, 1998, **37**, 3284.

33 M.-H. Baik, C. K. Schauer and T. Ziegler, *J. Am. Chem. Soc.*, 2002, **124**, 11167.

34 H. Reiss and A. Heller, *J. Phys Chem.*, 1985, **89**, 4207.

35 K. Nagata, N. Takeda and N. Tokito, *Angew. Chem. Int. Ed. Engl.,* 2002, **41**, 136.

1.-Vista la labilitat dels anions clorur en l'espècie $[\{Pt_2(\mu_3\text{-}S)_2(dppp)_2\}PtCl_2]$, es pot concloure que els complexos de formula general $[\{Pt_2(\mu_3\text{-}S)_2(L)_4\}PtCl_2]$, obren la porta cap a l'obtenció d'una família de nous compostos d'alta nuclearitat amb el centre $\{Pt_{2n}S_{2n}\}$ on n =1, 3, 7... El camí que es proposa per a l'obtenció d'aquestes espècies macromoleculars es pot expressar de la següent manera:

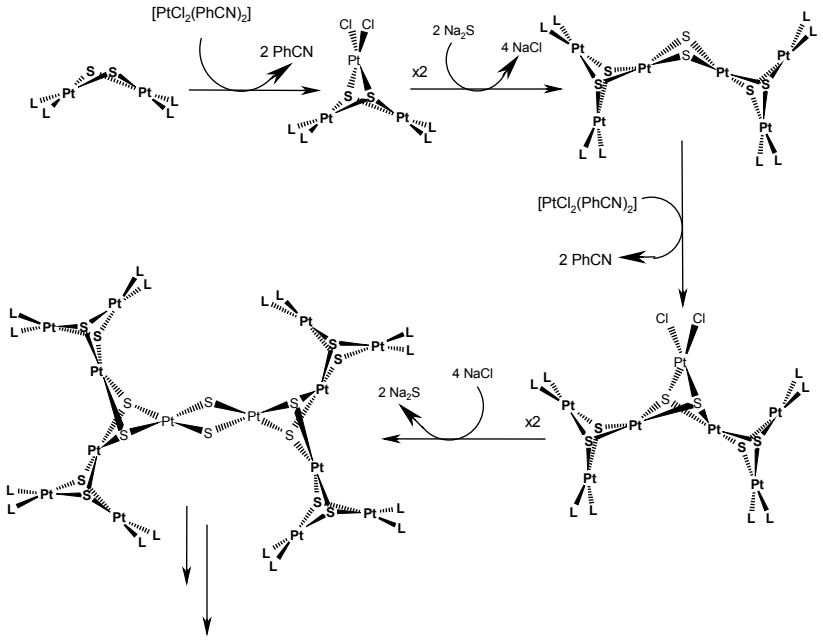

2.-En actuar com a lligand, el compost $[Pt_2(\mu\text{-}S)_2(dppp)_2]$, té una forta influencia sobre la reactivitat del fragment metàl·lic al qual es coordina. Aquest efecte s'ha demostrat de dues maneres en aquesta tesi doctoral:

a) En comparar el comportament químic dels compostos $[Pt_2(\mu\text{-}S)_2(L\cap L)_2]$, essent L∩L= dppp o $[Pt_2(\mu\text{-}S)_2(dppp)_2]$, s'observa una major basicitat dels anions sulfur del centre $\{Pt_2S_2\}$ quan el lligand quelatant terminal emprat és $[Pt_2(\mu\text{-}S)_2(dppp)_2]$.

b) El fragment metàl·lic $\{Pt(cod)\}^{2+}$ en coordinar-se a un metàl·lolligand del tipus $[Pt_2(\mu\text{-}S)_2(L\cap L)_2]$, mostra un comportament químic diferent al descrit fins al moment. Una d'aquestes anomalies químiques consisteix en una sorprenent inèrcia envers la substitució del lligand cod en el complex $[Pt_2(\mu\text{-}S)_2(dppp)_2\{Pt(cod)\}]^{2+}$. Per altra part, els compostos de tipus $[Pt_2(\mu\text{-}S)_2(L\cap L)_2\{Pt(cod)\}]^{2+}$ presenten la desprotonació del lligand cod en una posició al·lílica en reaccionar amb l'anió metòxid. Aquesta reacció de desprotonació és inèdita ja que la reactivitat descrita fins al moment per a complexos amb el fragment $\{Pt(cod)\}^{2+}$ amb MeO^- consisteix en la inserció de la base al lligand olefínic.

Mentre que el primer efecte comentat (a) és de naturalesa termodinàmica, el segon efecte esmentat (b) és, probablement, d'origen cinètic. Es pot dir, doncs, que la coordinació al lligand $[Pt_2(\mu\text{-}S)_2(P\cap P)_2]$ és una bona eina per modular i dirigir la reactivitat i les propietats químiques d'un centre metàl·lic.

3.- L'elevada densitat electrònica dels anions sulfur en els complexos $[Pt_2(\mu\text{-}S)_2(P\cap P)_2]$ (P∩P= dppe, dppp) fa possible que aquest compost activi l'enllaç C-Cl de la molècula de CH_2Cl_2. Aquest fet fa evident la forta nucleofilicitat del centre $\{Pt_2S_2\}$ i planteja la possibilitat de que aquests metàl·lolligands puguin ser utilitzats per a activar d'altres enllaços inerts. Aquesta tesi doctoral ha demostrat que tots els compostos descrits a la bibliografia referents a la reactivitat dels complexos$[Pt_2(\mu\text{-}S)_2L_4]$amb CH_2Cl_2 es poden encabir en el següent esquema general:

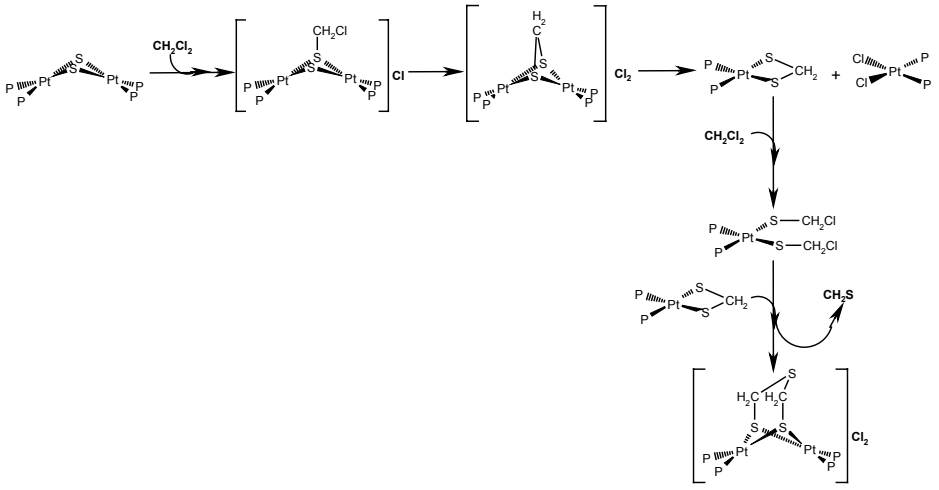

El procés químic descrit pot aturar-se a un o altre estadi de la reacció depenent del lligand terminal, la qual cosa explica la diversitat dels resultats publicats fins al moment i presenta la possibilitat de modular la reactivitat dels complexos $[Pt_2(\mu\text{-}S)_2L_4]$ controlant la naturalesa del lligand terminal L.

4.- La basicitat dels anions sulfur en el centre $\{Pt_2S_2\}$ queda reflectida en la reacció dels compostos $[Pt_2(\mu\text{-}S)_2(P\cap P)_2]$ (P∩P= dppe, dppp) envers àcids pròtics. El primer producte de la reactivitat d'aquests complexos amb àcids del tipus HX és el compost monoprotonat $[Pt_2(\mu\text{-}S)(\mu\text{-}SH)(P\cap P)_2]X$. La presència d'un segon lloc bàsic a la molècula del compost monoprotonat té dues conseqüències que han estat estudiades en aquesta tesi doctoral:

a) La coexistència d'un protó SH àcid i un lloc bàsic tal com l'anió sulfur sense protonar, en el complex $[Pt_2(\mu\text{-}S)(\mu\text{-}SH)(P\cap P)_2]X$, té com a conseqüència la interacció SH···S. Malgrat que aquesta interacció es considera habitualment com de

baixa intensitat, en el cas estudiat en aquesta tesi doctoral és tant important que no es limita a un simple enllaç d'hidrogen SH···S, sinó que el protó queda deslocalitzat entre els dos anions sulfur mitjançant un procés de transferència protònica intramolecular. Aquest treball el és primer precedent d'aquest procés i demostra que en els mecanismes de les reaccions en les que intervenen compostos amb el fragment S-M-SH es poden incloure processos de transferència protònica S-H···S.

b) Per altra part, en presencia d'un gran excés d'àcid (HX) es poden arribar a protonar ambdós anions sulfur del centre $\{Pt_2S_2\}$. El compost diprotonat és altament inestable, es trenca, i es desencadena un complex procés químic tal com es representa a continuació per HX = HCl o $HClO_4$:

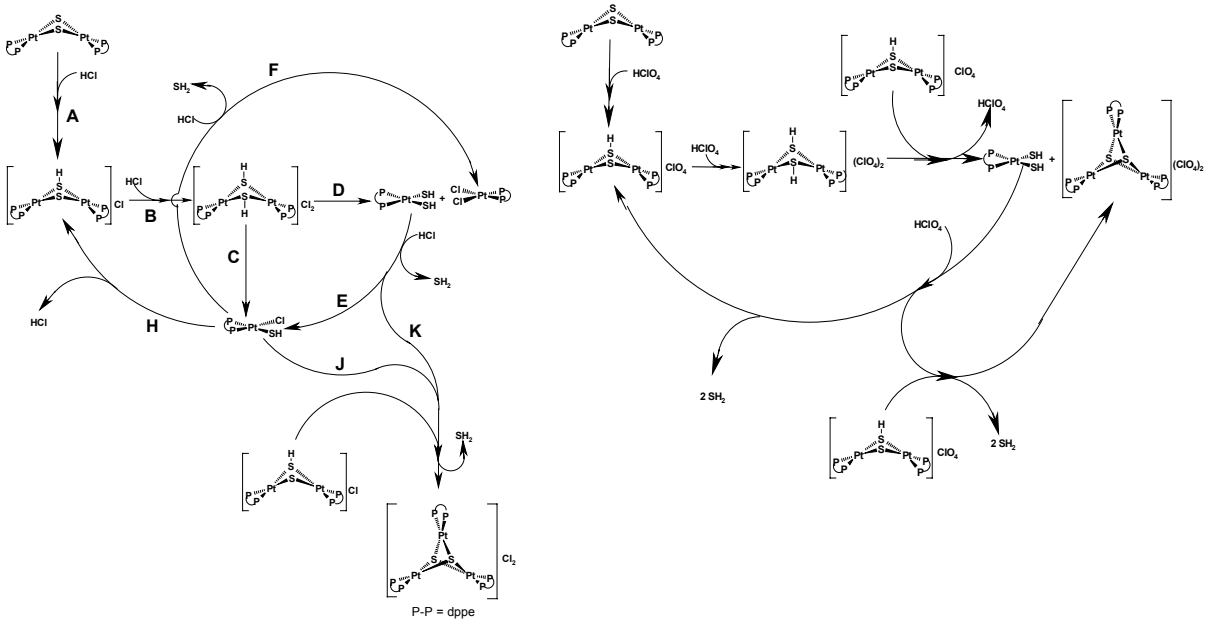

La riquesa química del sistema que es deriva de la segona protonació del centre $\{Pt_2S_2\}$, així com la naturalesa cíclica d'aquest procés, posada de manifest per la dimerització del compost $[Pt(SH)_2(P\cap P)]$, donen evidència de la diversitat que presenta la reactivitat dels compostos amb el fragment Pt-SH, i deixen entreveure la seva rellevància en processos catalítics tal com els de hidrodesulfuració.

5.- La combinació de dades experimentals obtingudes per mesures electroquímiques i dades teòriques obtingudes per càlculs DFT, ha permès establir que els compostos amb el centre $\{Pt_2S_2\}$ poden experimentar dos oxidacions monoelectròniques consecutives segons es representa a continuació:

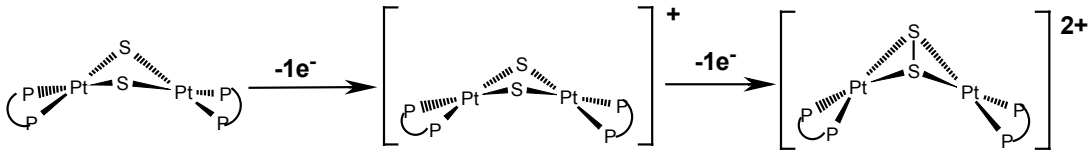

D'acord amb l'estudi presentat, el producte final de l'oxidació dels compostos $[Pt_2(\mu\text{-}S)_2(P\cap P)_2]$ és el complex $[Pt_2(\mu\text{-}S_2)(P\cap P)_2]^{2+}$ en el que s'ha format un enllaç S-S. Tanmateix, la ràpida degradació de l'espècie monooxidada $[Pt_2(\mu\text{-}S)_2(P\cap P)_2]^{+}$ ha impedit aïllar i caracteritzar aquest producte. Malgrat aquesta dificultat experimental, aquesta tesi doctoral ha demostrat que sistemes del tipus M_2S_2 poden presentar activitat redox com a conseqüència del canvi de l'estat d'oxidació dels anions sulfur donant lloc a lligands $(S\text{-}S)^{2-}$ pont.

6.- En conjunt, aquest treball ha demostrat la complexitat i diversitat que es deriva de la reactivitat que poden presentar els compostos amb l'anell $\{Pt_2S_2\}$. La clau de tota la química que presenten els compostos estudiats és l'elevada densitat electrònica dels anions sulfur en l'anell central $\{Pt_2S_2\}$. Així, la forta nucleofilictitat d'aquests complexos permetrà, per exemple, fer reaccions amb electròfils orgànics tal com ho faria l'anió sulfur lliure, però en un entorn inorgànic que permet tenir un major control sobre el sistema (solubilitat, modulació de la reactivitat variant el lligand L del complex $[Pt_2(\mu\text{-}S_2)L_4]$...). En conclusió, la recerca bàsica efectuada en aquesta tesi doctoral permet tenir un coneixement més profund d'uns sistemes que tenen rellevància de cara a possibles aplicacions sintètiques, a la major comprensió de processos biològics ,o de cara a futures innovacions en processos de catàlisi.